Measurements and Monte Carlo simulations for reference dosimetry of external radiation therapy beams

by

Bryan R. Muir

A thesis submitted to the Faculty of Graduate and Postdoctoral Affairs

in partial fulfillment of the requirements for the degree of

Doctor of Philosophy

in

Physics

Specialization in Medical Physics

Ottawa-Carleton Institute for Physics

Department of Physics

Carleton University

Ottawa, Ontario, Canada

Abstract

About 50 % of cancer patients receive some form of radiation therapy over the course of treatment. The accuracy of external beam radiation therapy relies on careful reference dosimetry, the calibration of treatment machine output. A comprehensive investigation of reference dosimetry of photon and electron beams is presented using measurements and Monte Carlo simulations, with specific focus on the determination of accurate beam quality conversion factors, k_Q, which are needed to convert the reading of an ionization chamber calibrated in a cobalt-60 reference field to the absorbed dose to water in a clinical beam. Measurements of k_Q factors for plane-parallel chambers are determined as the ratio of absorbed dose calibration coefficients, traceable to the Canadian primary standard water calorimeter, in a cobalt-60 beam to those from linac photon beams. The poor repeatability of these measurements indicates that plane-parallel chambers may not be suitable for reference dosimetry without a cross-calibration procedure. With the `EGSnrc` code system, k_Q factors are calculated as the ratio of the absorbed dose to water and the absorbed dose to the gas in fully modelled ionization chambers in clinical photon and electron beams to that in a cobalt-60 beam. Calculated k_Q factors for all chambers are within 0.7 % of those recommended by current dosimetry protocols although individual correction factors, used to explain the differences between k_Q factors, are up to 1.7 % different. Systematic uncertainties in calculated k_Q factors are less than 0.5 % using realistic assumptions and generally less than 1 % with conservative assumptions. Excellent agreement is observed when comparing the measured k_Q factors of this work and from the refereed literature to the present calculated values. This comparison is used to establish that the upper limit of $(W/e)_{air}$ variation with photon beam quality is 0.36 % with 95 % confidence. The level of agreement between measured and calculated k_Q factors and the low systematic uncertainties in Monte Carlo calculated k_Q factors give great confidence in adopting these calculations for updated reference dosimetry protocols.

Acknowledgments

I am greatly indebted to my supervisor and mentor, Dave Rogers, for all he has done for me over the course of this degree. Through his hard work, his unvarying availability to discuss even the most minor aspect of research and his attention to detail, he is the epitome of the physicist I aspire to be and a constant source of inspiration. I also owe a great deal of gratitude to Malcolm McEwen, with whom many hours were spent in the linac bunker at NRC where he taught me through his meticulousness with measurements, insightfulness and patience. The confidence Malcolm showed in my abilities meant a lot to me.

I appreciate the help of my former office mates, Daniel La Russa and Elsayed Ali. Dan taught me a lot about the `EGSnrc` code system when I was first starting this project. I enjoyed working with Ali and appreciate his help throughout this research. Ali's diligence also affected the quality of my work and my work ethic. I thank my colleagues for help in this work: Justin Sutherland, Rowan Thomson, Lilie Wang, Nicholas Humphreys and Benjamin Spencer from Carleton University; Ernesto Mainegra-Hing, Frédéric Tessier, Iwan Kawrakow, Claudiu Cojocaru, Dave Marchington and Carl Ross from NRC; Jan Seuntjens from McGill; and, Jörg Wulff and Klemens Zink from IMPS. For the ion chambers and chamber drawings used in this work, I thank Igor Gomola and Frantisek Gabris of IBA, Mark Szczepanski and Christian Pychlau of PTW, and Eric DeWerd and Brian Hooten of Exradin.

Generous funding from the OGSST program, the NSERC CGS program, the Dean of Graduate Studies and the Physics Department made this work possible.

I thank my mom and dad for their love and support and for always believing in me. I also thank my sister and lifelong best friend, Stephanie, for always being there for me. Finally, I thank Laura for being a wonderful companion and encouraging me during difficult times.

Statement of originality

This thesis summarizes the most significant portions of the author's research over the course of his doctoral studies. This work has been published in the peer-reviewed papers, technical reports and conference presentations listed below. Throughout this thesis, these publications are referenced by their Roman numeral labels given below.

Dr. David Rogers supervised this project, giving input on many aspects of the research, and provided comments on all of the manuscripts. Dr. Malcolm McEwen supervised and helped make the experimental measurements and provided input on several of the manuscripts. The author made the experimental measurements, performed all of the computational work, analyzed the results, wrote and prepared the manuscripts and revised them based on comments from referees.

Peer-reviewed papers

I. B. R. Muir and D. W. O. Rogers, "Monte Carlo calculations of k_Q, the beam quality conversion factor", Med. Phys. **37**, 5939 – 5950 (2010). Won the Farrington Daniels Award for the best scientific paper on radiation dosimetry in Med. Phys. in 2010.

II. B. R. Muir and D. W. O. Rogers, "The central electrode correction factor for high-Z electrodes in small ionization chambers", Med. Phys. **38**, 1081 – 1088 (2011).

III. B. R. Muir, M. R. McEwen and D. W. O. Rogers, "Measured and Monte Carlo calculated k_Q factors: Accuracy and comparison", Med. Phys. **38**, 4600 – 4609 (2011).

IV. B. R. Muir, M. R. McEwen and D. W. O. Rogers, "Beam quality conversion factors for parallel-plate ionization chambers in MV photon beams", Med. Phys. **39**, 1618 – 1631 (2012).

V. B. R. Muir, M. R. McEwen and D. W. O. Rogers, "Determination of relative ion chamber perturbation correction factors in high-energy electron beams and the impact of the effective point of measurement", Phys. Med. Biol., to be submitted (2013).

VI. B. R. Muir and D. W. O. Rogers, "Monte Carlo calculations for reference dosimetry of electron beams with the PTW Roos and NE2571 ion chambers", Med. Phys., submitted (June 2013).

VII. B. R. Muir and D. W. O. Rogers, "Monte Carlo simulations of electron beam quality conversion factors for several ion chamber types", Med. Phys., to be submitted (2013).

Technical reports

I. B. R. Muir and D. W. O. Rogers, "Ion Chamber Models for `EGSnrc` Calculations", Technical Report CLRP 08 – 02 (53 pp), Carleton University, Ottawa, Canada, (2008).

II. B. R. Muir and D. W. O. Rogers, "Monte Carlo calculations of the beam quality conversion factor, k_Q, for cylindrical ionization chambers", Technical Report CLRP 10 – 02 (23 pp), Carleton University, Ottawa, Canada. http://people.physics.carleton.ca/~drogers/pubs/papers/cylkQ_webreport.pdf, (2010).

III. B. R. Muir, M. R. McEwen and D. W. O. Rogers, "Depth-ionization measurements for high-energy electron beam dosimetry", Technical Report CLRP 12 – 06 (38 pp), Carleton University, Ottawa, Canada, (2012).

Conference abstracts (* indicates presenting author)

I. B. R. Muir* and D. W. O. Rogers, "A Monte Carlo Investigation of the Beam Quality Conversion Factor", Oral presentation at the American Association of Physicists in Medicine (AAPM) Meeting, Anaheim, California, U. S., Jul. 2009. Published in Med. Phys. **36**, 2732 (2009).

II. B. R. Muir* and D. W. O. Rogers, "Analysis of Systematic Uncertainties in Monte Carlo Calculated Beam Quality Conversion Factors", Oral presentation at the Canadian Organization of Medical Physicists (COMP) Meeting, Ottawa, Ontario, Canada, Jun. 2010. Published in Med. Phys. **37**, 3905 (2010).

III. B. R. Muir* and D. W. O. Rogers, "Central Electrode Correction Factor, P_{cel}, for Steel and Wire Electrodes", Moderated poster/short oral presentation at the American Association of Physicists in Medicine (AAPM) Meeting, Philadelphia, Pennsylvania, U. S., Jul. 2010. Published in Med. Phys. **37**, 3096 (2010).

IV. B. R. Muir*, M. R. McEwen and D. W. O. Rogers, "How accurate are Monte Carlo calculated k_Q factors for external beam radiotherapy?", Oral presentation at the European Society for Therapeutic Radiology and Oncology (ESTRO) Meeting, London, U. K., May 2011. Published in Radiother. Oncol. **99**, Supplement 1, S40 (2011).

V. B. R. Muir*, M. R. McEwen and D. W. O. Rogers, "Plane parallel ion chambers in MV photon beams: Monte Carlo calculated k_Q factors", Oral presentation at the

McGill International Workshop on Recent Advances in Monte Carlo Techniques in Radiation Therapy, Montreal, Quebec, Canada, Jun. 2011. Published in Abstract book for International Workshop on Recent Advances in Monte Carlo Techniques in Radiation Therapy.

VI. B. R. Muir*, M. R. McEwen and D. W. O. Rogers, "Making Plane – Parallel Ionization Chambers Available for Reference Dosimetry of High – Energy Photon Beams", Poster presentation at the joint Canadian Organization of Medical Physicists (COMP)/American Association of Physicists in Medicine (AAPM) Meeting, Vancouver, British Columbia, Canada, Jul. 2011. Published in Med. Phys. **38**, 3509 (2011).

VII. B. R. Muir*, M. R. McEwen and D. W. O. Rogers, "Monte Carlo simulations to obtain several parameters required for electron beam dosimetry", Oral presentation at the Canadian Organization of Medical Physicists (COMP) Meeting, Halifax, Nova Scotia, Canada, Jul. 2012. Finalist in J.R. Cunningham Young Investigator Symposium. Published in Med. Phys. **39**, 4623 (2012).

VIII. B. R. Muir, M. R. McEwen* and D. W. O. Rogers, "A New Method for the Measurement of Reference Dosimetric Quantities in Electron Beams", Oral presentation at the American Association of Physicists in Medicine (AAPM) Meeting, Charlotte, North Carolina, U. S., Jul. 2012. Published in Med. Phys. **39**, 3887 (2012).

IX. B. R. Muir* and D. W. O. Rogers, "Reference dosimetry of high-energy electron beams with a Farmer-type ionization chamber", Oral presentation at the American Association of Physicists in Medicine (AAPM) Meeting, Indianapolis, Indiana, U. S., Aug. 2013.

X. B. R. Muir* and D. W. O. Rogers, "Electron beam quality conversion factors for several plane-parallel and cylindrical ionization chambers", Poster presentation at the joint Canadian Association of Radiation Oncology (CARO)/Canadian Organization of Medical Physicists (COMP) Meeting, Montreal, Quebec, Canada, Sep. 2013.

Contents

List of Tables

List of Figures

Nomenclature

$(\Delta k_Q)_i$ Component of relative uncertainty in k_Q from a given parameter i at the k=1 limit (68 % confidence) [%]

$(w(E)/e)_{air}$ Energy deposited per unit of charge of one sign released by electrons of a certain energy coming to rest in dry air [J/C]

$(W/e)_{air}$ Average energy deposited per unit of charge of one sign released by an electron coming to rest in dry air [J/C]

$(W/e)_{gas}$ Average energy deposited per unit of charge of one sign released by an electron coming to rest in gas [J/C]

$\%dd(10)$ Percentage depth-dose at a depth of 10 cm with a 10×10 cm^2 field on the surface of a water phantom at an SSD of 100 cm [%]

$\%dd(10)_{\mathrm{x}}$ Photon component of the percentage depth-dose at a depth of 10 cm with a 10×10 cm^2 field on the surface of a water phantom at an SSD of 100 cm [%]

$\bar{E}_z$ Average electron energy at depth [MeV]

χ^2/df χ^2 per degree of freedom [unitless]

δ Parameter related to general ion recombination [mGy^{-1}]

Δ_i Percent difference between experimental and calculated k_Q values for chamber i [%]

$\frac{S(E)}{\rho}$ Unrestricted electron mass collision stopping power [MeV cm^2/g]

γ Parameter related to initial ion recombination [unitless]

$\left(\frac{\overline{L_\Delta}}{\rho}\right)^w_{air}$ Mean restricted water-to-air collision stopping power ratio [unitless]

$\left(\frac{\overline{S}}{\rho}\right)_{air}^{w}$ Mean unrestricted water-to-air mass collision stopping power ratio [unitless]

$\Phi(E)$ Differential charged particle primary fluence spectrum [cm^{-2} MeV^{-1}]

D_w Absorbed dose to water [Gy]

D_{air} Absorbed dose to dry air in an ideal ion chamber [Gy]

D_{ch} Absorbed dose to air in a real ion chamber [Gy]

d_{max} Depth of maximum dose [cm]

D_{pp} Dose per pulse [cGy]

d_{ref} Reference depth [cm]

Gy Gray, unit of absorbed dose [Gy=J/kg]

I Mean excitation energy [eV]

I_{50} Depth in electron beams at which the ionization or ion chamber reading has fallen to 50 % of its maximum value [cm]

$k'_{R_{50}}$ Electron quality conversion factor [unitless]

K_h Humidity correction factor [unitless]

k_Q Beam quality conversion factor [unitless]

k_{ecal} Photon-electron conversion factor, $k_{ecal} = k_{R_{50}}$ at R_{50}=7.5 cm [unitless]

$k_{R_{50}}$ Component of k_Q which is independent of the ionization gradient at the point of measurement [unitless]

L_Δ Collision stopping power restricted to energy losses less than Δ [MeV/cm]

M Fully corrected ion chamber reading [C]

m_{gas} Mass of the sensitive volume of gas in an ion chamber [kg]

M_{raw} Raw ion chamber reading [C]

$N_{D,w}$ Absorbed dose to water calibration coefficient [Gy/C]

P_{cel} Central electrode correction factor [unitless]

P_{fl} Fluence correction factor [unitless]

P_{gr} Gradient correction factor [unitless]

P_{Q} Overall ion chamber perturbation factor [unitless]

P_{repl} Replacement correction factor [unitless]

P_{stem} Stem correction factor [unitless]

P_{wall} Wall correction factor [unitless]

P_{elec} Electrometer correction factor [C/rdg]

P_{ion} Ion recombination correction factor [unitless]

P_{leak} Leakage correction factor [unitless]

P_{pol} Polarity correction factor [unitless]

P_{rp} Radial intensity profile correction factor [unitless]

P_{TP} Pressure and temperature correction factor [unitless]

R_{50} Depth in electron beams at which the absorbed dose to water has fallen to 50 % of its maximum value [cm]

r_{cav} Radius of a cylindrical ion chamber [cm]

SSD Source-to-surface distance [cm]

TPR_{10}^{20} Ratio of doses obtained at 20 and 10 cm with a constant source-to-detector distance and a field size of 10×10 cm^2 at the depth of measurement [unitless]

u_{k_Q} Combined relative uncertainty in k_Q at the k=1 limit (68 % confidence) [%]

Chapter 1

Reference dosimetry and beam quality conversion factors

Thirty to fifty per cent of cancer patients will receive some form of radiation therapy over the course of their treatment. The primary objective in radiation therapy is to conform the dose from ionizing radiation to the tumour while sparing the surrounding healthy tissue. Ultimately, the accuracy of treatment depends on the calibration of the output of the radiation source, the first step in the treatment process known as reference dosimetry. Dose delivery should be accurate to within 5 % requiring that the accuracy of treatment machine calibration be around 1-2 %[1] but the uncertainty associated with parameters required for treatment machine calibration should be as low as possible.

1.1 Ionization chambers

In modern radiation therapy clinics, ionization chambers are the detectors of choice for calibrating the output of radiation therapy treatment machines. Ionization chambers are used because of their simple design, sensitivity, high precision, real-time readout, stability and established history. Two types of ionization chambers are commonly used in radiotherapy clinics, plane-parallel and cylindrical chambers. Schematics of the two chamber types are shown in figure 1.1. Plane-parallel chambers consist of

an air-filled cavity between two electrodes (one in the front wall or window and one behind the chamber cavity known as the collector) with side walls required to water-proof the chamber and protect the sensitive volume from dust or debris, a guard ring and a stem (not shown in figure 1.1), which houses a triaxial cable to deliver the signal to an electrometer. The cylindrical chamber types commonly used in clinical practice were introduced by Aird and Farmer[2] and are also referred to as thimble- or Farmer-type chambers. With this chamber type, a central electrode is used and a voltage is applied between the central electrode and the cylindrical chamber walls. The guard is in the stem of the chamber and all three electrodes (central electrode or collector, cylindrical wall and guard) are connected through the stem to the triaxial cable. The cavity between the electrode and walls is vented to the surrounding air. For both chamber types, the purpose of the guard is to prevent leakage from the collector across the insulator since the guard is at the same potential as the collector. If the guard extends into the air volume of the chamber, the chamber is considered to be fully guarded. For plane-parallel chambers, the sensitive volume of the chamber is more uniformly defined if the chamber is fully guarded and fluence perturbation effects are decreased by reducing in-scattering of electrons from the side wall of the chamber.

The quantity of interest for the calibration of the output of clinical radiation therapy beams is the undisturbed absorbed dose to water at a specific point in the beam under consideration. In order to measure the output of a source of radiation, the signal from a detector (an ionization chamber) used for calibration, composed of materials different from water, is ideally proportional to the dose (absorbed energy per unit mass) to the sensitive material of the detector. As charged particles cross the cavity of an ionization chamber, from the incident beam or liberated by photon interactions in the surrounding media or chamber walls, they ionize the air in the

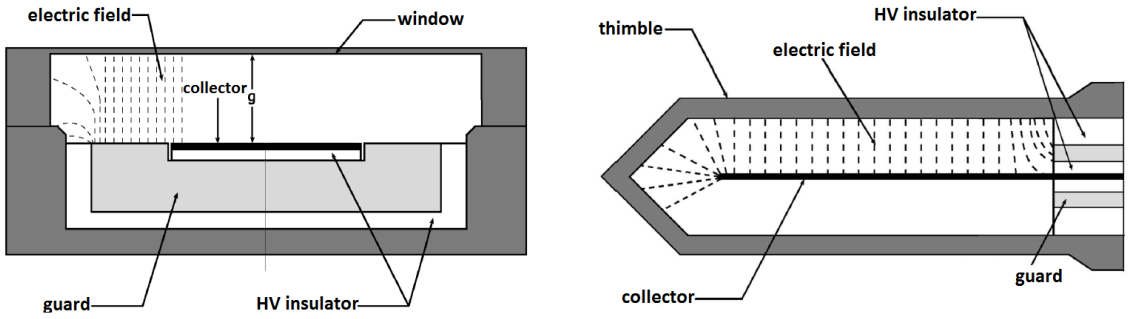

(a) (b)

Figure 1.1: General components of plane-parallel (a) and cylindrical (b) ionization chambers types [Redrawn from DeWerd *et al.*[3] with permission from American Association of Physicists in Medicine].

cavity. The charge released in the air is collected by the electrodes of the ion chamber and the signal obtained in Coulombs, M, is related to the absorbed dose to the sensitive volume of air in the ion chamber, D_{ch}, in units of Gray [Gy=J/kg] with

$$D_{ch} = \frac{M}{m_{gas}} \left(\frac{W}{e}\right)_{gas} \qquad [Gy], \tag{1.1}$$

where m_{gas} is the mass of the sensitive volume of air in the ion chamber in kg and $(W/e)_{gas}$ is the average energy deposited in humid air per unit of charge of one sign released in units of J/C. The raw signal from the ion chamber must also be corrected for various physical effects, discussed in section 1.3.

1.2 Cavity theory

Given that the absorbed dose to the sensitive air in the chamber is known from equation 1.1, the problem at hand is to relate the absorbed dose to the air in the chamber to the absorbed dose to water in the absence of the detector. This is dealt with using cavity theory, which forms the underlying basis of ion chamber dosimetry. The dose, D, from charged particles with a primary fluence spectrum differential in

energy, $\Phi(E)$, in a medium is given by

$$D = \int_0^{E_{max}} \Phi(E) \left(\frac{S(E)}{\rho} \right) dE \tag{1.2}$$

where $\frac{S(E)}{\rho}$ is the electron mass collision stopping power of the medium. Equation 1.2 is valid if so-called δ-equilibrium or secondary charged particle equilibrium (CPE) is achieved, that is, for each secondary charged particle of a given type and energy entering the region of interest an identical particle exits.

Consider now an air-filled cavity (an ideal ion chamber) at a specific point in a uniform tank of water, i.e., a water phantom, on which radiation is incident. The absorbed dose to the water, D_w, in the absence of the cavity is related to the absorbed dose to the air in the cavity, D_{air}, by the Bragg-Gray relation[4]

$$\frac{D_w}{D_{air}} = \frac{\int_0^{E_{max}} \Phi_w(E) \left(S(E)/\rho \right)_w dE}{\int_0^{E_{max}} \Phi_w(E) \left(S(E)/\rho \right)_{air} dE} = \left(\frac{\overline{S}}{\rho} \right)_{air}^{w}, \tag{1.3}$$

where $\left(\frac{\overline{S}}{\rho} \right)_{air}^{w}$ is the mean water-to-air mass collision stopping power ratio. Notice that in equation 1.3, the charged particle fluence spectrum in both the numerator and denominator is that for primary electrons in the water and is again differential in energy. In addition to the requirement of δ-equilibrium, the cavity considered to obtain equation 1.3 must fulfill the Bragg-Gray cavity requirements: that the cavity be small enough to (a) absorb energy *only* from electrons coming from the surrounding water; and, (b) not disturb the fluence of charged particles such that the fluence in the cavity is identical to the fluence in the water in the absence of the cavity. The preceding discussion was for the radiation dose from charged particles but the air in the cavity has a much lower density than the surrounding water. Therefore, even if the radiation source is a beam of photons, the majority of charged particles crossing the cavity are generated in the surrounding water and not from photon interactions

in the air.

In reality, because of the low density of air compared to water and the finite size of the cavity, δ-equilibrium is generally not achieved. Spencer and Attix[5] formulated a modified version of Bragg-Gray cavity theory that accounts for energy deposition of secondary particles. They introduced the concept of a cut-off energy, Δ, below which energy losses are assumed to be local - the energy loss remains in the cavity or medium where created. All charged particles entering the cavity from the surrounding medium have an energy greater than Δ. Local energy losses are treated with the use of the collision stopping power restricted to energy losses less than Δ, L_Δ. Equation 1.3 now becomes

$$\frac{D_w}{D_{air}} = \frac{\int_\Delta^{E_{max}} \Phi_w(E)\left(L_\Delta(E)/\rho\right)_w dE + \Phi_w(E)[S(\Delta)/\rho]_w\Delta}{\int_\Delta^{E_{max}} \Phi_w(E)\left(L_\Delta(E)/\rho\right)_{air} dE + \Phi_w(E)[S(\Delta)/\rho]_{air}\Delta} = \left(\overline{\frac{L_\Delta}{\rho}}\right)_{air}^{w}, \quad (1.4)$$

where $\int_\Delta^{E_{max}} \Phi_w(E)\left(L_\Delta(E)/\rho\right)_w dE$ represents the energy deposited by all electrons with energy greater than Δ and $\Phi_w(E)[S(\Delta)/\rho]_w\Delta$ is the 'track-end' term, accounting for energy deposition by electrons with energies less than Δ. Like equation 1.3, equation 1.4 still assumes that the fluence spectrum is identical in the cavity and the undisturbed water. The ratio of the dose to the water to the dose to the air in the cavity is then equal to the mean restricted water-to-air collision stopping power ratio, $\left(\overline{\frac{L_\Delta}{\rho}}\right)_{air}^{w}$. It was suggested[5] that Δ be set equal to the energy of an electron with a range just large enough to cross the cavity.

Equation 1.4 still assumes a perfect Bragg-Gray cavity - a cavity small enough that the fluence spectrum in the air is identical to that in the undisturbed water and without any effects present when considering a real ion chamber, that is, electrons generated by photon interactions in the chamber walls, stem or central electrode (if present). The deviation from perfect behavior is accounted for with perturbation

correction factors. Including these correction factors, the dose to the water is related to the dose to the humid air in a real ion chamber, D_{ch}, with

$$D_w = D_{ch}\left(\frac{\overline{L_\Delta}}{\rho}\right)^w_{gas} P_{\mathrm{Q}} = D_{ch}\left(\frac{\overline{L_\Delta}}{\rho}\right)^w_{gas} P_{\mathrm{repl}} P_{\mathrm{wall}} P_{\mathrm{stem}} P_{\mathrm{cel}}, \tag{1.5}$$

where P_{Q} is the overall ion chamber perturbation factor, which is factored into individual correction factors such that P_{repl} corrects for changes in the electron fluence spectrum in water due to the introduction of the air cavity, P_{wall} and P_{stem} correct for the non-water-equivalence of the chamber wall and stem, respectively, and the presence of the chamber's central electrode is corrected for with P_{cel}.

Except for P_{repl}, individual correction factors (in the notation of Seuntjens and Rogers[6]) are defined by

$$D_{air} = \frac{D_{air}}{D^w_{air}} \cdot \frac{D^w_{air}}{D^{w,c}_{air}} \cdot \frac{D^{w,c}_{air}}{D^{w,c,s}_{air}} \cdot D^{w,c,s}_{air} = P_{\mathrm{wall}} \cdot P_{\mathrm{cel}} \cdot P_{\mathrm{stem}} \cdot D^{w,c,s}_{air}, \tag{1.6}$$

where D_{air} is the average dose to the dry air in the bare chamber cavity while D^X_{air} are the doses to the cavity with X components included ($D^{w,c,s}_{air}$ includes contributions from the chamber wall, central electrode and stem such that $D^{w,c,s}_{air} = D_{ch}$ in equation 1.5). The replacement correction factor, P_{repl}, can be obtained using the stopping power ratio (SPR) method[7] with

$$P_{\mathrm{repl}} = \left(\frac{D_w}{D_{air}}\right) \Big/ \left(\frac{\overline{L}}{\rho}\right)^{water}_{air}. \tag{1.7}$$

Three other methods are available to obtain P_{repl} corrections but give consistent results in most cases.[7] For most experimental determinations of correction factors, assumptions are required. For example, Wittkamper *et al.*[8] assumed that the NACP-02 chamber correction factors are unity to obtain correction factors for the NE2571

and Markus chambers. More recent Monte Carlo calculated results show that these assumptions are not valid.[9]

1.3 Current dosimetry protocols based on absorbed dose to water

Current reference dosimetry protocols[10,11] are based on the use of ion chambers calibrated in terms of absorbed dose to water. Under reference conditions, the dose to water, D_w^Q, in a clinical beam of quality Q at the point of measurement of the ion chamber in the absence of the chamber, is given by

$$D_w^Q = MN_{D,w}^Q \qquad [Gy], \tag{1.8}$$

where M is the fully corrected chamber reading and $N_{D,w}^Q$ is the absorbed dose to water calibration coefficient, traceable to national standards. Normally, ion chambers are calibrated at primary standards laboratories (PSLs) or accredited dosimetry calibration laboratories (ADCLs). It is not usually practical or achievable to obtain $N_{D,w}^Q$ coefficients directly for ion chambers in the radiation quality of interest; only a few laboratories provide an absorbed dose calibration service in clinical radiation beam qualities. Instead, ion chambers are typically calibrated in a cobalt-60 reference field yielding the ion chamber calibration coefficient in cobalt-60, $N_{D,w}^{^{60}Co}$. With this, the beam quality conversion factor, k_Q, is required to convert a measurement of the fully corrected chamber reading, M, in a beam of arbitrary quality to determine D_w^Q in the clinical beam with

$$D_w^Q = MN_{D,w}^Q = Mk_QN_{D,w}^{^{60}Co} \qquad [Gy]. \tag{1.9}$$

Beam quality conversion factors vary with beam type and characteristics as well as ion chamber geometry and composition.

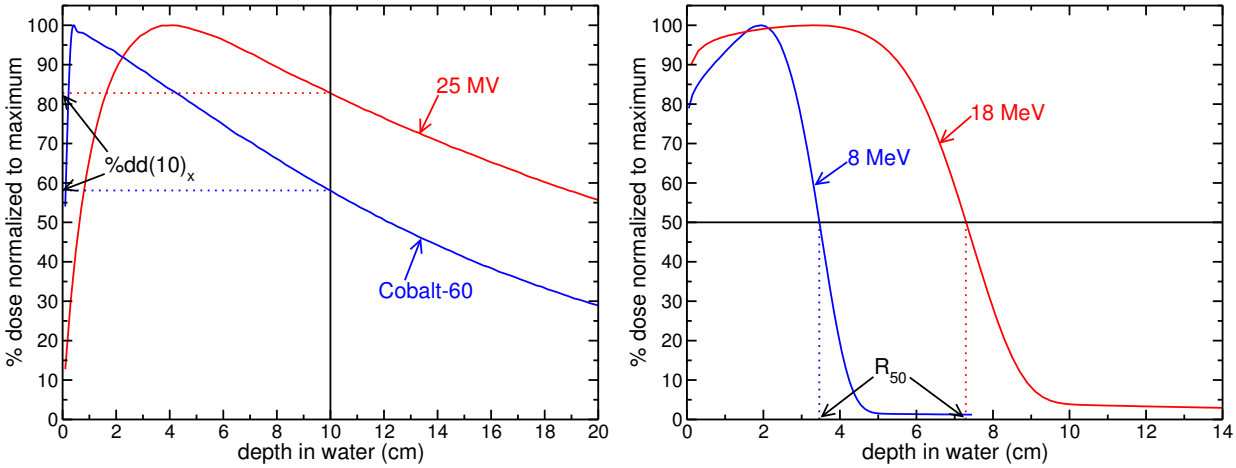

Figure 1.2: Beam quality specifiers used for reference dosimetry of external radiation therapy beams. Panel (a): the percentage depth-dose curves for photon beams from a cobalt-60 source and a 25 MV linear accelerator with the photon beam quality specifier, $\%dd(10)_x$. Panel (b): the percentage depth-dose in electron beams from linear accelerators with nominal energies of 8 and 18 MeV with the electron beam quality specifier, R_{50}.

Beam quality specification: In order to determine the beam quality conversion factor for the clinical beam of interest, the 'quality' of the beam must be specified in some way. In addition, to calculate k_Q factors with the approach used by dosimetry protocols described below, the accurate selection of various quantities (stopping power ratios and correction factors) requires a beam quality specifier that *uniquely* determines the value of the quantity to select. Figure 1.2 illustrates the beam quality specifiers used for (a) photon and (b) electron beams. In panel (a), the absorbed dose to water normalized to the maximum dose is shown as a function of depth in a water phantom (i.e., the percentage depth-dose curve). Beam quality is specified for photon beams with the photon component of the percentage depth-dose at a depth of 10 cm, $\%dd(10)_x$. In clinical beams, TG-51[10] details how to remove the component of the dose from contaminant electrons. One can see from figure 1.2 (a) that for a

cobalt-60 beam consisting of photons with 1.17 and 1.33 MeV energies, the $\%dd(10)_{\mathrm{x}}$ is 58.4 %, whereas for photons from a 25 MV linear accelerator with a spectrum of (on average higher) photon energies, the $\%dd(10)_{\mathrm{x}}$ is 82.8 %. The depth in water where the ion chamber measurement is made in the clinic (the reference depth, d_{ref}) is at 10 cm in photon beams. Figure 1.2 (b) shows percentage depth-dose curves in linear accelerator electron beams with 8 and 18 MeV energies. For electron beams, beam quality is specified by R_{50}, the depth at which the absorbed dose to water has fallen to 50 % of its maximum value. For the beams shown in figure 1.2 (b), R_{50} amounts to 3.46 cm in the 8 MeV beam and 7.29 cm in the 18 MeV beam. The reference depth for electron beams is calculated from R_{50} using $d_{ref} = 0.6R_{50} - 0.1$ cm.

Corrections to the measured ion chamber reading: As was alluded to previously, the raw ion chamber reading, M_{raw}, must be corrected for a variety of physical effects to obtain the fully corrected reading, M, with

$$M = M_{raw}P_{TP}P_{leak}P_{ion}P_{pol}P_{elec}P_{rp}, \tag{1.10}$$

where P_{TP} corrects for variations in temperature and pressure, P_{leak} corrects for leakage current, P_{ion} corrects for the lack of complete charge collection due to ion recombination, P_{pol} corrects for the polarity effect and P_{elec} is the electrometer correction factor (required to convert the reading to true Coloumbs if the electrometer and ion chamber are calibrated separately). Neither the AAPM[10] nor IAEA[11] protocols required P_{rp}, which corrects for variations in the radial intensity profile (field flatness) although the addendum[12] to the AAPM's TG-51 protocol does include this factor. The corrections to the raw chamber reading are revisited in more detail in chapters 2 and 3 when discussing the measurement of k_Q factors.

1.4 Protocol approach to determine k_Q factors

Current dosimetry protocols[10,11] calculated k_Q factors using an indirect approach, combining equations 1.1,1.5 and 1.9 to obtain (in the notation related to the AAPM's TG-51[13] protocol)

$$k_Q = \left[K_h (W/e)_{air} \left(\frac{\bar{L}}{\rho} \right)_{\text{air}}^{\text{water}} P_{\text{cel}} P_{\text{repl}} P_{\text{wall}} \right]_{^{60}Co}^{Q} . \tag{1.11}$$

where the humidity correction, K_h, accounts for the fact that measurements are made in humid air whereas $(W/e)_{air}$, m_{air} and $\left(\frac{\bar{L}}{\rho}\right)_{\text{air}}^{\text{water}}$ are all for dry air. The most accurate data available at the time were used to obtain k_Q factors but large uncertainties were present in some of the individual correction factors and some assumptions were required. In addition, there are now ion chambers available on the market for which data are not available to calculate accurate k_Q factors. In the following, a review of the data used for the TG-51[10] protocol calculations of k_Q factors is presented with comparison to more accurate data from recent publications where available.

Humidity effects: Equation 1.1 relates the signal from an ion chamber to the absorbed dose to the gas in the chamber. The quantity $(W/e)_{air}$ is thought to be constant with beam quality for dry air (see below). The factor K_h corrects for humidity effects and has been shown to be constant within 0.15 % with beam quality[14] at reasonable values of relative humidity between 10 and 90 %.

$\boldsymbol{(W/e)_{air}}$: For the calculation of k_Q factors in current dosimetry protocols,[11,13] the average energy deposited in dry air per unit of charge of one sign released as an electron slows completely in air, $(W/e)_{air}$, is assumed constant with beam energy. There is evidence that this is a poor assumption since $(w(E)/e)_{air}$, the energy lost in air per Coulomb of charge released by electrons of a *certain energy*, may vary

by up to 1.5 %[15] in monoenergetic electron beams. This leads to an uncertainty of 0.75 % in calculated k_Q factors from potential $(W/e)_{air}$ variation with beam quality. However, the reanalysis by Svensson and Brahme[15] of previous measurements made by Domen and Lamperti[16] used stopping power ratios for monoenergetic electrons, which do not reflect those for electrons crossing the cavity of an ion chamber at depth in water from real clinical beams, so it is hard to realistically assess the variation of $(W/e)_{air}$. In addition, the uncertainties in the original measurements of Domen and Lamperti[16] are estimated at 0.8 % so drawing conclusions on effects on the order of 1.5 % are suspect. The work of Svensson and Brahme[15] is cited by TRS-398[17] to assign uncertainty in calculated k_Q factors from potential $(W/e)_{air}$ variation with beam quality, estimated at 0.5 %. The variation of $(W/e)_{air}$ with beam quality is a significant focus of this work; in chapter 5, the first quantitative estimate of the uncertainty in k_Q factors from variation in $(W/e)_{air}$ with beam quality in photon beams is determined (papers III and IV).

Stopping power ratios: A point of contention at the time that current dosimetry protocols[10,11] were written was the choice of beam quality specifier to determine stopping power ratios in photon beams. The IAEA[11] protocol used TPR^{20}_{10}, the ratio of doses obtained at 20 and 10 cm with a constant source-to-detector distance, while the TG-51[10] protocol used $\%dd(10)_{\mathrm{x}}$, described above. The reason for the use of $\%dd(10)_{\mathrm{x}}$ by TG-51[10] was that, if TPR^{20}_{10} was used, up to 1 % differences in stopping power ratios at the same value of TPR^{20}_{10} could occur depending on the filtration of the photon beam, making it a poor beam quality specifier. Specifying beam quality with $\%dd(10)_{\mathrm{x}}$ allows a more accurate determination of stopping power ratios independent of the characteristics of the beam under consideration.[18–21]

The stopping power ratios used by TG-51[13] to determine k_Q factors for photon beams are based on Monte Carlo calculations by Rogers and Yang.[22] More recently,

Kalach and Rogers[20] calculated stopping power ratios for about 50 beams and observed agreement within about 0.2 % with those of Rogers and Yang[22] while the results for unfiltered beams of Xiong and Rogers[21] were in agreement within 0.4 % compared to those used for TG-51[13] k_Q calculations.

Similarly, beam quality specification and the associated reference depth for electron beams were chosen for the accurate selection of stopping power ratios. Both current dosimetry protocols[10,11] recommend R_{50} for beam quality specification and $d_{ref} = 0.6R_{50} - 0.1$ cm for the reference depth.

The stopping power ratios used to obtain electron beam k_Q factors[11,13] are based on the stopping power ratios calculated using realistic Monte Carlo simulations of linear accelerator electron beams by Ding *et al.*[23] The fit proposed by Burns *et al.*[24] to the stopping power ratios at d_{ref} as a function of R_{50} was used to calculate stopping power ratios for TG-51.[13] Burns *et al.*[24] also proposed a fit to these data as a function of depth and R_{50} but Rogers[25] pointed out that this fit is only accurate at the 1 % level for depths less than $1.2R_{50}$. More recently, Zink and Wulff[26] calculated stopping power ratios (albeit using sources from electron beam spectra that do not include contaminant photons) that are within 0.2 % of those calculated by the Burns *et al.*[24] fit to stopping power ratios at d_{ref}. Using realistic accelerator models, Verhaegen *et al.*[27] observed differences up to 0.9 % at d_{ref} compared to the results of Burns *et al.*[24]

Central electrode correction factors: To correct for the presence of an aluminum central electrode in cylindrical chambers in photon beams, TG-51[13] used a fit to the Monte Carlo calculated P_{cel} correction factors of Ma and Nahum.[28] For chambers that use a graphite or air-equivalent plastic central electrode, P_{cel} was assumed to be unity. Measurements of P_{cel} made by Palm and Mattson[29] are in good agreement with the calculations of Ma and Nahum.[28] More recent Monte Carlo calculations by Buckley *et al.*[30] for cylindrical chambers that employ graphite and aluminum electrodes and

Wulff *et al.*[31] for an aluminum electrode are also in good agreement with the results of Ma and Nahum.[28] In this work (paper II), up to 1.5 % effects on k_Q factors are observed for chambers that use high-Z (Z>13) electrodes but these chambers were not included in TG-51.[10]

For electron beam k_Q factors, again TG-51[13] used the P_{cel} calculations of Ma and Nahum[28] for chambers that use an aluminum central electrode and for a graphite electrode P_{cel} was assumed unity. The calculations of Buckley *et al.*[30] indicate that P_{cel} is up to 0.2 % from unity for a graphite central electrode in electron beams but observed fairly good agreement with the results of Ma and Nahum[28] for an aluminum electrode. As in photon beams, this work (paper II) shows much larger effects on k_Q factors (up to a 2.3 %) for chambers (not included in TG-51[10]) that use high-Z electrodes in electron beams.

Wall correction factors: For cylindrical chambers in photon beams, TG-51[13] used P_{wall} correction factors based on the formalism of Almond and Svensson[32] and ignored the effect of a water-proofing sleeve (although many cylindrical chambers do require a sleeve). Buckley and Rogers[33] showed up to 0.8 % differences in P_{wall} corrections compared to those used by TG-51[13] with up to 0.6 % differences in the effect on k_Q factors. Several investigations,[18,33–35] including paper III of this work, have shown that a water-proofing sleeve has up to a 0.3 % effect on k_Q factors in high-energy photon beams.

For plane-parallel chambers in photon beams, P_{wall} values were not available at the time TG-51[10] was written in beam qualities other than cobalt-60 and there existed evidence for large chamber-to-chamber variability (up to 3.6 %) of P_{wall} correction factors for these chambers in cobalt-60.[36] This led to the recommendations that (a) plane-parallel chambers not be used for reference dosimetry of photon beams; and, (b) a cross-calibration procedure against stable cylindrical chambers be employed

(to avoid incurring high uncertainties from the variability of P_{wall} for plane-parallel chambers in cobalt-60) to enable the use of plane-parallel chambers in electron beams. However, k_Q factors were still provided for plane-parallel chambers in electron beams in case it was not possible to perform the cross-calibration procedure. Also note that $k'_{R_{50}}$ values (the electron quality conversion factor, values of k_Q normalized to unity in a high-energy electron beam to remove the cobalt-60 and gradient components) were required for the determination of absorbed dose in low-energy electron beams with cross-calibrated plane-parallel chambers. Calculations of P_{wall} values for plane-parallel chambers in a cobalt-60 beam (required for electron beam k_Q factors) used `EGS4`[37] calculations that had known systematic uncertainties of up to 1 %. Mainegra-Hing *et al.*[38] and Buckley and Rogers[9] showed up to 1.2 % differences from the `EGS4`[37] P_{wall} calculations for plane-parallel chambers used for the cobalt-60 component of k_Q factors by TG-51.[13]

For electron beams, P_{wall} was assumed to be unity by TG-51[13] for all chambers. Buckley and Rogers[9] indicate up to 1.7 % differences from unity in low-energy electron beams for plane-parallel chambers. For cylindrical chambers, the difference in P_{wall} from unity in electron beams is up to 0.6 %.[33]

Replacement correction factors: The replacement correction factor, P_{repl}, corrects for changes in the fluence spectrum caused by the introduction of a cavity into a uniform medium. It is thought to consist of two components, the gradient correction, P_{gr}, and the fluence correction, P_{fl}, such that $P_{\text{repl}} = P_{\text{gr}}P_{\text{fl}}$.

The electron fluence in a cavity is actually representative of the fluence in the medium at a point closer to the source because of less attenuation in the cavity than in the medium. This effect can be accounted for with the use of a gradient correction, P_{gr}, termed so because the magnitude of the effect depends on the dose gradient. The gradient correction effectively moves the point of measurement upstream from the

center of a cylindrical chamber. For well-guarded plane-parallel chambers in photon beams, it is thought that using the front of the cavity as the point of measurement accounts for any gradient effect so that P_{gr} is taken as unity (even in regions where there is a dose gradient). The other component of the replacement correction factor is the fluence correction, P_{fl}. In photon beams, the fluence correction is not required because the reference depth is in a region with transient charged particle equilibrium.

There are two common methods for correcting gradient effects. One is to shift the depth-dose curve with an effective point of measurement while the other uses a multiplicative correction factor to correct for gradient effects. The TG-51[10] protocol uses some form of both approaches. For the determination of beam quality specifiers with cylindrical chambers, the use of an effective point of measurement shifts the entire depth-dose curve to account for gradient effects. The gradient correction at the reference depth is accounted for using a multiplicative correction factor. For photon beams, this is implicitly included in the k_Q factors provided by TG-51[13] but for electron beams, k_Q is factored into

$$k_Q = P_{\text{gr}}^Q k_{R_{50}}, \tag{1.12}$$

where $k_{R_{50}}$ is the component of k_Q which is independent of the ionization gradient at the point of measurement and P_{gr}^Q is the gradient correction. In electron beams, P_{gr}^Q is taken to be unity for well-guarded plane-parallel chambers but for cylindrical chambers, a clinically measured gradient correction factor is applied, which is determined with

$$P_{\text{gr}}^Q = M_{raw}(d_{ref} + 0.5\, r_{cav})/M_{raw}(d_{ref}). \tag{1.13}$$

The shift of $0.5\ r_{cav}$, where r_{cav} is the radius of the cylindrical chamber, was measured by Johansson *et al.*[39] by comparison of depth-dose curves measured with cylindrical

chambers to those obtained with well-guarded plane-parallel chambers. Correcting for gradient effects with the measured value of $P_{\rm gr}^{Q}$ obtained with equation 1.13 is equivalent to using the effective point of measurement approach (for both beam quality specification *and* measurements at the reference depth) recommended by the IAEA.[11]

Gradient corrections for TG-51[13] calculated k_Q factors in photon beams are based on the measurements of Cunningham and Sontag.[40] Wang and Rogers[7] found P_{repl} in a cobalt-60 beam to be 0.9964 for a cylindrical chamber compared to the value of 0.992 used by TG-51[10] (a difference of 0.4 %). However, for k_Q factors, Wang and Rogers[41] found that the ratio of $P_{\rm repl}$ values in a high-energy photon beam to that in a cobalt-60 beam are consistent within 0.2 % with the values used by TG-51.[13] For plane-parallel chambers in cobalt-60 (needed for electron beam k_Q factors), the protocol determination[13] of k_Q factors assumed that the fluence correction was unity but recent Monte Carlo simulations showed differences from unity of up to 0.8 %[26] and 0.6 %[7] (for PTW Roos and IBA NACP-02 chambers, respectively).

For TG-51[13] calculations of k_Q factors for cylindrical chambers in electron beams, the measurements of $P_{\rm fl}$ by Johansson *et al.*[39] are used as a function of $\bar{E}_z$, the average electron energy at depth. These measurements were determined at d_{max} in a PMMA phantom so they may not be directly applicable to d_{ref}, which is far from d_{max} in high-energy beams. This determination[39] also required the assumption that the wall correction factor for the plane-parallel chamber used was unity. Recent Monte Carlo calculations show that the wall correction factor is actually larger than unity in electron beams by 0.5-1.5 %.[9] Other measurements by Wittkamper *et al.*[8] and Van der Plaetsen *et al.*[42] are in agreement with the Johansson *et al.*[39] results within 0.26 % but required the same assumption. Wang and Rogers[43] showed that P_{repl} is 0.5-1.0 % different from that used by TG-51[13] for cylindrical chambers in electron beams. This difference can be explained with the required wall correction for plane-

parallel chambers that was ignored to determine P_{fl} for cylindrical chambers.

For well-guarded plane-parallel chambers, the replacement correction in high-energy electron beams is taken as unity for TG-51[10] k_Q calculations. In fact, Wang and Rogers[7] showed that P_{repl} was between 0.996 and 1.0005 for the IBA NACP-02 chamber and Zink and Wulff[44] showed that it was between 0.997 and 1.003 for the PTW Roos chamber.

1.5 The EGSnrc Monte Carlo system

The EGSnrc[45,46] (Electron Gamma Shower) code system is a package of computer codes for the Monte Carlo simulation of coupled photon-electron transport in arbitrary geometries. It is applicable to particles with kinetic energies between a few keV to hundreds of GeV. The code system is based on the EGS4 system,[47] which has been in development since the 1970s. EGSnrc offers many improvements and upgrades to the EGS system and is considered to be the gold standard for medical physics applications. EGSnrc has been shown[48] (using the Fano test - one of the most rigorous benchmarks of coupled photon-electron transport) to be accurate to within 0.1 % with respect to its own cross sections for calculations of ion chamber response.

The EGSnrc back-end handles the physics of particle transport but, to perform calculations for practical applications, user-codes are required to model geometries and score quantities of interest. In this study, a variety of user-codes are employed depending on the desired quantity of interest but the majority of simulations use the egs_chamber user-code,[49] which uses the egs++ geometry package[50] to allow modelling of arbitrary geometries. The egs_chamber user-code[49] provides several powerful variance reduction techniques to increase the efficiency of in-phantom ion chamber simulations. For the simulations performed in this work, other user-codes include BEAMnrc[51,52] for accelerator source simulation, which is then used as an input

to `egs_chamber`, as well as calculations of absorbed dose to water as a function of depth for beam quality specification of photon beams and `SPRRZnrc`[53] for calculations of stopping power ratios.

1.6 Motivation, goals, and thesis organization

Motivation and goals: In section 1.4, differences of up to 1.7 % are indicated between the individual correction factors used to obtain k_Q factors provided by current dosimetry protocols[10,11] and recent, more accurate, determinations of individual correction factors. These differences provide motivation for an in-depth investigation of beam quality conversion factors. The AAPM is currently in the process of updating their protocol for high-energy reference dosimetry, further motivating this study. With the availability of the `EGSnrc` Monte Carlo code system to accurately calculate the response of ion chambers of arbitrary geometry and the access to high-quality equipment and collaboration with experts at the National Research Council of Canada (NRC) for the accurate measurement of ion chamber calibration coefficients, this type of study is now possible. The goals of this work are therefore to (a) provide direct calculations of k_Q factors using Monte Carlo simulations of ion chamber response in photon beams at the reference depth; (b) measure photon beam k_Q factors at the reference depth for plane-parallel chambers; (c) investigate the potential variation of $(W/e)_{air}$ with beam quality in photon beams; (d) use measurements as a function of depth to investigate absorbed dose calibration coefficients (with the end-goal of determining measured k_Q factors) for ion chambers in electron beams; (e) simulate the response of ion chambers as a function of depth in electron beams to investigate gradient effects and protocol recommendations to obtain beam quality specifiers; (f) extract data at the reference depth using the results of (d) and (e) to provide electron beam k_Q factors for ion chambers; and, (g) using the combined re-

sults of (a)-(f), provide general recommendations for high-energy reference dosimetry and the use of ion chambers.

Thesis organization: The bulk of this thesis focuses on reference dosimetry of photon beams because of the much more complicated nature of electron beam dosimetry. In chapter 2, the methods used to perform this study are laid out with specific emphasis on the determination of k_Q factors at the reference depth in photon beams. Measured k_Q factors for plane-parallel chambers in photon beams are presented in chapter 3. The results for Monte Carlo calculated k_Q factors for both chamber types in photon beams are presented in chapter 4. Comparison of high-quality measured and calculated k_Q factors in photon beams is performed in chapter 5 and the results of this comparison are used to estimate the upper limit on the potential variation of $(W/e)_{air}$ with beam energy. In chapter 6, Monte Carlo calculations for electron beam reference dosimetry are presented with emphasis on a few ion chamber types. A summary of the thesis and conclusions are provided in chapter 7. Appendix A describes a study of the central electrode correction factor and is referred to in chapter 4. Measurements of ion chamber response in electron beams are presented in appendix B and are referred to in chapter 6. The variation of the overall ion chamber correction factor with depth is investigated with Monte Carlo simulations for select chambers in appendix C and is also referred to in chapter 6.

Chapter 2

Determination of beam quality conversion factors

This chapter presents the methods employed throughout this thesis to obtain beam quality conversion factors using measurements (section 2.1) and Monte Carlo simulations (section 2.2).

2.1 Experimental measurements of k_Q factors

There is substantial interest in the measurement of k_Q factors traceable to primary standards for absorbed dose. Measured values of k_Q are valid for the specific ion chamber under investigation. This is different from Monte Carlo calculations where results are valid for a chamber type in general. If a specific ion chamber behaves as the manufacturer intends, Monte Carlo calculated k_Q factors should give accurate results for reference dosimetry. With measurements, several chambers of the same type should be considered to investigate chamber-to-chamber variation of measured k_Q factors. Significant variation of k_Q factors among chambers of the same type could lead to errors if a generalized k_Q factor is used for reference dosimetry. However, most experimental investigations are only able to inspect a few chambers of the same type. In addition, measured k_Q factors have been extensively investigated for only a few

types of ion chamber.

McEwen[34] presented the first investigation on measured k_Q factors for a wide range of cylindrical chamber types (27) in photon beams. Of those chamber types, different sample sizes were available ranging from nine different NE2571 chambers to only one chamber for several other chamber types. The standard uncertainty on measured k_Q factors was 0.3 % for typical chamber types. Of the 27 chamber types investigated by McEwen,[34] 25 overlap with the chamber types investigated with the Monte Carlo simulations of this work. This provides an excellent basis for comparison of measured (chamber-specific) and calculated (general chamber type) k_Q factors. This comparison is presented in chapter 5.

As was indicated previously, plane-parallel chambers were not recommended by dosimetry protocols[10,11] for use in photon beams because (a) a lack of data made it impossible to calculate k_Q factors with the method used in dosimetry protocols; and, (b) there was evidence for large variation (3.6 %) of measured P_{wall} values for plane-parallel chambers of the same type in ^{60}Co,[36] which would result in significant errors if generic k_Q factors were provided. Missing data is no longer a problem; it is now possible to provide direct calculations of k_Q factors with the method presented in section 2.2. Recent evidence[54,55] indicates reduced chamber-to-chamber variation of measured k_Q factors for plane-parallel chambers in photon beams, at least for a few chamber types. The goals of the present experimental investigation are to determine measured k_Q factors for several plane-parallel chamber types in photon beams with methods similar to McEwen[34] and, over the course of this study, to characterize the behavior of these chamber types in terms of long-term stability and chamber-to-chamber variability.

Method of indirect calibration: The direct calibration of ion chambers against primary standards for absorbed dose is impractical for routine calibrations. For

this reason, laboratory maintained reference chambers with well established levels of stability are normally used for routine calibrations of other 'user' ion chambers. These reference chambers are directly calibrated periodically against the primary standard for absorbed dose. The Canadian primary standard for absorbed dose is a water calorimeter, located and operated at NRC. The basic principle behind water calorimetry is the measurement of absorbed dose from radiation-induced temperature rise. Ross *et al.*[56] describe the NRC water calorimeter in detail while McEwen and Ross[57] and Seuntjens *et al.*[18] discuss the direct calibration of ion chambers against the calorimeter. The relative standard uncertainty in the absorbed dose to water calibration coefficient is 0.34 % when an ion chamber is calibrated directly against the primary standard.[57] The correlation of some uncertainties results in a reduced standard uncertainty on measured k_Q factors of 0.27 % for well-behaved ion chambers.

With $N_{D,w,ref}$ coefficients known for secondary standard reference chambers, absorbed dose calibration coefficients can be obtained indirectly for plane-parallel ('user') chambers with

$$N_{D,w,pp} = N_{D,w,ref} \frac{M_{ref}}{M_{pp}}, \tag{2.1}$$

where the fully corrected chamber readings (applying the corrections to the raw reading in equation 1.10 [p. 9], discussed below) are obtained close in time for reference and plane-parallel chambers. With calibrations in a cobalt-60 reference field and high-energy linear accelerator beams, measured k_Q factors are realized (from equation 1.9) with

$$k_Q = \frac{N^Q_{D,w}}{N^{Co}_{D,w}}. \tag{2.2}$$

The accuracy of the calibration of 'user' chambers ultimately rests on the calibration of the reference chambers, which consist of a set of five NE2571 chambers. The two main issues that deserve specific attention are (a) k_Q factors for all cham-

bers depend on the original comparison of the NE2571 chambers to water calorimetry measurements meaning that the accuracy of NE2571 k_Q factors is crucial; and, (b) the accuracy of measurements for all chambers obtained through comparison to reference chambers depend on the stability of reference chambers over the short time period between measurements made for calibrations and the longer time period between calorimetry measurements. In paper III these two issues were reviewed in detail to establish confidence in the indirect method of calibration.

Chamber types and set-up: Absorbed dose calibration coefficients are obtained at NRC in the cobalt-60 reference field and beams from the Elekta *Precise* clinical linear accelerator with nominal energies of 6, 10 and 25 MV. Measurements of chamber readings are obtained with chambers centred on the axis of the beam at the reference depth in a 30×30×30 cm^3 water phantom. A horizontal geometry is used allowing accurate positioning of the chamber to 0.1 mm[58] along the beam axis. The field size is set to 10×10 cm^2 at the thin entrance window of the phantom with an SSD of 100 cm. The thickness of the PMMA entrance window is accounted for when positioning chambers along the beam axis. In cobalt-60, the calibration depth is 5.3 g/cm^2 whereas in linac beams it is 10.2 g/cm^2. Cylindrical reference chambers are positioned with the center of the chamber at the reference depth. Plane-parallel chambers are positioned with the front of the cavity at the reference depth, taking into account the chamber window with water-equivalent scaling of the physical thickness. This is different from the geometry modelled for Monte Carlo simulations where the front of the cavity is at the reference depth without water-equivalent scaling of the front window. To compare consistently, the measured results are adjusted using the slopes of the depth-dose curves resulting in a correction of up to 0.2 %.

The plane-parallel chambers investigated include (number of chambers of each type in parentheses): PTW Roos (2), Markus (2) and Advanced Markus (2), Exradin

A11 (2, one of which was obtained before the manufacturer made major changes in chamber construction), A10 (1), P11TW (1) and P11 (1), and IBA NACP-02 (4, two obtained when Scanditronix was manufacturing these chambers), PPC-05 (2) and PPC-40 (2).

Irradiation delivery: Ion chambers are preirradiated to 1000 MU in linac beams for stabilization of the chamber reading. Dose delivery is monitored with the internal linac monitor chamber and an external thin-windowed transmission chamber mounted on the linac. These allow the transfer of the absorbed dose calibration coefficients from reference chambers to the 'user' ion chamber being calibrated. Following preirradiation, a series of seven 100 MU irradiations are delivered. No trend is ever observed in the chamber reading among the seven irradiations. The standard deviations of the chamber readings are used for analysis of the standard uncertainty from the reproducibility of the chamber reading (generally less than 0.05 %). The standard deviations of the monitor chamber readings are used to estimate the standard uncertainty from the transfer of the monitor calibration (less than 0.07 %). The drift of reference chamber readings compared to monitor chambers from the beginning to the end of calibrations is generally much better than 0.1 %.

For calibration in the cobalt-60 reference field, measurements of the charge collected by the chambers are taken during continuous dose delivery. No preirradiation is performed in order to investigate chamber stabilization, which can be significant[59] especially in cobalt-60, and is a good indicator of the behavior of a given chamber.[34] Charge is collected for 30 second periods typically for a total of 13.5 minutes. The average of the last seven readings is used for calibration.

Corrections to the raw reading: Corrections for various physical effects are required in equation 1.10 (p. 9) to obtain the fully corrected chamber reading. In most cases, these corrections are obtained following the recommendations of the TG-

51 protocol.[10]

The correction P_{TP} corrects for variations in temperature and pressure. Readings of pressure and temperature are made during irradiations of each chamber to correct the reading to standard environmental conditions ($T_0 = 22.0°$C, P_0=1 atm or 101.33 kPa) with

$$P_{TP} = \frac{273.2 + T}{273.2 + 22.0} \times \frac{101.33}{P}. \tag{2.3}$$

Variations in temperature and pressure introduce a small, differential effect when comparing chamber readings over the short time period between calibrations. The correction factor is applied regardless.

The correction P_{leak} corrects for leakage of signal in the absence of radiation. Leakage currents are measured for each chamber for at least 30 seconds following irradiation to investigate any effect from radiation-induced leakage.[60] For most chambers, leakage contributes less than 0.01 % to the signal measured during irradiation so no leakage correction is applied. However, for some chambers significant leakage currents are measured that appear to depend on environmental conditions (humidity levels), indicating problems with those chambers as discussed further in chapter 3.

The recombination correction, P_{ion}, accounts for the lack of complete charge collection due to ion recombination. Ion recombination includes effects from ion diffusion, initial recombination (the process of ions from the same track combining) and general recombination (combination of ions from different tracks). A plot of 1/reading vs. 1/applied voltage (known as a Jaffé plot) at a given dose per pulse, D_{pp}, is linear over a range of 'safe' operating voltages, limited such that charge multiplication does not occur. The ratio of the intercept of this plot, obtained through extrapolation to infinite voltage, to the value of 1/reading at the operating voltage gives a measure of the total ion recombination correction at a given D_{pp}.[61] The recombination correc-

tion is known to be a linear function of dose per pulse.[62,63] The component of initial recombination is independent of D_{pp} while the component of general recombination depends on D_{pp}. Therefore, in the formalism of Burns and McEwen,[61] the linear function of the total ion recombination correction vs. D_{pp} is parameterized with

$$P_{ion} = 1 + (\gamma + \delta D_{pp})/V, \tag{2.4}$$

where γ and δ are related to initial and general recombination, respectively, and V is the polarizing voltage.

TG-51[10] recommends a two-voltage method to obtain P_{ion} in the clinical beam of interest, which is a simplification to using a Jaffé plot at the specific D_{pp} of interest. In this work, the more robust procedure used in previous publications[61,64] is employed where recombination measurements are extracted from Jaffé plots for each chamber for at least three D_{pp} values. Using a wide range of randomized polarizing potentials between 300 and 30 V, a Jaffé plot (1/I vs. 1/V) is made. The maximum operating voltage is determined through observation of the range of voltages that result in linear behavior on the plot and is subsequently used for calibration measurements. The recombination correction at a given D_{pp} is then determined through extrapolation to infinite voltage. Normally, it is assumed that the correction for initial recombination is small (<0.1 %) for continuous radiation (D_{pp}=0 Gy) such as that from a cobalt-60 source and therefore not corrected. However, components of initial recombination of up to 0.5 % are observed in this work from measurements in pulsed beams. For this reason, recombination measurements are also performed in cobalt-60 for comparison. It is difficult to separate the effects of initial and general recombination in cobalt-60 because D_{pp} cannot be varied. However, using these results to calculate P_{ion} from 1/I vs. $1/V^2$ (general recombination is predicted by theory[62,65] to depend on $1/V^2$)

in cobalt-60 indicates that general recombination contributes effects less than 0.1 % for almost all chambers in continuous beams.

The polarity correction factor, P_{pol}, is determined by the application of voltages of opposing polarities. This effect is thought to arise from radiation interactions in the collecting electrode of the ion chamber (Compton current), which if not balanced, can add or subtract from the measured signal or from extracameral current caused by ionizations outside of the defined collecting volume[3] or in an electron beam by a net deposition of charge by electrons stopping in the collector. The recommendation of TG-51[10] is used here to obtain the polarity correction with

$$P_{pol} = \left| \frac{M^+_{raw} - M^-_{raw}}{2M_{raw}} \right|, \tag{2.5}$$

where M^+_{raw} is the uncorrected reading of the chamber when collecting positive charge (negative polarizing potential), M^-_{raw} is that when collecting negative charge and M_{raw} is the uncorrected reading corresponding to the sign of charge collected for calibration measurements (M^+_{raw} at NRC for these measurements). This equation indicates that the mean of values obtained when collecting opposite charge should be taken as the 'true' reading.

The electrometer correction factor, P_{elec}, is required to convert the ion chamber reading to true Coloumbs if the electrometer and ion chamber are calibrated separately. Chambers are calibrated together with computer controlled Keithley 6517A electrometers such that no electrometer correction is required.

The correction for radial intensity variations, P_{rp}, required by the addendum[12] to the AAPM's TG-51 protocol is obtained by measuring the 2-D beam profile at the reference depth with a diode detector (e.g., a PTW SFD, 0.03 mm^3) scanned in directions perpendicular to the beam axis in steps of 0.3 cm in a random order. Again,

this is a differential effect correcting for field flatness for chambers with different dimensions and results in a correction of up to 0.4 % but usually much less. The overall effect for the Farmer-type chamber is up to 0.5 % in a 10 MV photon beam, whereas for the smallest plane-parallel chambers with radii ∼3 mm, the effect is only 0.1 %.

2.2 Monte Carlo calculations of k_Q factors

Equation for calculated k_Q factors: Combining equations 1.1 (p. 3) and 1.9 (p. 7), one obtains

$$k_Q = \left(\frac{D_w}{D_{ch}}\right)^Q_{Co}, \tag{2.6}$$

where k_Q is determined at the reference depth through the ratio of the absorbed dose to water, D_w, in the absence of the chamber, to the absorbed dose to the air in an ion chamber, D_{ch}, with the notation outside of the parentheses indicating that the ratio of D_w/D_{ch} is made in a high-energy beam relative to that in a cobalt-60 beam. Equation 2.6 requires the assumption made in current dosimetry protocols that $(W/e)_{air}$ remain constant with beam energy and this is a topic of major discussion in chapter 5. All of the required quantities in equation 2.6 can be calculated accurately using Monte Carlo simulations to obtain direct calculations of k_Q factors. This approach is used in papers I, IV, VI and VII of this work. It was also used in other recent publications[26,31,66–68] for only a few chamber types and sometimes with high values of statistical uncertainties (0.5-1.0 %).

General simulation geometry: All quantities are calculated in a 30×30×30 cm^3 water phantom. Monte Carlo calculations of the response or absorbed dose to the air in an ion chamber averaged over the active cavity volume, D_{ch}, are performed with the `EGSnrc`[45,46] `egs_chamber` user-code of Wulff *et al.*[49] The use of `egs_chamber` allows

faithful modelling of ion chambers in detail with the egs++ geometry package.[50] The ion chamber models are discussed below. Ion chamber simulations are performed at the point of measurement in water in photon beams and as a function of depth in water close to the phantom surface to a depth well into the bremsstrahlung tail in electron beams with steps between 0.05 and 0.2 cm depending on beam energy.

In photon beams, the quantities required in equation 2.6 are calculated at the point of measurement. For cobalt-60 calculations, the point of measurement is on the central axis of the beam and the reference depth is at a depth of 5 cm (the depth of calibration at calibration laboratories). In all other photon beams, the reference depth is at 10 cm. The absorbed dose to water in the absence of the chamber is calculated with the egs_chamber user-code[49] for a disk of water with a thickness of 0.025 cm and a radius of 1 cm centered on the point of measurement.

In electron beams, the absorbed dose to water is calculated as a function of depth in water along the central axis of the beam with the egs_chamber user-code.[49] Dose is scored in individual disks of water with 0.5 cm radii and thicknesses between 0.05 cm in the lowest-energy beams and 0.2 cm in the highest-energy beams. Using egs_chamber calculations of D_w and D_{ch} as a function of depth in electron beams allows: (a) extraction of k_Q factors at the reference depth; (b) linear fitting of D_w/D_{ch} as a function of depth close to the reference depth to reduce statistical fluctuations in k_Q factors; (c) the study of gradient effects; (d) investigation of the conversion of I_{50} obtained from chamber simulations to R_{50} from depth-dose calculations; and, (e) study of the overall ion chamber correction and its variation with depth. Topics (a)-(d) are discussed in chapter 6 while (e) is left for appendix C.

EGSnrc transport parameters and variance reduction: EGSnrc[45,46] Monte Carlo transport parameters are set to their default values except for the use of xcom photon cross sections[69] and NIST bremsstrahlung cross sections,[70,71] which are the

most accurate available compilations of cross sections. The default Monte Carlo transport parameters are specifically selected because they allow an efficient, accurate simulation in the energy range of interest. However, Wulff *et al.*[72] performed calculations after systematically changing each of the `EGSnrc` transport parameters to their most accurate settings (at the cost of increased computing time) and the effects on calculated k_Q factors were less than 0.1 %. In this work, electron and photon cut-off energies (the particle energy at which the code stops tracking the particle with the energy deposited locally) and particle production thresholds (the energy a particle must have to generate a secondary particle) are set to 521 and 10 keV, respectively. However, several test calculations are performed with 512 and 1 keV energy cut-offs and thresholds. Differences in results are less than 0.1 % compared to using higher values in most cases.

Calculation efficiency is increased using several variance reduction techniques:
Photon cross section enhancement[49] - photon interaction cross sections are increased in a region surrounding the geometry of interest with weights of the resulting secondary particles adjusted such that results are not biased. Since the volume of typical ion chambers is small compared to the mean free path of photons with energies in the range of interest, increasing the probability for photon interactions around the chamber cavity greatly reduces computing time for photon beam calculations without biasing the results.
Electron range-based Russian Roulette[49] - if the predicted range of an electron located outside of a user-specified geometry close to the region of interest is less than the distance to that geometry, the electron can either survive and continue to be tracked or have its energy deposited locally with given probabilities. Efficiency is increased by terminating electron histories if it is unlikely that the electron will ever reach the region of interest. Again, the adjustment of particle weights assures that

results are not biased.

Intermediate phase-space storage[49,73] - the phase space of a particle - e.g., type, energy, position, direction - is stored at the boundary of an artificial geometry and used as a source for subsequent calculations. This is useful when only a small part of the geometry changes from simulation to simulation as in the calculation of ion chamber response as a function of depth in water - most of the geometry (the phantom outside of the central axis) remains unchanged while the ion chamber is translated through a small region along the central axis.

Correlated sampling[30,49,74] - similar to intermediate phase-space storage but, when calculating dose ratios, the correlations in the individual doses are used to decrease the statistical uncertainty on the dose ratio. This technique is especially useful for the calculation of individual correction factors (a high degree of correlation exists between the individual geometries) through equation 1.6 (p. 6), which are sometimes required in this work to compare to other publications.

Ion chamber models: Ion chambers are modelled according to information from manufacturers' user's manuals, catalogs or brochures, insight from relevant publications or specifications from blueprints or drawings from the manufacturer, if available. Calculations for k_Q factors in photon beams are performed with 33 cylindrical ionization chamber models. These models are described in technical report I. Cylindrical chambers are modelled with their central axis perpendicular to the axis of the incident beam, centred on the point of measurement. A subset of the same chambers, including only those considered reference-class detectors,[34] are used for calculations in electron beams. Specifications for the cylindrical ion chamber models are given in table 2.1. For chambers that are not inherently water-proof, the model includes a 1 mm PMMA sleeve since this is required for calibration and clinical measurements in water and, as noted above, affects k_Q factors by up to 0.3 %.

Table 2.1: The specifications of the cylindrical ionization chamber models used. The materials are air-equivalent plastic (C552), tissue-equivalent plastic (A150), silver plated copper covered steel (SPC), polymethylmethacrylate (PMMA), graphite (Gr), aluminum (Al) and polyoxymethylene (POM). Chambers with similar characteristics are divided into groups referenced by letters a to i, given here. Chambers considered to be reference-class detectors[34] are in italics. Modified from paper I.

Chamber (Group, V(cm^3))	Wall		Electrode			Active Cavity		Water-proof
	Material	Thickness (mm)	Material	Radius (mm)	Length (mm)	Radius (mm)	Length (mm)	
Exradin								
A12 (a, 0.65)	C552	0.5	C552	0.5	21.6	3.05	24.8	Y
A19 (a, 0.62)	C552	0.5	C552	0.5	21.6	3.05	25.0	Y
A2 (a, 0.54)	C552	1.0	C552	0.5	8.4	4.7	12.0	Y
T2 (b, 0.54)	A150	1.0	A150	0.5	8.4	4.7	12.0	Y
A12S (a, 0.25)	C552	0.5	C552	0.5	7.4	3.05	10.6	Y
A18 (a, 0.125)	C552	1.0	C552	0.5	5.9	2.45	8.3	Y
A1 (a, 0.057)	C552	1.0	C552	0.5	4.4	2.0	6.0	Y
T1 (b, 0.057)	A150	1.0	A150	0.5	4.4	2.0	6.0	Y
A1SL (a, 0.057)	C552	1.1	C552	0.5	4,4	2.025	6.0	Y
A14 (g, 0.016)	C552	1.0	SPC	0.165	1.5	2.0	2.0	Y
T14 (h, 0.016)	A150	1.0	SPC	0.165	1.5	2.0	2.0	Y
A14SL (g, 0.016)	C552	1.1	SPC	0.165	1.5	2.025	2.0	Y
A16 (g, 0.007)	C552	0.5	SPC	0.165	1.3	1.2	2.4	Y
PTW								
30010 (e, 0.6)	PMMA/Gr	0.335/0.09	Al	0.55	20.4	3.05	23.4	N
30011 (d, 0.6)	Gr	0.425	Gr	0.5	20.4	3.05	23.4	N
30012 (c, 0.6)	Gr	0.425	Al	0.55	20.4	3.05	23.4	N
30013 (e, 0.6)	PMMA/Gr	0.335/0.09	Al	0.55	20.5	3.05	23.4	Y
31013 (e, 0.3)	PMMA/Gr	0.55/0.15	Al	0.45	14.25	2.75	16.25	Y
31010 (e, 0.125)	PMMA/Gr	0.55/0.15	Al	0.55	6.0	2.75	6.5	Y
31016 (i, 0.016)	PMMA/Gr	0.57/0.09	Al	0.09	1.45	1.45	2.9	Y
31014 (i, 0.015)	PMMA/Gr	0.57/0.09	Al	0.09	4.0	1.0	5.0	Y
IBA								
FC65-G (c, 0.65)	Gr	0.43	Al	0.5	21.3	3.1	23.1	Y
FC65-P (f, 0.65)	POM	0.4	Al	0.5	21.3	3.1	23.1	Y
CC25 (a, 0.25)	C552	0.4	C552	0.5	7.6	3.0	10.0	Y
FC23-C (a, 0.23)	C552	0.4	C552	0.5	7.0	3.1	8.8	Y
CC13 (a, 0.13)	C552	0.4	C552	0.5	3.2	3.0	5.8	Y
CC08 (a, 0.08)	C552	0.4	C552	0.5	1.4	3.0	4.0	Y
CC04 (a, 0.04)	C552	0.4	C552	0.5	2.5	2.0	3.6	Y
CC01 (g, 0.01)	C552	0.5	Steel	0.175	2.7	1.0	3.6	Y
Other								
NE2581 (b, 0.6)	A150	0.36	A150	1.5	20.5	3.15	24.0	N
NE2571 (c, 0.6)	Gr	0.36	Al	0.5	20.5	3.14	24.0	N
NE2611/2561 (c, 0.3)	Gr	0.53	Al	1.0*	6.5	3.7	9.0	N
Capintec								
PR06C/G (a, 0.65)	C552	0.28	C552	0.8	22.0	3.22	24.0	N

* The NE2561 has a hollow electrode with a 0.2 mm thick aluminum shell. The air inside the aluminum layer is not considered part of the active cavity.

As a result of availability, all of the Exradin chambers as well as the IBA CC01 chamber are modelled from blueprint specifications. In some cases, results for k_Q factors are calculated with simplified models for comparison. Figure 2.1 shows three different models of the Exradin A12 chamber. Comparing k_Q factors in photon beams using these three models results in differences less than 0.2 % (with 0.1 % statistical

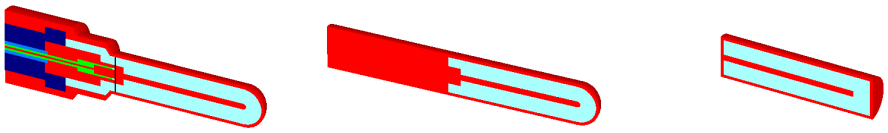

(a) (b) (c)

Figure 2.1: Three models of the Exradin A12 ionization chamber. (a) blueprint model; the solid line shows where the active cavity begins; (b) user manual, with a spherical top and a 2 cm long stem; (c) user manual, purely cylindrical geometry. From paper I.

uncertainties). This is also the level of variation observed when comparing calculations with simplified and detailed models of the Exradin A18, A2 and IBA CC01 chambers. In the worst case, the difference between k_Q factors using simplified and detailed models is 0.4 % for the Exradin A19 chamber. Tantot and Seuntjens[67] also investigated the use of simplified models and differences outside of statistical uncertainties were not detected when all of the stem materials in the Exradin A12 chamber were changed to C552.

For other cylindrical chambers, blueprints were not made available to us. The NE2571 chamber model is based on that used by La Russa *et al.*,[75] which is close to the original chamber design by Aird and Farmer.[2] The PTW Farmer-type chamber models use specifications from the PTW Product Catalog. The composition of the PTW chamber stems are unknown so they are based on the stem of the NE2571 model used here. The PTW 31010 chamber is modelled from information given by Wulff *et al.*[31] IBA chambers are modelled from information given in the IBA Detector Brochure. Again, the composition of the stems used by IBA chambers are not known so solid 2 cm C552 stems are used, justified by the sensitivity analysis reported above for the Exradin chambers.

In order to explain differences between Monte Carlo calculated k_Q factors and those provided in protocols and to analyze systematic uncertainties in calculated k_Q factors, each chamber in table 2.1 was loosely sorted into one of nine groups for paper I. The groups are referenced by letters a-i (given in table 2.1) with chambers grouped by wall material, central electrode material, and chamber volume. Chambers are classified as those with (a) C552 walls and central electrodes; (b) A150 walls and central electrodes; (c) graphite walls and aluminum central electrodes; (d) graphite walls and graphite central electrodes; (e) PMMA and graphite walls and aluminum central electrodes; (f) polyoxymethylene (POM, trade name Delrin) walls and aluminum central electrodes; (g) small volume (<0.02 cm^3), C552 walls and electrodes made from high-Z materials (silver plated copper covered steel [SPC] or steel); (h) small volume (<0.02 cm^3), A150 walls and SPC electrodes; and, (i) small volume (<0.02 cm^3), PMMA and graphite walls and aluminum electrodes.

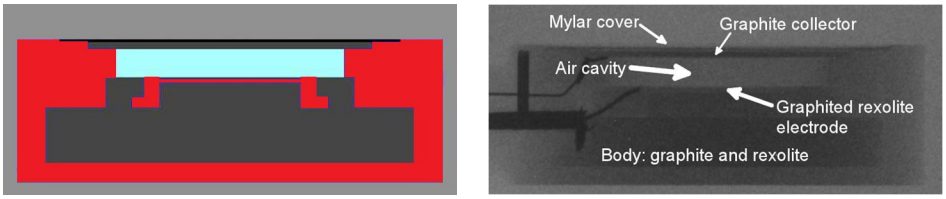

(a) (b)

Figure 2.2: The IBA NACP-02 geometry. Panel (a) is the Monte Carlo model of the chamber while panel (b) is a radiograph of the chamber taken for aid with modelling and to ensure no significant differences between design and manufacture. Major components of the ion chamber are labeled in the radiograph of panel (b). From paper IV.

All of the plane-parallel chambers investigated are modelled using blueprints or drawings from ion chamber manufacturers and insights from the literature. An example of the plane-parallel chamber models used here is shown with the IBA NACP-02 model in figure 2.2 (a) with a radiograph of the same chamber in figure 2.2 (b) to show similarities between the model used for Monte Carlo simulations and the real

Table 2.2: Major dimensions and materials for the plane-parallel ion chambers investigated. Materials are MYLAR, graphite (Gr), rexolite (cross-linked polystyrene, Rex), polyetheretherketone (PEEK), air-equivalent plastic (C552), polyoxymethylene (POM, trade name Delrin), polystyrene-equivalent plastic (D400), Kapton (Ka) and polyethylene (PE). The abbreviation Gr'd refers to a graphited material where a thin layer of graphite is applied to the material in question. Chambers indicated by an asterisk require a water-proofing cap. Modified from paper IV.

Chamber	Volume (cm^3)	Cavity		Window		Wall Materials	Collector
		Depth (mm)	Radius (mm)	Material	Thickness (mm)		
Exradin							
A11	0.622	2	9.9 (15.7)	C552	1	C552 POM	C552
P11	0.622	2	9.9 (15.7)	D400	1	D400 POM	D400
P11TW*	0.920	3	9.9 (14.3)	Ka	0.03	D400 POM	D400
A10*	0.050	2	2.8 (7.3)	Ka	0.03	C552 POM	C552
IBA							
NACP-02	0.157	2	5 (8)	MYLAR Gr	0.17 0.5	Gr Rex	Gr'd Rex
PPC-05	0.039	0.5	5 (8.5)	C552	1	C552 MYLAR	Gr'd PEEK
PPC-40	0.402	2	8 (12)	Gr'd PMMA	1	PMMA	Gr'd PMMA
PTW							
Roos	0.384	2	7.8 (12)	Gr'd PMMA	1.1	PMMA	Gr'd PMMA
Markus*	0.044	2	2.7 (3)	PE	0.03	PMMA	Gr'd PMMA
Adv. Mark.*	0.020	1	2.5 (4.5)	PE	0.03	PMMA	Gr'd PMMA

ion chamber. Plane-parallel chamber specifications are provided in table 2.2. Plane-parallel chambers are modelled in photon beams with the front of the cavity (i.e., the inside of the front window determined with the physical thickness of the window) at the point of measurement, with the axis of the chamber parallel to and centred on the axis of the incident beam. In electron beams, all of the plane-parallel chambers used for photon beam calculations are investigated as a function of depth in water.

Radiation source models: All sources in this work are modelled at a source-to-surface distance (SSD) of 100 cm collimated to a field size of 10×10 cm^2 at the surface

of the phantom. The majority of photon beam sources are modelled as collimated point sources using realistic photon beam spectra for filtered, clinical beams. Table 2.3 provides the photon beams used for the bulk of this work along with the provenance of photon spectra and the beam quality specifiers: the photon component of the percentage depth-dose at 10 cm, $\%dd(10)_x$, and the tissue-phantom ratio at 20 and 10 cm, TPR^{20}_{10}. For the determination of $\%dd(10)_x$ in photon beams, the absorbed dose to water is calculated with `BEAMnrc`[51,52] along the central axis of the beam in individual disks of water with 0.2 cm thicknesses and 0.5 cm radii. An example of the determination of $\%dd(10)_x$ from these depth-dose calculations was shown in figure 1.2 (a) on p. 8. The relative uncertainty of the $\%dd(10)_x$ calculations is 0.1%. Source models from photon beam spectra do not include electron contamination so no conversion from $\%dd(10)$ to $\%dd(10)_x$ is required. The TPR^{20}_{10} is obtained from $\%dd(10)_x$ calculations with the formula of Kalach and Rogers[20] for heavily filtered beams.

Table 2.3: Photon beams and beam quality specifiers. Modified from paper I.

Beam	Nominal Energy (MV)	$\%dd(10)_x$	TPR^{20}_{10}
^{60}Co Eldorado 6[76]	-	58.4	0.569
Siemens KD[77]	6	67.0	0.671
	18	77.7	0.762
Elekta SL25[77]	6	67.3	0.672
	25	82.8	0.791
Varian Clinac[77]	4	62.7	0.623
	6	66.5	0.666
	10	73.8	0.734
	15	77.8	0.763
	18	81.5	0.785
Varian Clinac[78]	24	86.1	0.805

Electron beam sources are modelled with realistic `BEAMnrc`[51,52] accelerator simulations for input as a shared library source to the `egs_chamber` simulations described above. These accelerator simulations use energy cut-offs and production thresholds

of 700 and 10 keV for electrons and photons, respectively. The `BEAMnrc` accelerator models used here were created for other investigations[51,79,80] and paper VI of this work. In addition, modifications to the Elekta *Precise* beams are made to greatly affect the shape of calculated depth-dose curves for sensitivity analysis of resulting k_Q factors. This is done by varying the incident electron energy spread from about 10 to 30 % and by removing the last layer of the applicator.

Less realistic beams are also used for electron beam calculations including those modelled as collimated point sources using electron beam spectra from Ding and Rogers[79] or using monoenergetic electrons with incident energies of 4, 8 and 15 MeV.

Table 2.4 provides the electron beams investigated along with the electron beam quality specifier, R_{50}, and the percentage bremsstrahlung tail - a measure of photon contamination from interactions in the accelerator head and, less importantly, in the phantom. Calculations of R_{50} use the `egs_chamber`[49] simulations of absorbed dose to water as a function of depth described above. An example of the calculation of R_{50} was presented in figure 1.2 (b) on p. 8. The R_{50} values are generally within 1 mm of the calculated values of Ding and Rogers[79] despite the change from `EGS4` to `EGSnrc`. Calculations of R_{50} are unchanged in the Elekta *Precise* 4 and 18 MeV beams within 0.02 mm after varying the mean excitation energy used to calculate the stopping power of water by 1.5 % (the k=1 uncertainty estimate on I from ICRU-37[81]). Estimating the systematic uncertainty in R_{50} is difficult because Monte Carlo transport parameters and uncertainties about the incident beam will also have effects but our results indicate that the uncertainties in the R_{50} calculations in table 2.4 from variation of water stopping power are negligible. As for an estimate of the statistical uncertainty in the percentage bremsstrahlung tail, the standard deviation of the % depth-dose values at depths greater than the projected range by 2 cm in the Elekta *Precise* 22 MeV beam is 0.2 % of the maximum dose and much lower for

Table 2.4: Characteristics of the electron beam models used for source simulation. The source of the `BEAMnrc` accelerator model is indicated beside the accelerator name. Electron beam spectra from Ding *et al.*[79] are used to model a 10×10 cm^2 point source incident on the surface of the phantom. In some cases denoted by an ^{R} or ^{N} beside R_{50}, sources are only used for chamber simulations for one of the Roos or NE2571 chamber. Beams that are considered to be clinical accelerators are in italics. Modified from paper VI.

Accelerator	Source simulation: Nominal Energy (MeV)	BEAMnrc accelerator models		Electron beam spectra	
		R_{50} (cm)	Brem. Tail % of D_{max}	R_{50} (cm)	Brem. Tail % of D_{max}
Elekta Precise	4	1.79	0.36	1.79	0.06
	8	3.29	1.18	3.28^R	0.21
	12	4.93	2.03	4.91^R	0.43
	18	7.04	3.00	6.99^R	0.67
	22	8.73	4.94	8.58^R	0.99
Modified Precise (σ_{E_0}=30%)	8	3.36	1.25		
	18	7.13	3.16		
Modified Precise (applicator)	8	3.31	1.13		
	18	7.08	2.76		
Elekta Precise (only electrons)	4	1.79^R	0.08		
	18	7.00^R	0.69		
	22	8.63	1.04		
Varian Clinac 2100C[51]	6	2.64	0.99	2.64	0.13
	9	3.99^N	2.17	4.02	0.31
	12	5.20^N	2.83	5.19	0.48
	15	6.51^N	3.07	6.49	0.57
	18	7.72	3.78	7.72	0.80
Varian Clinac (only electrons)	18	7.64^R	0.75		
Siemens KD2[79]	6			2.31	0.12
	11			4.21	0.34
	21	8.32	4.82	8.23	0.91
AECL Therac-20[51]	6			2.22	0.09
	9	3.44^N	0.38	3.44	0.23
	13			5.18	0.48
	17			6.86	0.64
	20	8.09^N	1.59	8.08	0.89
Elekta SL25	4			1.69	0.05
	8			2.80	0.15
	22			8.79	1.04
Elekta SL75-5	5			2.11	0.09
	10			4.15	0.33
	14			6.03	0.68
	17			6.95	0.64
	20			8.05	0.87
Siemens MD2 (cut-out)[80]	6	2.43^N	0.21		
	11	4.57^N	1.78		
NRC Vickers	10			3.97	0.30
	20			8.24	0.92
Monoenergetic	4			1.55^N	0.04
	8			3.30^N	0.21
	15			6.35^N	0.54

low-energy beams. The source models used here represent a broad range of electron beams including realistic clinical beams as well as a variety of beams that are not typical of modern clinical treatment machines (e.g., AECL *Therac-20* scanned beams, the NRC *Vickers* research accelerator and monoenergetic beams).

The focus in this thesis and paper VI for electron beam calculations is on two of the most widely used chamber types: the PTW Roos plane-parallel chamber and the NE2571 cylindrical chamber. Table 2.4 indicates that not all sources are used for calculations with both chamber types - as insight was gained throughout the project, the use of some of the less realistic sources became meaningless while it was found that some could be used without affecting the accuracy of the simulations. For other chamber types, even fewer sources in table 2.4 are used. These calculations and the rationale for using given sources are presented in paper VII but the majority of these results are not the focus of this thesis.

Systematic uncertainties in calculated k_Q factors: Relative statistical uncertainties on Monte Carlo calculated k_Q factors obtained in this work are less than 0.1 %. As mentioned above, the `EGSnrc` code system has been shown to be accurate within 0.1 % with respect to its own cross sections for calculations of ion chamber response.[48] Aside from these small components of uncertainty, there exist several sources of systematic uncertainty in calculated k_Q factors; material properties used for the simulations such as photon cross sections and electron stopping powers, ion chamber dimensions, the radiation source model and potential variation of $(W/e)_{air}$ with beam quality. In this work, most systematic uncertainties in calculated k_Q factors are investigated by varying individual components of uncertainty within reasonable limits and assessing the resulting effect on k_Q. The exception is the uncertainty introduced by possible variation of $(W/e)_{air}$ with beam quality. In this case, an estimate of the uncertainty in calculated photon beam k_Q factors is established through comparison

of calculated and measured k_Q factors, taking advantage of the fact that experimental results do not require the assumption of constant $(W/e)_{air}$ with beam quality (see chapter 5). For electron beam k_Q calculations, an estimate of the uncertainty from $(W/e)_{air}$ variation is assigned using previous experimental results.[15]

Individual systematic uncertainties on calculated k_Q factors are combined using the equation for combined standard uncertainty from uncorrelated variables,[82]

$$u_{k_Q} = \left[\sum_{i=1}^{n} \left(\frac{\partial k_Q}{\partial x_i} \right)^2 u^2(x_i) \right]^{1/2}, \tag{2.7}$$

where u represents the uncertainty on the input quantity in question. This equation is simplified by approximating $\partial k_Q/\partial x_i$ by $\Delta k_Q/\Delta x_i$. Then the change in calculated k_Q factors, Δk_Q, is calculated when $\Delta x_i = u(x_i)$ such that equation 2.7 becomes

$$u_{k_Q} = \left[\sum_{i=1}^{n} (\Delta k_Q)_i^2 \right]^{1/2}, \tag{2.8}$$

where the combined uncertainty in k_Q is the sum of the squared components of uncertainty in k_Q when the influence quantities are changed by one standard deviation.

For external beam radiation therapy, the energy range of interest and materials considered lead to Compton scattering being the dominant effect for photon interactions, implying that the incoherent photon scattering cross section is most relevant. The uncertainty in incoherent cross sections is estimated to be at the 1-2 % level.[83] To estimate the effect from these uncertainties on calculated k_Q factors, photon cross sections are scaled for each material in the simulated geometry by 1 %. There is, however, some question about whether photon cross sections should be considered correlated or uncorrelated. Photon cross sections could be considered correlated because they are based on the same theoretical model[84] for all low-Z materials. Considering

this, if photon cross sections are incorrect by 1 % for one material, it is likely that similar errors in the same direction will be present for other materials with similar properties, potentially resulting in cancellation of errors on dose ratios. In this work, uncertainties in k_Q calculations from both correlated and uncorrelated photon cross sections are investigated. Uncertainties in k_Q calculations from correlated photon cross sections are studied by varying photon cross sections for all materials by 1 % in the same direction for calculations of the quantities in equation 2.6 (p. 28) in three beam qualities spanning the energy range of interest. The component of uncertainty in k_Q is then given by

$$\Delta k_Q = \left| \left[\left(\frac{D_w}{D_{ch}} \right)^{Q}_{^{60}Co} \right]^{\text{scaled}}_{\text{default}} - 1 \right| \times 100\%. \tag{2.9}$$

Another method of analyzing the sensitivity of k_Q calculations to correlated photon cross sections is to change the Monte Carlo transport options used to simulate Compton scattering. Calculations of k_Q factors are unchanged within 0.1 % when different Compton options are used: bound Compton scattering turned on and radiative Compton corrections off, both options on and both options off. Uncertainties in k_Q calculations from uncorrelated photon cross sections are investigated with equation 2.9 by varying photon cross sections for each material by 1 % in separate simulations. This is done in three beam qualities to obtain Δk_Q when graphite or water cross sections are varied. The resulting Δk_Q is largest in the high-energy beam (likely because the photon spectrum is most different from cobalt-60) so calculations of Δk_Q for all other materials are only performed for this beam. For these calculations, correlated sampling is used to decrease the relative statistical uncertainty on dose ratios but the reader is referred to paper I for details.

The largest source of uncertainty in electron stopping powers is the mean excita-

tion energy, I. The ICRU Report-37[81] provides uncertainties on I-values for common materials. The uncertainty in k_Q calculations from stopping powers is determined with equation 2.9 but instead of scaling photon cross sections, stopping powers are varied by changing I-values according to their one standard deviation limits from ICRU Report-37.[81] The I-values in ICRU Report-37[81] were obtained with independent experiments so stopping powers are considered uncorrelated and I-values are changed for each material in separate simulations to estimate Δk_Q. Uncertainties in stopping powers from density effects may also be present, especially in cobalt-60, but the stopping power variation from this effect is about one seventh compared to that from I-value uncertainty.[85] This is considered negligible and uncertainties in k_Q calculations from these effects are ignored in most cases.

Uncertainties in calculated k_Q factors may stem from the ion chamber models used for simulations. In some cases, simplified models of the chamber stem are used because the real characteristics of the stem are unknown. Uncertainties from these simplifications are investigated by comparing calculations using detailed and simplified models or by changing the stem material (e.g., the stem of a cylindrical chamber is changed from air-equivalent plastic to aluminum to investigate sensitivity of electron beam k_Q factors to the stem model). Manufacturing tolerances could impact the actual thickness of chamber walls or cavity dimensions of real ion chambers. Calculations of k_Q are performed after changing these dimensions within reasonable limits to obtain Δk_Q. The actual variation used to investigate the uncertainty from a given parameter depends on the ion chamber geometry and type, so the details are provided when results are presented in chapters 4 and 6.

There may exist uncertainties in k_Q calculations from the model of the radiation source used for simulations. For photon beams, the use of $\%dd(10)_x$ to specify beam quality has been shown to reduce fluctuations of k_Q factors at the same value

of $\%dd(10)_x$ from accelerators with different properties.[18–21] However, there may be uncertainty from using simplified source models derived from photon spectra to calculate k_Q factors and this is investigated with calculations using `BEAMnrc`[51,52] accelerator models. Photon beam k_Q calculations are also performed for some chambers with spectra for several unfiltered photon beams to investigate sensitivity to beam properties. For electron beam k_Q factors, the situation is more complicated because of the variation of stopping power ratios at the reference depth from the amount of photon contamination in the beam.[23] In chapter 6, it is established that using electron beam spectra to model high-energy electron beams can result in errors of up to 0.5 % in k_Q calculations. In addition, the method for correcting gradient effects is optimized to obtain more accurate k_Q factors from electron beams with different properties. However, no component of uncertainty is assigned in electron beam k_Q factors from the model of the source because realistic `BEAMnrc`[51,52] accelerator models are used for these calculations.

Chapter 3

Measured k_Q factors for plane-parallel chambers in photon beams

In this chapter, the behavior of plane-parallel chambers in photon beams is characterized using measurements to obtain k_Q factors. Systematic uncertainties on measured photon beam absorbed dose calibration coefficients and k_Q factors for these chambers are discussed and the resulting measured k_Q factors are compared to the limited data in the literature.

3.1 Chamber behavior and corrections to the reading

Chamber stabilization: In the cobalt-60 reference field, the readings for most of the chambers investigated settled to within 0.05 % of the mean of the last seven readings within six minutes, consistent with the stabilization results observed by McCaffrey *et al.*[59] for well-guarded cylindrical chambers. For two comparatively smaller volume chamber types, the PTW Markus and IBA PPC-05, stabilization of the reading took up to 15 minutes. Longer settling times for small volume cylindrical chambers compared to their larger volume counterparts were also observed by McEwen.[34] For linac beam calibrations, the chambers are preirradiated to 1000 MU without measuring chamber stabilization. For polarity and recombination measurements, readings are taken consecutively in linac beams without preirradiation after changing voltage and

typically settled in much less than three minutes in these high dose rate beams.

Leakage currents: When initial calibration measurements were made in winter, the relative humidity was low (25 %) and leakage typically contributed less than 0.01 % (maximum 0.05 %) to the chamber reading taken during irradiation. During follow-up measurements made to investigate long-term stability in summer, when relative humidity was higher (60 %), much larger leakage currents were measured, sometimes 10-20 times that measured in winter. To investigate this unexpected behavior, an environmental enclosure was used to determine that the leakage was directly affected by relative humidity levels for some chambers, but for other chambers leakage behavior was not so predictable, exhibiting short-term fluctuations. The stability of plane-parallel chamber calibrations also seemed to be more sensitive to relative humidity levels than that of cylindrical chambers (see section 3.2).

Polarity effects: In paper IV, polarity effects for plane-parallel chambers in photon beams result in a correction of less than 0.3 % for all chambers investigated and less than 0.1 % for most chambers. The standard deviation of the polarity corrections for different ion chambers of the same type determined in different linac beam energies (the polarity correction has been shown[18,34] to be independent of energy in photon beams) and different experimental set-ups (to change the dose per pulse for recombination measurements) is less than 0.08 % for all chambers investigated. This is assigned as the uncertainty in absorbed dose calibration coefficients from polarity effects. The polarity corrections observed here for NACP-02 and PTW Roos chambers are in reasonable agreement with those determined by McEwen *et al.*[86] However, the small differences between the polarity corrections among the two studies could be due to chamber-to-chamber variability indicating the importance of measuring the polarity correction for the specific chamber under investigation.

Ion recombination: Figure 3.1 shows a Jaffé plot (1/reading vs. 1/applied voltage)

for a PTW Advanced Markus chamber when the dose per pulse at the point of measurement from the pulsed linac beam is 0.024 cGy (500 MU/min nominal dose rate, 200 Hz pulse repetition frequency). The linear region is shown which determines the maximum safe operating voltage of 100 V before nonlinear behavior is observed on the Jaffé plot. This safe voltage is then used for calibration measurements. For many of the plane-parallel chambers investigated here, the maximum safe applied voltage is between 100-200 V, lower than that for cylindrical chambers. The recombination correction determined at D_{pp}=0.024 cGy for the Advanced Markus chamber from figure 3.1 is 1.0042, determined as the ratio of 1/M at the operating voltage to the value obtained through extrapolation to infinite voltage on the Jaffé plot. Comparison of the ion recombination correction obtained from Jaffé plots to that determined with the two-voltage method recommended by TG-51,[10] typically with applied voltages of 100 and 33 V, is used to estimate the uncertainty in chamber calibrations from the recombination correction.

For all chambers, P_{ion} is determined for at least three D_{pp} values. Figure 3.2 shows P_{ion} as a function of D_{pp} when collecting positive charge with an applied voltage of 100 V for all plane-parallel chambers investigated. The linear behavior of the ion recombination with D_{pp} is consistent with theoretical predictions,[61–63] which also predict that the slopes of the linear fits are dependent on plate separation because of variations in electric field when the same voltage is applied. These slopes are predicted to increase with the square of plate separation.[61] Most chambers use plates separated by 2 mm explaining why the slopes of the linear fits are similar for several chambers in figure 3.2. However, the Exradin P11TW uses a 3 mm plate separation resulting in a much steeper gradient in figure 3.2 while the PTW Advanced Markus and IBA PPC-05 use smaller plate separations (1 mm and 0.5 mm, respectively) and decreased gradients are observed in figure 3.2.

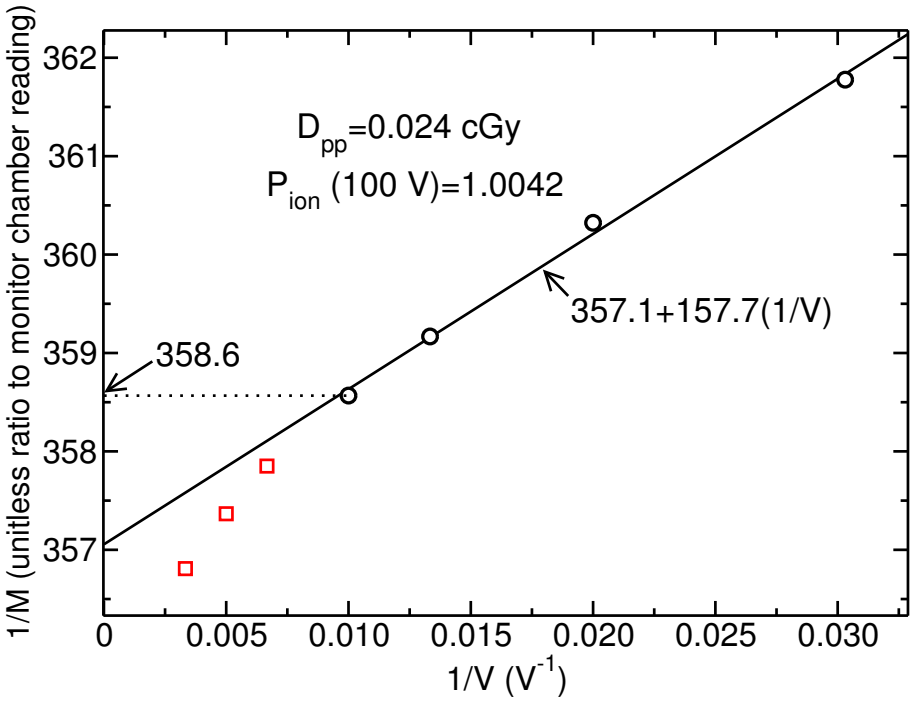

Figure 3.1: An example Jaffé plot for an Advanced Markus chamber showing the region of linear behavior that allows the selection of the maximum safe operating voltage (100 V) and determination of the ion recombination correction factor.

Figure 3.3 shows ion recombination corrections as a function of D_{pp} for selected chambers when collecting opposite charge. Most chambers investigated behaved predictably, giving similar P_{ion} vs. D_{pp} gradients when collecting opposite charge as for the NACP-02 shown in figure 3.3. The difference in the intercepts obtained when collecting opposite charge is consistent with the polarity correction. Strange recombination behavior is observed for two chamber types, the PTW Advanced Markus and the IBA PPC-05. Different gradients are observed for both chambers when reversed voltages are applied and, for the IBA PPC-05 when collecting negative charge, the recombination correction *decreases* as a function of D_{pp} anomalous to theoretic predictions.[61–63] McEwen[34] also observed strange recombination behavior for small volume cylindrical chambers. Both of the chamber types investigated here that exhibit this type of behavior use comparatively small active volumes resulting in an increased

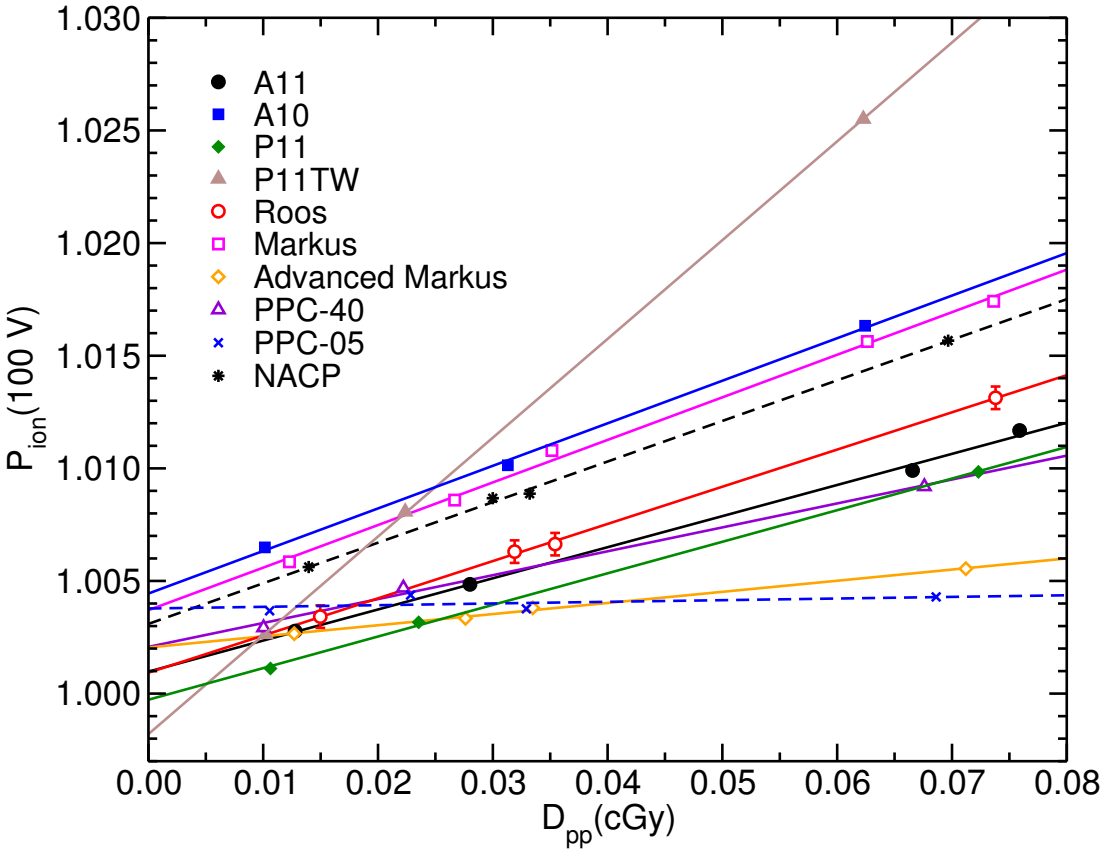

Figure 3.2: The corrections for ion recombination as a function of dose per pulse for all plane-parallel ion chambers investigated here in photon beams. The lines show linear fits to the data. For the PTW Roos chamber, systematic uncertainties are represented by error bars. From paper IV.

electric field. This problematic behavior could indicate that a given chamber is not suitable for reference dosimetry.[34]

Recombination parameters, in the formalism of Burns and McEwen[61] (equation 2.4 [p. 26]), are extracted from the data in figure 3.2. As indicated above, δ values are related to general recombination and are expected to depend on the square of the plate separation for plane-parallel chambers. Differences in δ values among the chambers investigated in this work are consistent with variations in chamber dimensions.

The recombination parameters are not provided here for brevity and only a brief

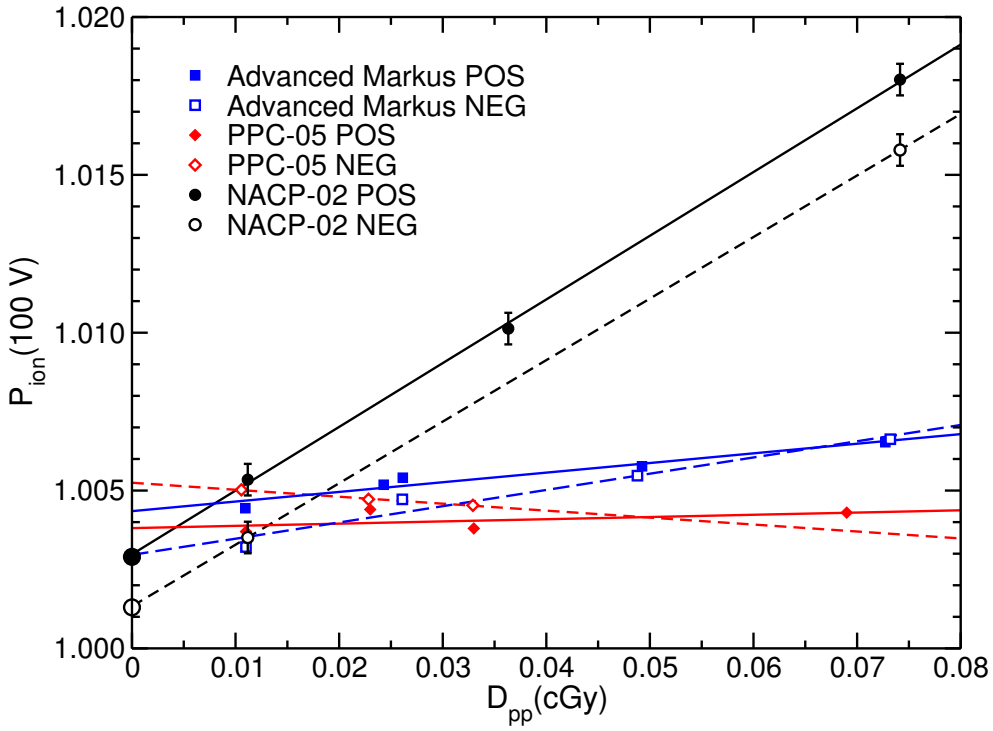

Figure 3.3: Ion recombination correction factors as a function of dose per pulse for select chambers to demonstrate unexpected differences in recombination behavior depending on the polarity of charge collected. Linear fits are shown. Error bars representing systematic uncertainties are shown for the IBA NACP-02 chamber. Values of P_{ion} obtained in cobalt-60 (D_{pp}=0 Gy) are shown. From paper IV.

summary of the comparison of recombination parameters to those from the literature is presented. The interested reader is referred to Paper IV for details. Except for the study of Bass *et al.*[87] who investigated a large sample of NACP-02 and Roos chambers, recombination parameters are only available in the literature for a few chambers of selected types.[61,64,88,89] Of the eight values of γ and δ compared to those from other publications that investigated only a few chambers of each type, only one γ value and four δ values are in agreement within systematic uncertainties. The common practice at most standards laboratories other than NRC is to collect negative charge for ion chamber calibrations. The differences between the γ values obtained here and those from other publications are likely due to this difference in applied polarity;

when collecting negative charge, a smaller value of γ is almost always observed here. The other possible explanation for the differences in γ and δ values is sensitivity to changes in chamber construction. Bass *et al.*[87] investigated recombination parameters for about 40 NACP-02 and Roos chambers, the average of which are in agreement with the results of this work. The standard deviation of δ values of Bass *et al.*[87] amount to 20 % and 8 % for NACP-02 and Roos ion chambers, respectively, indicating the large variability of recombination parameters for a large sample of different chambers of the same type. Therefore, it is not surprising that resulting recombination parameters are in poor agreement when only a few chambers of a given type are investigated.

Although it is commonly assumed that initial ion recombination in cobalt-60 affects the response of a chamber by less than 0.1 % and can be ignored, the large intercepts in figure 3.2 from measurements in pulsed beams indicate that initial recombination can introduce up to 0.5 % effects for these chambers. Other authors have stressed the importance of correcting for initial recombination in continuous beams, indicating effects of up to 0.2 % for cylindrical chambers[90] and up to 0.7 % for plane-parallel chambers.[91] To compare to the results from pulsed beams, measurements of recombination corrections are obtained in cobalt-60 (D_{pp}=0 Gy) for a sample of chambers to determine the component of initial recombination directly. Figure 3.3 shows the recombination correction extracted from a Jaffé plot obtained in cobalt-60 for an NACP-02 chamber. The resulting correction is in good agreement with the intercept from pulsed beams as is the case for six of the eight chambers for which ion recombination corrections are obtained in cobalt-60. Differences between initial recombination measurements in continuous and pulsed beams are up to 0.28 % for two chambers but these are the chambers that exhibit strange recombination behavior in figure 3.3 discussed above. The results of this work confirm the results of Derikum[92] that, for well-behaved chambers, the intercept of P_{ion} vs. D_{pp} from pulsed beams

results in the same correction for initial recombination as measurements in cobalt-60. These results also indicate that ignoring the correction for ion recombination in cobalt-60 can introduce systematic errors of up to 0.5 % for plane-parallel chambers.

3.2 Long-term stability of $N_{D,w}$ coefficients and k_Q factors

Measurements to investigate long-term stability of $N_{D,w}$ coefficients and k_Q factors were obtained eight and eleven months after initial calibrations were performed in January 2011. Repeated calibrations of plane-parallel chambers to obtain $N_{D,w}$ in cobalt-60 in August 2011 (a period of eight months after initial calibrations were performed) are on average 0.6 % lower than initial calibration measurements with a standard deviation of 0.3 %. The maximum difference between repeated calibrations in cobalt-60 is up to 1.2 %. There was no change in the calibration coefficients for the cylindrical chambers investigated. These large systematic differences for plane-parallel chambers in cobalt-60 prompted repeated calibrations in the 6 MV linac beam. Calibration coefficients in the 6 MV beam were again systematically lower by 0.3 % on average with a standard deviation of 0.5 % and a maximum difference of 1.5 %. However, the average difference in k_Q factors determined after a period of eight months was only 0.17 % with a standard deviation of 0.28 % and a maximum change of 0.7 %.

Only a few other authors have reported repeated calibration measurements for plane-parallel chambers in electron or photon beams. Christ *et al.*[93] suggested that long-term stability was not an issue for plane-parallel chambers. The standard deviation of calibration coefficients measured by Palm *et al.*[94] in cobalt-60 three or four times during a period of several months was between 0.3 to 0.7 % for different plane-parallel chambers. A large sample of electron beam calibrations for plane-parallel chambers by Bass *et al.*[87] were stable at the 0.1 to 0.2 % level on average but dif-

ferences of up to 1 % were observed between repeated calibrations. These levels of stability are consistent with the observations of this work.

The unexpected sensitivity of leakage currents to levels of relative humidity discussed above suggests that plane-parallel chambers are more sensitive to environmental conditions than cylindrical chambers. To investigate if the change in calibration coefficients obtained in August 2011 (when relative humidity was much higher than January 2011 when initial calibrations were performed) was related to variations in environmental conditions, calibrations were repeated in the 6 MV beam in December 2011 when relative humidity levels were similar to those during the initial calibration measurements made eleven months previously. These repeated calibrations were within 0.16 % on average (0.32 % standard deviation) compared to the initial calibration measurements. The maximum difference was observed for the same chamber that had changed by 1.5 % in August 2011 but had returned to within 0.75 % of the initial measurement. The relative humidity level in August 2011 was 65 % compared to 25 % in January and December 2011. Although these levels of humidity are still well within the limits for which dosimetric quantities have been shown to be constant within 0.15 %,[14] the results of this work suggest that calibration coefficients for plane-parallel chambers can be adversely affected by humidity levels.

The uncertainty from the stability of $N_{D,w}$ coefficients is estimated using the mean difference between calibrations and the root mean square deviation from zero and amounts to 0.36 %. The k_Q factors determined here appear to be more stable than $N_{D,w}$ coefficients introducing a component of uncertainty of only 0.19 %.

Although k_Q factors for these chambers appear to be stable, these unsatisfactory results regarding the stability of plane-parallel chamber calibration coefficients have implications regarding their use for reference dosimetry. Reference-class detectors should have stable calibration coefficients at the 0.3 % level after a period of

two years.[12,95] This means that many of the chambers investigated here can not be deemed suitable for reference dosimetry. A cross-calibration procedure against a stable cylindrical chamber would avoid these problems, although this would need to be done each time these chambers are used.

3.3 Measured k_Q factors

Uncertainty budget: The uncertainty budget for measured k_Q factors and calibration coefficients for plane-parallel chambers in photon beams is provided in table 3.1, derived using the ISO "Guide to the expression of uncertainty in measurement"[82] recommendations. The use of the indirect method of calibration against a stable secondary standard cylindrical chamber is discussed in chapter 2 and the individual components of uncertainty are discussed in the preceding sections 3.1 and 3.2.

Chamber-to-chamber variability of measured k_Q factors: Variability of measured k_Q factors for plane-parallel chambers of the same type has been investigated by several authors,[36,55,86,93,94,96] usually based on measurements in cobalt-60. The main reason that these chambers were not recommended for use in photon beams by reference dosimetry protocols[10,11] was evidence for unacceptable (up to 3.6 %) chamber-to-chamber variations of cobalt-60 P_{wall} values for chambers of the same type.[36] That evidence was for older chambers that were likely manufactured by hand potentially resulting in variable manufacturing processes. More recent investigations[55,93] suggest that chamber-to-chamber variability for plane-parallel chambers of the same type is no longer an issue.

Measurements of k_Q factors in this work are performed with more than one chamber of a given type for several chamber types, including two of each of the Exradin A11 (although significant differences are present in the chamber construction), IBA PPC-05 and PPC-40 and PTW Roos, Advanced Markus and Markus chambers as

Table 3.1: Combined uncertainty in measured $N_{D,w}$ coefficients and k_Q factors for plane-parallel ion chambers where estimates are given using a k=1 coverage factor. Modified from paper IV.

Type	Source	$N_{D,w}$ (%)	k_Q (%)
A			
1	Reproducibility in chamber reading (R/MU)	0.04	0.04
2a	Transfer of monitor calibration (NRC ref.)	0.07	0.07
2b	St. dev. of ref. chamber calibration	0.05	0.05
3	Chamber-to-chamber repeatability	-	0.11
4	Long-term stability	0.36	0.19
B			
5	Uncertainty in NE2571 standard	0.34	0.27
6	P_{ion}	0.05	0.05
7	P_{pol}	0.08	0.08
8	P_{rp}	0.05	0.05
9	P_{leak}	0.01	0.01
10	P_{TP}	0.05	0.05
11	Chamber Positioning	0.06	0.06
Combined		0.52	0.45

well as four NACP-02 chambers (two manufactured by Scanditronix and two manufactured by IBA). Aside from the IBA PPC-05 and NACP-02 chambers, all k_Q factors for chambers of the same type are within 0.2 % of each other. This includes the two Exradin A11 chambers that are different in construction because of changes in manufacturing. Due to the cancellation of correlated uncertainties, the standard uncertainty estimate on relative k_Q factors is only 0.1 %, indicating that the 0.2 % variation in k_Q factors for chambers of the same type is a real effect. The k_Q factors for the IBA PPC-05 chambers are 0.3 % different from each other, although the problems with ion recombination discussed above may indicate other issues with these chambers. The four NACP-02 k_Q factors are up to 0.5 % different from one

another, although two of the chambers investigated were manufactured much earlier by Scanditronix and two were manufactured just before the onset of this study by IBA. However, the standard deviation of the mean of the NACP-02 k_Q factors is only 0.11 %, which is used as the uncertainty estimate from chamber-to-chamber variation of k_Q factors in table 3.1. The amount of variation of k_Q factors for chambers of the same type observed here is much lower than early investigations and does not contribute a significant component to the overall uncertainty in measured k_Q factors.

Measured k_Q factors and comparison to literature values: Measured k_Q factors are shown in figure 3.4 for chambers for which literature values are available. The present measurements are shown with the point of measurement of the chamber at the same position as that used for the Monte Carlo simulations discussed above and corrected for ion recombination. The measured values of this work shown in figure 3.4 are all in agreement within systematic uncertainties with the calculated k_Q factors of this work, discussed in chapter 4. The largest difference between the calculations and measurements of this work for all chambers investigated is 0.7 % for the Exradin A11 chamber. A detailed comparison of the measured and calculated values of this work is discussed in chapter 5.

Also shown in figure 3.4 are the measurements of this work adjusted for comparison to measurements from the literature, which were not corrected for ion recombination in cobalt-60 and used slightly different water-equivalent shifts to account for the front window of the chambers. The measurements of McEwen *et al.*[86] for the NACP-02 and PTW Roos chambers are traceable to the NPL graphite calorimeter, the primary standard for absorbed dose in the UK. The combined uncertainty on the NPL measurements is 1.0 % so, although the measured values of this work are systematically higher by about 0.5 %, the results of the two studies are in agreement within systematic uncertainties. That the results are systematically different

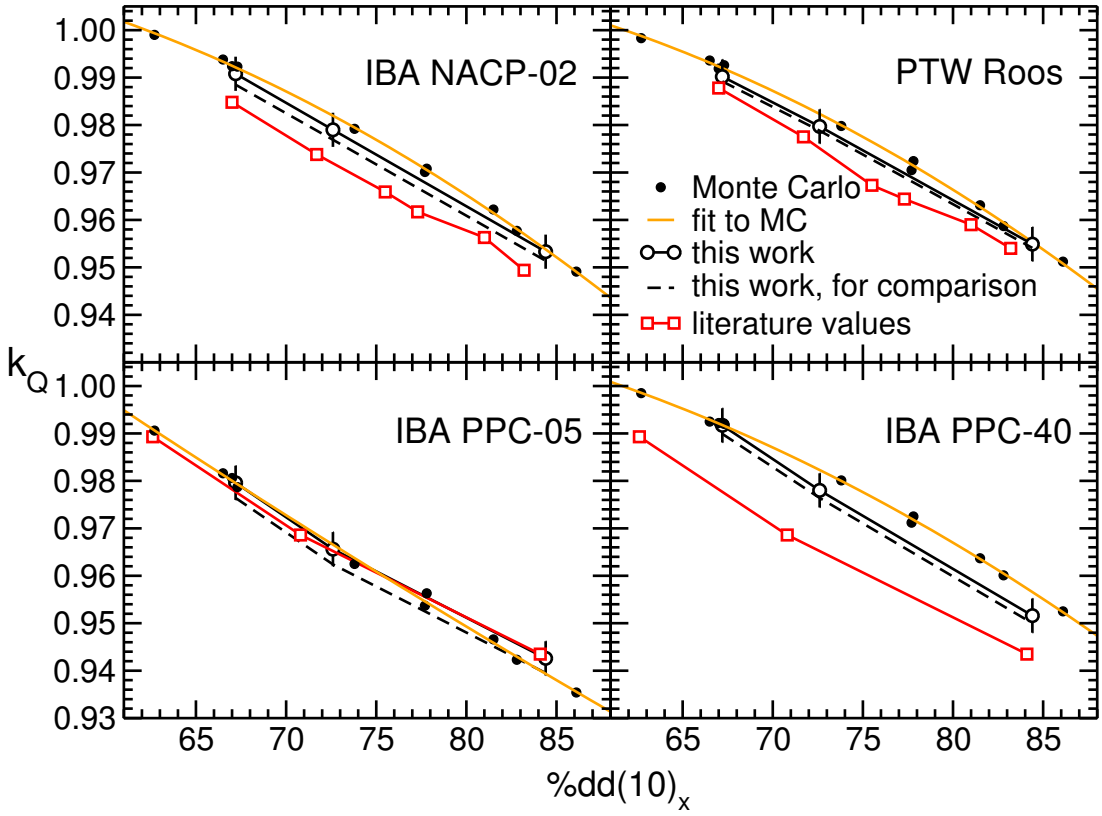

Figure 3.4: Beam quality conversion factors with comparison to literature values and Monte Carlo calculations for the subset of chambers for which literature values are available. Filled symbols are calculated k_Q factors with a fit to the values shown by the lightly coloured line. Present measurements, shifted so that the inside of the chamber window is at the measurement depth and corrected for recombination in cobalt-60, are open circles with error bars representing combined systematic uncertainties. Measured literature values are shown by open squares, connected with straight lines. The dashed lines represent our measurements modified for comparison to literature values as described in the text. In the upper two panels, values are compared to measurements from McEwen *et al.*[86] In the lower two panels, values are compared to k_Q factors measured by Kapsch and Gomola.[55] From paper IV.

by a similar amount for both chambers suggests that the difference may result from measurements in cobalt-60.

The measured values for the IBA PPC-05 and PPC-40 chambers of Kapsch and Gomola[55] were determined using measurements at PTB but also relied on the use of k_Q factors from the IAEA TRS-398[11] protocol for a cylindrical NE2561 chamber.

Since the measurements of McEwen[34] and the calculated results of this work are up to 0.5 % different from those in TRS-398,[11] to compare consistently, the results of Kapsch and Gomola[55] are adjusted with the fit to Monte Carlo k_Q calculations for the NE2561 from paper III of this work. In figure 3.4, the results of this work for the IBA PPC-05 are in excellent agreement with those of Kapsch and Gomola[55] but the two sets of results are systematically different by about 1 % for the IBA PPC-40 chamber. The problematic behavior of these chambers in terms of long-term stability of calibration coefficients could explain the differences among measured k_Q factors.

3.4 Summary

In the process of obtaining measured photon beam k_Q factors for plane-parallel chambers, the behavior of these chambers in photon beams is analyzed. The settling behavior observed for plane-parallel ion chambers is not an issue; all chamber readings settled to a stable reading within 15 minutes, much less than that observed with problematic small volume cylindrical chambers.[34] These chambers display unexpected sensitivity to relative levels of humidity. Leakage currents for all plane-parallel chambers measured at a time when relative humidity was low are less than 0.05 % of the reading with radiation present but increased dramatically at a time of higher relative humidity. Polarity correction factors for all of the plane-parallel chambers investigated show effects of up to 0.3 %. This is within the allowable range of polarity corrections for a reference-class ion chamber.[12,34]

For most chambers, the behavior of the recombination correction factor as a function of dose per pulse is consistent with theoretical predictions[61–63] but anomalous behavior is observed for two chamber types indicating potential problems with these chambers. Recombination parameters are in variable agreement with literature values, indicating that these parameters are likely sensitive to variations in cham-

ber construction for chambers of the same type. In addition, some chambers exhibit large (up to 0.5 %) components of initial recombination determined from the intercept of P_{ion} vs. D_{pp} in pulsed beams. Direct measurements of initial recombination in cobalt-60 (D_{pp}=0 Gy) are consistent with measurements from pulsed beams for most chambers. These measurements indicate that initial recombination should not be ignored for calibration measurements in continuous beams.

Significant issues are observed regarding the long-term repeatability of calibration coefficients for these chambers, which appear to be sensitive to environmental conditions. Plane-parallel calibration coefficients are different by up to 1.5 % in photon beams after a period of eight months suggesting that many of these chambers can not be considered reference-class ion chambers.[12,34,95] This has implications for the use of these chambers in reference dosimetry protocols where the determination of absorbed dose relies on stable cobalt-60 calibration coefficients. The stability of k_Q factors for plane-parallel chambers does not appear to be as poor provided that measurements in linac beams and cobalt-60 are made close in time as in this work.

The measured k_Q factors of this work are obtained with a systematic uncertainty estimate of 0.45 %. The variability of measured k_Q factors for chambers of the same type is less than 0.5 % with typical variations less than 0.2 %, much less than that suggested by early publications.[36] The measured and calculated k_Q factors of this work are generally in good agreement within systematic uncertainties with a maximum difference of 0.7 %. These measurements are in variable agreement with those from other publications, depending on the chamber type and calibration laboratory of origin. The problems indicated above regarding the stability of calibration coefficients and the sensitivity of these chambers to environmental conditions indicate that plane-parallel chambers, as a class, are not suitable for reference dosimetry without cross-calibration against a stable cylindrical chamber.

Chapter 4

Calculated k_Q factors in photon beams

This chapter presents Monte Carlo calculated k_Q factors for cylindrical and plane-parallel ion chambers in photon beams. These results are compared to values from the literature for a few chamber types for which literature data are most abundant. Calculated k_Q factors for cylindrical chambers are compared to those recommended in current dosimetry protocols and differences are explained. This comparison cannot be performed for plane-parallel chambers because current dosimetry protocols did not recommend these chambers for use in photon beams so k_Q factors were not provided. Systematic uncertainties in calculated k_Q factors in photon beams are analyzed and presented.

4.1 Results for calculated k_Q factors

One of the most commonly used ion chambers for reference dosimetry of photon beams is the NE2571 Farmer-type chamber. The design is based on the original conception of Aird and Farmer[2] who made modifications to an existing chamber to obtain a uniform response over the therapy energy range and reduce conductivity of the insulator to improve precision. This chamber type has been shown to produce absorbed dose calibration coefficients that are stable for decades. Consequently, it is the chamber of choice for many investigations of reference dosimetry.

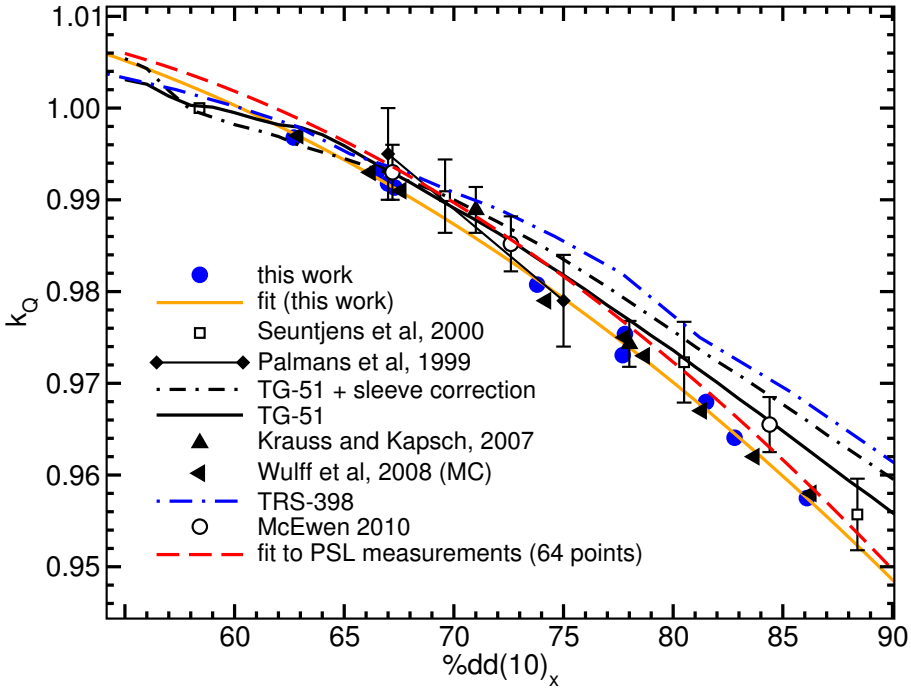

Figure 4.1: Monte Carlo calculated k_Q factors for the NE2571 ion chamber (c, 0.6 cm^3) in photon beams along with measurements from Palmans *et al.*,[97] McEwen,[34] Seuntjens *et al.*,[18] Krauss and Kapsch[96] and a fit to 64 measurements from a large comparison of primary standard laboratories [Stucki, G., private communication (2011)], Monte Carlo calculated values from Wulff *et al.*[31] and values from the TG-51[10] and TRS-398[11] protocols. Modified from paper I.

Monte Carlo calculated k_Q factors of this work are shown for the NE2571 chamber type in figure 4.1 compared to results from previous investigations. The calculated results of this work are in excellent agreement with those of Wulff *et al.*[31] The measured values are all from direct calibrations of different NE2571 chambers against water calorimetry measurements, usually at primary standard laboratories (PSL). The calculations of this work are in excellent agreement with those obtained by Palmans *et al.*[97] at Ghent University and Krauss and Kapsch[96] at Physikalisch-Technische Bundesanstalt (PTB, a PSL). Values traceable to the NRC primary standard water calorimeter are from McEwen[34] and Seuntjens *et al.*[18] Figure 4.1 shows that the calculated results of this work are in reasonable agreement with the NRC measurements, although they are lower by up to 0.3-0.4 % at high energy. Also in figure 4.1 is a fit

to k_Q factors from an international comparison [Stucki, G., private communication (2011)] of primary standard laboratories, where $N_{D,w}$ factors were determined at each laboratory for the same four NE2571 ion chambers to compare standards. The 64 high-quality data points which ranged up to %dd(10)$_x$ of 84.4 % are omitted from figure 4.1 for clarity but the root-mean-square deviation of the fit to the data is 0.24 %. Figure 4.1 shows that the calculated results of this work are in excellent agreement (within 0.24 %) with the fit to comparison data, although they are systematically slightly lower. The fit to the calculated data of this work agrees within 0.78 % of all of the individual measured values from the comparison (not shown).

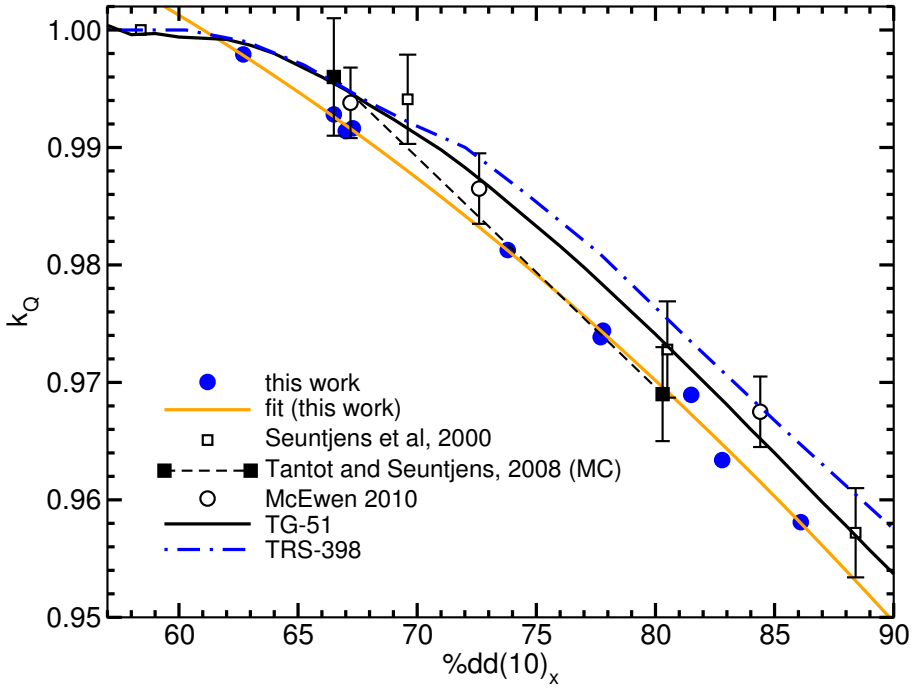

Figure 4.2: Monte Carlo calculated k_Q factors for the Exradin A12 ion chamber (a, 0.65 cm^3) in photon beams along with measurements from Seuntjens *et al.*[18] and McEwen,[34] Monte Carlo calculated values from Tantot and Seuntjens[67] and protocol values.[10,11] Modified from paper I.

Another commonly used chamber for dosimetry of high-energy photon beams is the Exradin A12 chamber. Its volume is similar to the NE2571 chamber but other characteristics are substantially different; the A12 uses water-proof C552 walls

and central electrode while the NE2571 uses a graphite wall and aluminum central electrode and is not inherently water-proof requiring a sleeve for calibrations in water. Figure 4.2 shows the calculated k_Q factors of this work compared to measurements from Seuntjens *et al.*[18] and McEwen[34] traceable to the Canadian primary standard for absorbed dose and other calculated results from Tantot and Seuntjens.[67] The calculations of this work are in good agreement with those of Tantot and Seuntjens,[67] although the results from that work have much higher statistical uncertainties (0.5 % compared to 0.1 % here). The k_Q factors obtained here are systematically lower than measured values by up to 0.6 %.

Figure 4.3 shows k_Q factors for cylindrical chambers chosen to be representative of the chamber groups from section 2.2. In addition, paper I provided fits (not included in this thesis) to k_Q factors as a function of $\%\mathrm{dd}(10)_x$ for all chambers investigated (33 chambers in total). The results of paper I have been recommended for clinical use for reference dosimetry across North America in the addendum[12] to the AAPM's TG-51 protocol. Technical report II provided plots of k_Q factors for all cylindrical chambers investigated in photon beams with comparison to literature data where available. In general, the results of this work are in good agreement with other publications. The level of agreement with literature data shown in figures 4.1 and 4.2 is typical for other chambers investigated. In chapter 5 these calculated results are compared to the measurements of McEwen[34] for the 25 chambers that overlap between the two studies.

Calculated k_Q factors are also obtained for plane-parallel ion chambers in photon beams. Only a few authors have investigated a small number of these chamber types in photon beams. Measurements using plane-parallel chambers in photon beams are investigated in chapter 3 and figure 3.4 (p. 56) shows the measured and calculated k_Q factors of this work compared to the limited data in the literature.[55,86] In addition,

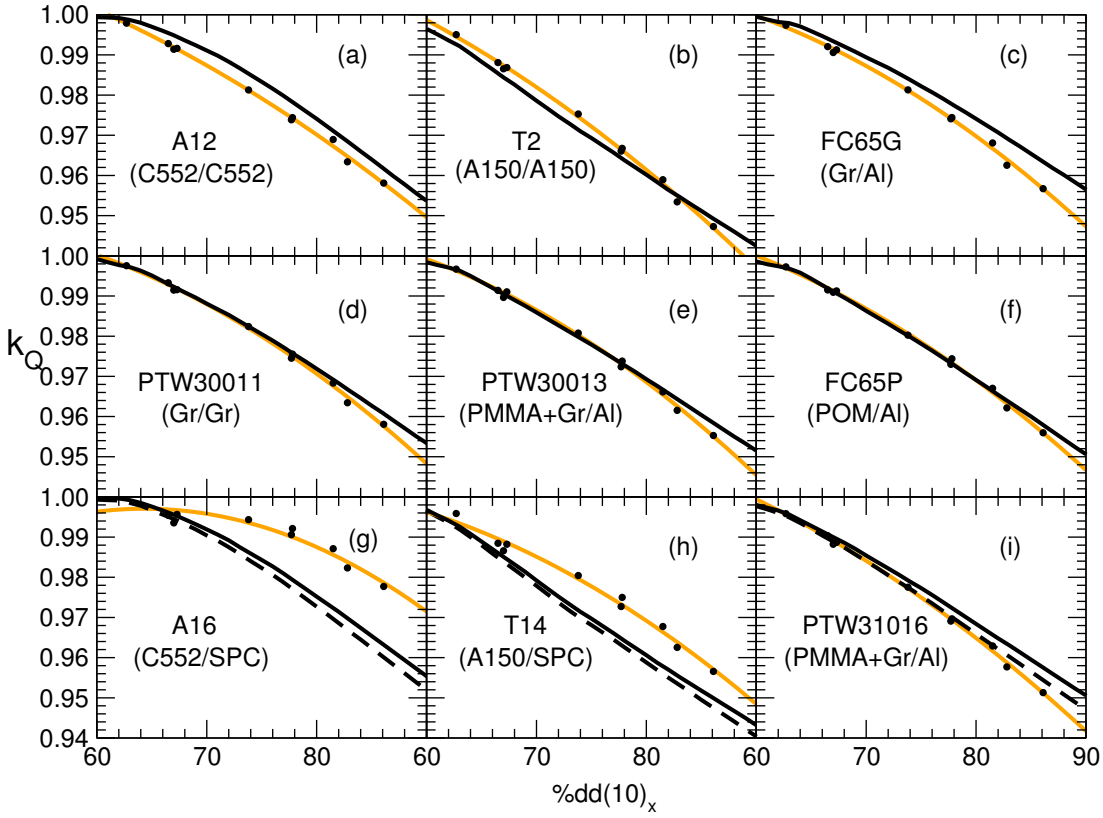

Figure 4.3: Representative Monte Carlo calculated k_Q values (solid points) along with a fit to the data (light-coloured lines) and the TG-51 calculated values (black lines). The chambers with small cavities and metal electrodes have two sets of TG-51 calculated values, one with a 0.5 mm radius aluminum electrode (solid black lines) and another without (dashed lines). The chamber that is used as a representative is given along with a brief classification given as (wall/electrode). From paper I.

paper IV provided fits to the calculated k_Q factors for all plane-parallel chambers investigated in photon beams. The calculated results for all chambers in figure 3.4 (p. 56) agree within systematic uncertainties with the measurements of chapter 3. Of all plane-parallel chambers investigated, the largest difference between measured and calculated values of k_Q was 0.7 % for the Exradin A11 chamber. The measured results of this work are compared to those from other publications[55,86] in chapter 3.

There are no other publications that investigate calculated k_Q factors for plane-parallel chambers in photon beams but two[98,99] provided D_w/D_{ch} for cobalt-60 source

models. The results of this study agree within 0.2, 0.6 and 0.2 % for the IBA NACP-02, PPC-05 and PPC-40 chambers, respectively, with those of Panettieri *et al.*,[98] who calculated the dose ratio for IBA chambers with the PENELOPE code system. This level of agreement is promising given that the calculations were done with independent chamber models and different code systems. Similarly, Wulff and Zink[99] calculated the D_w/D_{ch} ratio in cobalt-60 for the IBA NACP-02 chamber, which is in agreement within 0.1 % with the result of this work when the same specifications are used for the chamber window and back wall. Over the course of this investigation, calculations are performed using different back wall specifications in the chamber model and D_w/D_{ch} in cobalt-60 was sensitive to these specifications at the 0.5 % level. The effect of using different back wall specifications is only 0.2 % on k_Q factors.

4.2 Comparison of calculated k_Q factors with protocol values

In section 1.3, the equation used for protocol calculations of k_Q factors was presented (equation 1.11 [p. 10]) with the origin of the individual quantities used for TG-51.[10] Differences of up to 1.7 % are noted between the individual correction factors used by TG-51 and more accurate Monte Carlo calculated values. The differences in figure 4.3 between the k_Q calculations of this work for cylindrical chambers and those in dosimetry protocols can be explained entirely by differences in individual correction factors.

The emphasis here is on comparison to the North American TG-51[10] protocol but the values used in the European IAEA TRS-398 protocol[11] are similar except for their values of $(P_{\text{repl}})^Q_{Co}$, which are about 0.3 % higher than the TG-51[10] values in high-energy photon beams. This explains why the TRS-398 values are higher than TG-51 values in figures 4.1 and 4.2. Wang and Rogers[41] showed that, for Farmer-

type chambers, TG-51 $(P_{\text{repl}})^{Q}_{Co}$ values are up to 0.2% higher than the more accurate Monte Carlo calculations. This will result in protocol k_Q factors being higher than these calculated results by 0.2 % for TG-51 and 0.5 % for TRS-398 in the highest-energy photon beams. Differences between P_{cel} corrections for chambers that use low-Z central electrodes are not observed compared to TG-51. However, the central electrode correction factor can be significant for chambers that use high-Z electrodes. Central electrode corrections for these chambers were not available when TG-51 was written so the comparison in figure 4.3 is for TG-51 calculations without an electrode or with an aluminum central electrode. Figure 4.4 shows the ratio of P_{wall} calculations of the present work in a high-energy beam to that from cobalt-60 compared to those used in TG-51, $\left[(P_{\text{wall}})^{Q}_{Co}\right]^{TG51}_{MC}$. This figure helps explain differences between these k_Q factors and TG-51 values - if the ratio is greater (less) than unity, the TG-51 calculations will be higher (lower) than these calculated k_Q factors.

For chambers in groups a, c, d, e and f, TG-51 $(P_{\text{wall}})^{Q}_{Co}$ values are all higher in high-energy photon beams than the more accurate results from Monte Carlo simulations. The $(P_{\text{repl}})^{Q}_{Co}$ values used for TG-51 calculations are also higher by 0.2 % at high energy than the more accurate results of Wang and Rogers.[41] This explains why TG-51 k_Q factors are all higher than Monte Carlo calculated results for these chamber groups. For the chambers in this group that require a water-proofing sleeve, the differences in k_Q factors at high energy between TG-51 calculations are compensated by up to 0.3 % - TG-51 ignored the effect of a sleeve but it has been shown[18,33–35] to increase k_Q factors by 0.3 % in high-energy beams.

For chambers in group b, TG-51 $(P_{\text{wall}})^{Q}_{Co}$ values are lower than the Monte Carlo calculations by up to 0.2 % in low-energy beams but agree at high energy causing TG-51 k_Q factors to be lower in low-energy beams. The 0.2 % effect from $(P_{\text{repl}})^{Q}_{Co}$ in high-energy beams results in the TG-51 k_Q calculations being higher than the Monte

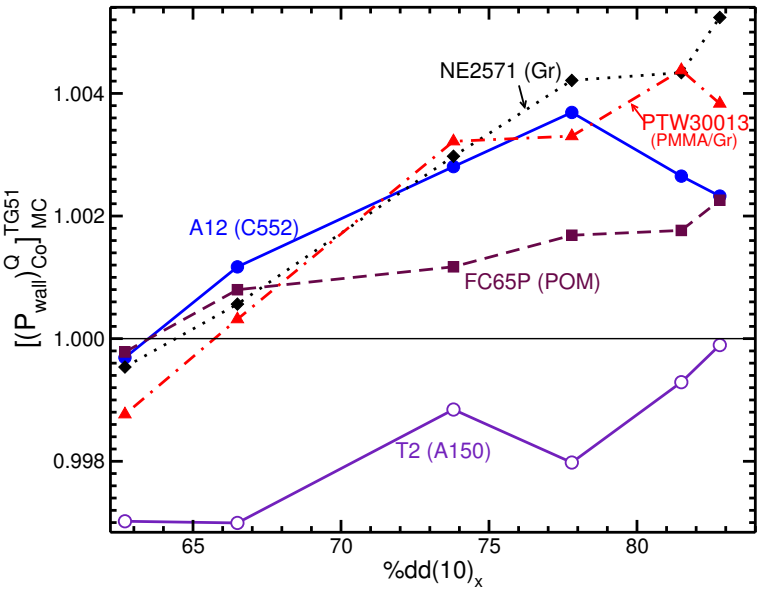

Figure 4.4: The ratio of $(P_{\text{wall}})^{Q}_{Co}$ values used in TG-51 to the more accurate values calculated using Monte Carlo simulations. The ratios are a function of wall thickness and thus specific to the chambers mentioned although the differences for chambers with the same wall materials are explained using the ratios from this plot. Multiplying Monte Carlo calculated k_Q values by these ratios indicate what the value of k_Q would be if TG-51 values of P_{wall} were used. From paper I.

Carlo calculated values in this region.

For the small volume chambers of groups g and h, a large effect is observed due to the use of a central electrode composed of high-Z materials. TG-51 calculations could only be done with an aluminum electrode or without an electrode. These TG-51 calculations are both shown in figure 4.3 and the results using aluminum electrodes are in slightly better agreement with Monte Carlo calculated values. The differences from $(P_{\text{wall}})^{Q}_{Co}$ observed for Farmer-type chambers are also present but are not as significant as the effect from the high-Z central electrode. These observations prompted an investigation into P_{cel} for these ion chambers (see paper II and appendix A). McEwen[34] showed that these small volume chambers are not suitable for reference dosimetry so the large differences between TG-51 k_Q calculations and results from Monte Carlo

simulations may not be practically important.

For group i chambers with small active collecting regions and aluminum central electrodes, the differences between Monte Carlo calculated values and TG-51 calculations are similar to those for their larger volume counterparts of group e. The aluminum central electrode in these chambers does not cause a large effect compared to the other small volume chambers of group g and h that use high-Z electrodes. Wang and Rogers[41] indicate that the replacement correction factor varies by less than 0.2% as a function of cavity length. The agreement between Monte Carlo calculated k_Q factors and TG-51 calculations verify this statement since the TG-51 calculations assume a 24 mm long chamber cavity. These small volume chambers are still not suitable for reference dosimetry.[12,34]

4.3 Systematic uncertainties in calculated k_Q factors

Systematic uncertainties in calculated k_Q factors are analyzed according to the methods in section 2.2. The relative statistical uncertainty in Δk_Q calculations is less than 0.05%. This means that in cases where Δk_Q is less than 0.05% the contribution to the uncertainty is negligible. A sample uncertainty budget is provided for the NE2571 chamber in table 4.1. This chamber is chosen to represent chambers in group c with graphite walls and aluminum electrodes. An 18 MV photon beam is used to determine the systematic uncertainty in calculated k_Q factors because the properties of that beam are very different from a cobalt-60 source resulting in greater sensitivity of k_Q factors to variations in individual components of uncertainty. If a lower-energy beam is used, the resulting systematic uncertainty in k_Q calculations is smaller.[72]

Varying the mean excitation energy, I, to alter the stopping powers used for the water phantom and the materials of the chamber results in a maximum variation in calculated k_Q factors of 0.19 % in table 4.1 from the graphite of the chamber

Table 4.1: Sample uncertainty budget for a cylindrical ion chamber in group c (NE2571 - graphite wall, Al electrode) indicating the relative change in each variable, u(x_i), which contributes a component, $\Delta(k_Q)_i$, to the overall systematic relative uncertainty in calculated k_Q factors, u_{k_Q}. Values are given in percent. Modified from paper I.

Variable, x_i	u(x_i) (%)	$\Delta(k_Q)_i$ (%)
Mean Excitation Energy, I		
Water	1.5	0.03
Air	2.5	0.03
Graphite Wall	4.5	0.19
Aluminum Electrode	0.5	0.00
Photon cross sections		
Water	1.0	0.55
Air	1.0	0.03
Graphite Wall	1.0	0.29
Aluminum Electrode	1.0	0.01
All (Correlated)	1.0	0.0
Other Sources		
Statistical Uncertainty	-	0.1
`EGSnrc`[48]	-	0.1
Wall Thickness	5.0	0.1
Cavity Dimensions	5.0	0.00
Source model	-	0.1
$(\frac{W}{e})_{air}$ (see Ch. 5)	-	0.25
u_{k_Q}		
corr, no W/e	-	0.28
uncorr, no W/e	-	0.68
corr, with W/e	-	0.38
uncorr, with W/e	-	0.72

wall. Considering the unlikely situation that photon cross sections are uncorrelated, the maximum effect on k_Q factors is 0.55 % from scaling photon cross sections by 1 % in the water phantom. In the more likely event that photon cross sections are correlated, scaling photon cross sections introduces a negligible component of uncertainty in calculated k_Q factors. For other chambers, the uncertainty in k_Q factors from uncertainties in material properties is provided in table 4.2. Other than the uncertainty from scaling photon cross sections in the water phantom, the largest

component of uncertainty in k_Q factors from uncorrelated photon cross sections is 0.53 % for chambers in groups a, b and h with C552 or A150 walls. The largest component of uncertainty from varying the stopping powers in the chamber walls is 0.33 %, also for chambers in group b with A150 walls.

Table 4.2: Components of uncertainty in k_Q, in percent, due to variations in photon cross sections and electron stopping powers. Photon cross sections are varied separately for each material by 1%. Electron stopping powers are varied by changing the mean excitation energy, I, for each material separately. The first column shows the percent variation in I values used. The chambers used in each case are given in brackets. Modified from paper I.

Material	Mean Excitation Energy		Photon cross sections
	ΔI (%)	Δk_Q (%)	Δk_Q (%)
Water (NE2571)	1.5	0.03	0.55
C552 (Exradin A12)	5	0.30	0.53
Graphite Wall (NE2571)	4.5	0.19	0.29
PMMA (PTW 30013)	2	0.09	0.16
Air (NE2571)	2.5	0.03	0.02
Aluminum (NE2571)	0.5	0.00	0.01
POM/Delrin (IBA FC65P)	5	0.23	0.21
A150 (Exradin T2)	5	0.33	0.53
Steel Wire (IBA CC01)	5	0.01	0.05
SPC Electrode (Exradin A16)	5	0.03	0.02

Other than material properties, additional sources of uncertainty are considered in calculated k_Q factors in table 4.1. The relative statistical uncertainty in k_Q calculations is 0.1 %, achieved by increasing the number of histories used for the simulations. The `EGSnrc` code system has been shown[48] to be accurate to within 0.1 % with respect to its own cross sections with the rigorous Fano test of photon-electron transport. Varying the wall thickness used for the chamber model by 5 % only results in a 0.1 % effect on k_Q calculations. The uncertainty in k_Q from the cavity dimensions of the chamber model is considered for cylindrical chambers with a linear fit to the $(P_{\text{repl}})^Q_{Co}$ data of Wang and Rogers.[41] The component of uncertainty in k_Q factors from cavity dimensions is then estimated by multiplying the slope of this fit by the uncertainty in cavity radius, assumed to be $\pm$5% of a typical Farmer

chamber radius (3 mm). The small variation of $(P_{\text{repl}})^{Q}_{Co}$ with cavity radius results in a negligible component of uncertainty in calculated k_Q factors. One could also introduce a component of uncertainty in k_Q factors from using a simplified stem in the chamber model of 0.2 % from the difference in calculated k_Q factors for Exradin chambers when simplified and detailed chamber models are used (see chapter 2). For most chambers including the NE2571, the most detailed possible model of the chamber stem is used for calculations, so in table 4.1 this component of uncertainty in not included. The component of uncertainty from the use of photon spectra for source simulation is investigated by calculating k_Q factors with realistic `BEAMnrc` accelerator models and the effect on k_Q is less than 0.1 %. Finally, the component of uncertainty in k_Q from potential $(\frac{W}{e})_{air}$ variation with beam quality is estimated to be 0.25 % (see chapter 5).

Table 4.3: The total relative systematic uncertainty in Monte Carlo calculated k_Q values using different assumptions - with and without correlated photon cross section uncertainties and with and without the uncertainty on $\frac{W}{e}$, sorted by chamber group. The values are given in percent. Modified from paper I.

	u_{k_Q}			
Group (Wall/Electrode)	corr no W/e	uncorr no W/e	corr with W/e	uncorr with W/e
a (C552/C552)	0.36	0.85	0.44	0.89
b (A150/A150)	0.39	0.86	0.46	0.90
c (Graphite/Al)	0.28	0.68	0.38	0.72
d (Graphite/Graphite)	0.28	0.68	0.38	0.72
e/i (PMMA+Graphite/Al)	0.31	0.71	0.40	0.75
f (POM/Al)	0.32	0.66	0.41	0.71
g (C552/SPC)	0.36	0.85	0.44	0.89
h (A150/SPC)	0.39	0.86	0.46	0.90

Adding the individual components of uncertainty in k_Q, Δk_Q, in quadrature as in equation 2.8 (p. 40) the combined systematic uncertainty in calculated k_Q factors, u_{k_Q}, is realized. For the NE2571 chamber and other chambers in group c, table 4.1 shows u_{k_Q} when different assumptions are made. If one assumes correlated photon cross

sections and that $(\frac{W}{e})_{air}$ does not vary with beam quality, u_{k_Q} amounts to 0.28 % in table 4.1. However, if the more conservative approach is taken assuming uncorrelated photon cross sections and uncertainty of 0.25 % from $(\frac{W}{e})_{air}$ variation with beam quality, the combined relative uncertainty in calculated k_Q factors amounts to 0.72 %. These values are similar to those determined by Wulff *et al.*[72] who also estimated uncertainties in calculated k_Q factors for the NE2571 chamber, although there are many small differences between their approach and the one taken in this work. For cylindrical chambers in all groups, the combined relative systematic uncertainties in k_Q calculations of this work are in table 4.3. Assuming correlated photon cross sections and negligible $(\frac{W}{e})_{air}$ variation with beam quality, systematic uncertainties in calculated k_Q factors for cylindrical chambers are between 0.28 and 0.39 %. With conservative assumptions, the systematic uncertainty estimates increase to between 0.71 and 0.9 %.

As with cylindrical chambers, systematic uncertainties are estimated on calculated k_Q factors for plane-parallel chambers in photon beams. For plane-parallel chambers, only the realistic situation that photon cross sections are correlated is considered such that they introduce a negligible component of uncertainty in k_Q calculations. A sample uncertainty budget is provided for the IBA NACP-02 chamber in table 4.4. Again, the statistical uncertainty on k_Q calculations is less than 0.1 % and the accuracy of `EGSnrc` for calculations of ion chamber response with respect to its own cross sections is 0.1 %.

The largest component of uncertainty in k_Q factors from stopping power variation is 0.16 % when changing the I-value of the graphite wall. This is not surprising since the NACP-02 chamber is composed mostly of graphite. The overall effect on k_Q calculations when changing stopping powers by varying I-values is 0.19 %.

When the thickness of the graphite window of the chamber model is varied by

Table 4.4: Sample uncertainty budget for Monte Carlo calculated k_Q factors for the plane-parallel IBA NACP-02 chamber. Modified from paper IV.

Source	Uncertainty in k_Q (%)
Stopping Powers (%ΔI)	
Mylar (5)	0.08
Rexolite (5)	0.02
Graphite (4.5)	0.16
Air (2.5)	0.04
Water (1.5)	0.04
Combined (Stopping powers)	0.19
Chamber dimensions	
Graphite window (±0.1 mm = 20 %)	0.11
MYLAR cover (+0.1 mm = 100 %)	0.02
Collector spacing (±0.3 mm)	0.10
Guard width (or r_{eff})	0.11
Combined (Dimensions)	0.19
Others	
Source Model	0.06
Statistical Uncertainty	0.06
`EGSnrc`[48]	0.10
Combined uncertainty without W/e	0.30
Uncertainty from W/e (see Ch. 5)	0.25
Combined uncertainty	0.39

20 %, the resulting effect on k_Q is only 0.11 % and if the thickness of MYLAR cover on the chamber window is doubled the effect on k_Q is negligible. There is some confusion about whether the graphite density in the front window of the NACP-02 chamber is 1.7 g/cm^3 as specified by the manufacturer or 2.25 g/cm^3 as suggested by Chin *et al.*[100] Calculations of k_Q using the two graphite densities differing by 26 % are different by up to 0.3 %. However, it is very unlikely that the manufacturer would use grain graphite density (2.25 g/cm^3) since it is much more expensive than bulk graphite density which performs just as well in the window of an ion chamber. In addition, for paper V the graphite density from the window of a sacrificed NACP-02

chamber is measured at NRC and amounts to 1.7 g/cm^3. Therefore, no component of uncertainty in calculated k_Q factors is assumed from variations in graphite density since we are fairly confident in the manufacturer specification of 1.7 g/cm^3. It was noted above that the back wall specifications used for the NACP-02 chamber model affect k_Q calculations by up to 0.2 % but since the manufacturer's blueprints are used to model this chamber, no component of uncertainty in k_Q calculations from this effect is included. Changing the dimensions of the NACP-02 air cavity, by either changing the collector spacing by 0.3 mm (15 %) or performing the calculation without a guard (effectively changing the radius of the active cavity by 60 %) results in a maximum effect on k_Q of 0.11 %. The combined uncertainty from possible uncertainties in specifications of the chamber model is 0.19 %.

The effect of using a more accurate `BEAMnrc` source model instead of a collimated point source from photon spectra is tested and the effect on k_Q calculations for the NACP-02 chamber is less than 0.1 %. This is also investigated for the Exradin A11 and A10 chambers that use steel screws for chamber construction, and the resulting effects on k_Q are less than 0.14 %. For the rest of the plane-parallel chambers, the uncertainty in k_Q calculations from the source model is taken as the average of the variation in k_Q when using different source models for the three chambers investigated. The k_Q factors determined here and for cylindrical chambers in photon beams are for spectra from filtered beams. To investigate differences for accelerators that do not include a flattening filter, calculations of k_Q are performed for six unfiltered beams covering the energy range of interest for plane-parallel IBA NACP-02 and Exradin A10 chambers and cylindrical NE2571 and Exradin A12 chambers. For all of these chambers, including the A10 chamber that includes steel screws in the model which might make it more sensitive to beam filtration, k_Q calculations are within 0.2 % of the fit to calculated values using filtered beams.

Table 4.5: Combined uncertainty in Monte Carlo calculated k_Q factors for plane-parallel chambers. Uncertainty in calculated k_Q factors from possible variation in $(W/e)_{air}$ with beam quality is assumed to be 0.25 % as estimated in chapter 5. Modified from paper IV.

Chamber	Combined uncertainty without W/e	Combined uncertainty with W/e component
Exradin		
A11	0.36	0.44
P11	0.43	0.50
P11TW	0.40	0.47
A10	0.32	0.41
IBA		
NACP-02	0.30	0.39
PPC-05	0.37	0.45
PPC-40	0.24	0.34
PTW		
Roos	0.24	0.34
Markus	0.32	0.40
Advanced Markus	0.34	0.42

The combined systematic uncertainty in k_Q factors for plane-parallel chambers in photon beams is again dependent on assumptions made. If no component of uncertainty from $(\frac{W}{e})_{air}$ variation with beam quality is assumed, the overall uncertainty in k_Q factors for the NACP-02 chamber is 0.3 %. For all plane-parallel chambers, the overall systematic uncertainty in k_Q calculations is tabulated in table 4.5 and, depending on the chamber type, amounts to between 0.24 and 0.43 % if $(\frac{W}{e})_{air}$ variation is ignored. If a component of uncertainty in k_Q calculations from potential $(\frac{W}{e})_{air}$ variation with beam quality estimated to be 0.25 % in chapter 5 is assigned for plane-parallel chambers, the overall systematic uncertainty in calculated k_Q factors is between 0.34 and 0.5 % depending on the chamber model.

4.4 Summary

Monte Carlo calculated k_Q factors for cylindrical and plane-parallel chambers in photon beams are presented. These results for cylindrical chambers are being used in the addendum[12] to the AAPM's TG-51 protocol. The calculated results of this work are compared to literature values where available and are well within 0.8 % of all measured and calculated results for k_Q factors. The differences between the present values and those recommended in current dosimetry protocols are explained with the use of more accurate Monte Carlo calculated individual correction factors. Systematic uncertainties in Monte Carlo calculated k_Q factors are analyzed and the combined overall uncertainty in k_Q calculations is less than 0.9 % using conservative assumptions but less than 0.5 % if more realistic assumptions are made for all chambers investigated.

Chapter 5

Comparison of measured and calculated k_Q factors in photon beams and $(W/e)_{air}$ variation

In this chapter, a thorough comparison of high-quality measured k_Q factors[34] to the calculated values of this work is presented for cylindrical chambers, representing the largest data set of overlapping cylindrical ion chambers ever investigated. This was the focus of paper III, which also provided additional consistency checks to verify the accuracy of the k_Q factors determined in each study but the focus here is on comparison of the two data sets. The results of this work for measured and calculated k_Q factors for plane-parallel chambers in photon beams are also compared. Using the entire data set consisting of both cylindrical and plane-parallel chambers, an upper limit on the variation of $(W/e)_{air}$ with photon beam quality is analyzed to give the first quantitative uncertainty estimate on calculated k_Q factors in photon beams from the variation of $(W/e)_{air}$ with beam quality.

5.1 Motivation

Prior to the study of McEwen,[34] measured k_Q factors had been determined using water calorimetry[18,96,97,101–103] or Fricke dosimetry[104–107] but only for a few chamber

types. Additionally, many of the measured values suffer from large uncertainty (in most cases >0.5 %) or use Fricke chemical dosimetry, which must be corrected for intrinsic energy dependence. McEwen[34] published k_Q factors with low systematic uncertainties (typically 0.3 %) for a large number (27) of cylindrical chamber types.

Calculated photon beam k_Q factors were also determined in other publications[31,66–68] using a very similar approach to that presented above but for a small subset of chambers and, in the case of the work of González-Castaño *et al.*,[66] with much larger statistical uncertainties. Therefore, the focus of this chapter is on comparison of the calculated photon beam k_Q factors of this work and the measured values of McEwen[34] for cylindrical chambers. The measured and calculated values for plane-parallel chambers determined here are also compared in this chapter as they represent the largest data set of photon beam k_Q factors for plane-parallel chambers. However, in chapter 4 the calculated results of this work are compared to those from several other investigations for the chambers for which literature data are most extensive and, additionally, technical report II shows the calculated results with many available experimental and calculated values of k_Q for all of the cylindrical ion chambers simulated in this work.

Monte Carlo calculated k_Q factors represent the ideal chamber using specifications provided by the chamber manufacturers. Therefore, if a given chamber behaves exactly as the manufacturer intends, Monte Carlo calculated k_Q factors should give accurate results for reference dosimetry. Measured values of k_Q are relevant for the specific chamber for which the measurements were performed - for most chamber types investigated by McEwen[34] k_Q factors were determined for only one to three chambers of each type. For the chamber types for which more than one chamber was characterized, McEwen[34] did not observe variability of k_Q factors outside of systematic uncertainties. Although generally not significant for cylindrical ion chambers as demonstrated by McEwen[34] as well as NPL data[108] for a large set of

NE2561/2611 chambers and the data for multiple chambers in Seuntjens *et al.*,[18] if there are chamber-to-chamber variations for chambers of the same type, agreement between measured and calculated k_Q factors may be fortuitous. In particular, agreement between measured and calculated k_Q factors for a single chamber cannot be taken as demonstrating that the measured data are typical of the chamber type as a whole. However, by analyzing the results for the large number of different chambers as a single data set, one can make stronger statements than would otherwise be possible.

As discussed above, potential variation of $(W/e)_{air}$ with beam quality is still an important topic. The analysis of Svensson and Brahme[15] suggests that $(w(E)/e)_{air}$, the energy lost in air per Coulomb of charge released by electrons of a specific average energy, may vary by up to 1.5 %.[15] However, in that work, the stopping power ratios used to reanalyze previous measured data were for monoenergetic electrons, not reflecting those for electrons crossing the cavity from the accelerators used for the original experiments. If $(W/e)_{air}$ does vary with beam quality, a significant component of uncertainty is introduced in both the Monte Carlo calculated values of k_Q obtained with equation 2.6 as well as those published in dosimetry protocols.[10,17] Experimental determination of k_Q does not require the assumption that $(W/e)_{air}$ be constant with photon energy, unlike determination via Monte Carlo simulation. Comparing experimental and Monte Carlo values of k_Q allows a realistic analysis of the upper limit on the variation of $(W/e)_{air}$ between cobalt-60 and up to the highest measured beam energy of 25 MV.

Table 5.1: Percent difference $\left(\Delta = \frac{k_Q(calc.)-k_Q(meas.)}{k_Q(meas.)}\right)$ between experimental[34] and Monte Carlo calculated k_Q factors for cylindrical chambers for each energy and chamber. Chambers that are suitable for reference dosimetry are in italics. Chamber wall and electrode (el.) materials are given in brackets. The χ^2/df is calculated at all energies for each chamber and for all chambers at each energy. Modified from paper III.

chamber (wall,el.)	nominal MV/%$dd(10)_x$			χ^2/df (all energies)
	6/67.2	10/72.6	25/84.4	
	Δ (%)			
Exradin				
A12 (C552, C552)	-0.22	-0.33	-0.62	0.83
A19 (C552, C552)	-0.17	-0.27	-0.70	0.90
A12S (C552, C552)	-0.26	-0.11	-0.49	0.50
A18 (C552, C552)	-0.38	-0.27	-0.59	0.86
A1SL (C552, C552)	-0.28	-0.28	-0.54	0.65
A14SL (C552, SPC)	-0.18	-0.22	0.14	0.07
A16 (C552, SPC)	0.09	-0.10	0.22	0.03
PTW				
30010 (PMMA/Gr, Al)	0.15	0.12	0.00	0.06
30012 (Gr, Al)	0.12	0.24	0.00	0.15
30013 (PMMA/Gr, Al)	0.16	0.37	0.16	0.34
31013 (PMMA/Gr, Al)	0.00	0.33	0.21	0.28
31010 (PMMA/Gr, Al)	0.28	0.81	0.23	0.74
31016 (PMMA/Gr, Al)	-0.32	-0.05	-0.21	0.11
31014 (PMMA/Gr, Al)	0.06	-0.06	-0.45	0.19
IBA				
FC65-G (Gr, Al)	-0.01	-0.12	-0.15	0.07
FC65-P (POM, Al)	0.10	-0.08	-0.04	0.03
CC25 (C552, C552)	-0.27	-0.22	-0.30	0.32
FC23-C (C552, C552)	-0.07	-0.14	-0.16	0.07
CC13 (C552, C552)	-0.13	0.02	-0.02	0.03
CC08 (C552, C552)	-0.21	-0.02	-0.18	0.11
CC04 (C552, C552)	0.03	-0.06	-0.08	0.01
CC01 (C552, Steel)	-0.08	-1.05	-0.87	1.97
NE				
2581 (A150, A150)	-0.12	-0.05	-0.48	0.35
2571 (Gr, Al)	-0.16	-0.19	-0.45	0.52
2611 (Gr, Al)	-0.05	0.24	-0.28	0.25
Capintec				
PR06C (C552, C552)	-0.16	-0.26	-0.36	0.33
χ^2/df (all chambers)	0.14	0.39	0.60	
χ^2/df (ref. chambers)	0.17	0.35	0.63	

5.2 Comparison results

The percent differences between experimental and calculated k_Q values for each chamber and for each energy are calculated for chamber i as

$$\Delta_i = \frac{k_{Q,i}(calculated) - k_{Q,i}(measured)}{k_{Q,i}(measured)} \times 100\%, \tag{5.1}$$

so that a negative percent difference indicates a higher measured than calculated k_Q factor. The χ^2 per degree of freedom (df), χ^2/df, for each chamber and for each energy is determined via

$$\chi^2/df = \frac{1}{f}\sum_{i=1}^{f}\frac{\Delta_i^2}{s_m^2 + s_c^2}, \tag{5.2}$$

where f is the number of degrees of freedom (3 beams for each chamber or 26 [10] chambers for each energy for cylindrical [plane-parallel] chambers), and s_m and s_c are the standard percentage uncertainties on the measured and calculated k_Q factors, respectively. The systematic uncertainties on the calculated values, s_c, are those in tables 4.3 (p. 70) for cylindrical chambers and 4.5 (p. 74) for plane-parallel chambers, assuming correlated photon cross sections and ignoring possible $(W/e)_{air}$ variation with beam quality.

Table 5.1 shows the percent difference between measured and calculated k_Q factors for cylindrical chambers in photon beams with the χ^2/df at all energies for each chamber and for all chambers at each energy. For cylindrical chambers, the χ^2/df, i.e., reduced χ^2, is less than 1.0 for all chambers at each energy, indicating agreement between experimental and Monte Carlo calculated k_Q values. There is a 0.13 % mean percent difference for the entire data set with a sample % RMS deviation of 0.31 %. The χ^2/df for the whole data set of cylindrical chambers is only 0.38, suggesting

good agreement between measured and calculated k_Q factors or that the already low values of systematic uncertainties are overestimated. Calculating the reduced χ^2 for each chamber by summing over energies results in only one chamber with a reduced χ^2 larger than unity, indicating a significant discrepancy for that chamber. This chamber, the IBA CC01, does not meet the specifications for a reference-class ion chamber[12,34] and this type of deviation is perhaps expected.

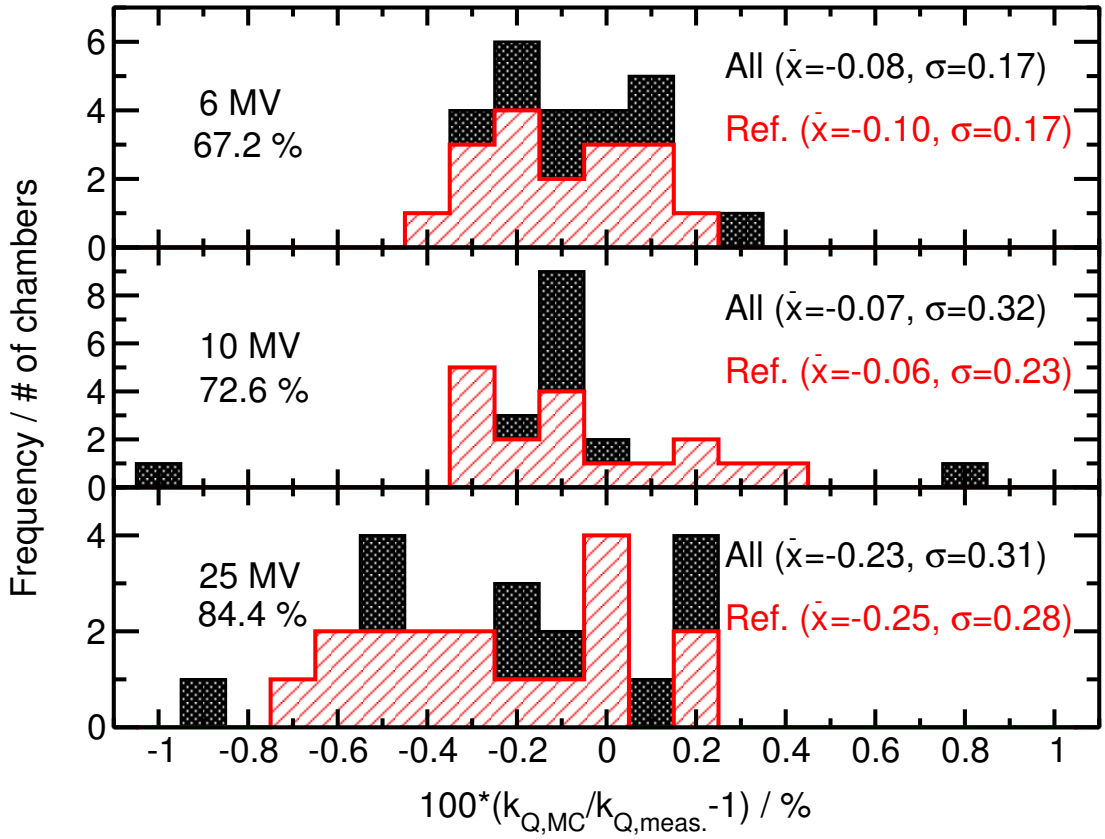

Figure 5.1: Histograms comparing measured k_Q values of McEwen[34] to those calculated in this work for cylindrical chambers in photon beams. There are 17 chambers in the reference set (light hashed area) and 26 in the full set of chambers (dark area), which includes chambers not suitable for reference dosimetry. From paper III.

Figure 5.1 presents histograms for each beam quality of the percent differences between experimental and Monte Carlo calculated k_Q factors for the entire overlap of cylindrical chambers between the two data sets, as well as histograms showing

the subset of chambers considered suitable for reference dosimetry. The mean and standard deviation of the sample is displayed on each plot. Overall, the agreement is very good with some outliers, mostly those chambers that are not suitable for reference dosimetry. However, even with these outliers, the maximum percent difference between experimental and calculated k_Q values is only 1.05 %. At 6 MV, the mean percent difference is -0.08 and -0.10 % for all and reference chambers only, respectively, with a very tight distribution; the standard deviation of the sample is 0.17 % for both samples. For the 10 MV beam, the mean percent difference is -0.07 or -0.06 for all and reference chambers, respectively. The standard deviation of the sample is slightly larger than that for the 6 MV beam, being 0.32 % for the entire sample and 0.23 % for reference chambers. Both distributions have a mean percent difference very close to zero and much less than the standard combined uncertainty of both studies, indicating the excellent agreement between the two data sets. However, at 25 MV the mean percent differences are -0.23 and -0.25 % with a standard deviation of the sample of 0.31 and 0.28 % for the entire sample and only reference chambers, respectively. Again, this deviation is less than the combined standard uncertainty in both studies but does indicate a systematic difference between the two data sets, with the Monte Carlo calculated values being lower on average than the experimentally determined values at high energy.

All of the Monte Carlo calculated k_Q factors for the Exradin C552-walled cylindrical ion chambers are significantly lower than the experimental values. The C552-walled chambers of IBA do not exhibit such a large discrepancy. To investigate this discrepancy, a sample of the C552 used for the Exradin chambers was obtained from the manufacturer. Chemical analysis, using X-ray fluorescence, showed some differences in composition to that being used for the Monte Carlo calculations but additional simulations performed using this composition of C552 gave k_Q values that

Table 5.2: As in table 5.1 but for plane-parallel chambers. Modified from paper IV.

chamber	nominal MV/%$dd(10)_x$			χ^2/df (all energies)
	6/67.2	10/72.6	25/84.4	
	Δ (%)			
Exradin				
A11	-0.19	-0.17	-0.66	0.54
P11	-0.17	0.07	-0.42	0.20
P11TW	0.00	0.25	-0.49	0.31
A10	-0.32	-0.11	-0.32	0.24
IBA				
NACP-02	0.14	0.30	0.05	0.13
PPC-05	-0.01	0.10	-0.35	0.14
PPC-40	0.01	0.43	0.52	0.63
PTW				
Roos	0.19	0.28	0.04	0.15
Markus	0.27	0.64	0.49	0.82
Advanced Markus	-0.12	0.12	-0.17	0.06
χ^2/df (all chambers)	0.10	0.32	0.55	

are unaffected within the statistical uncertainty of the calculations. Perhaps what is most surprising is that all of the Exradin chambers are modelled in detail from blueprints, so one might expect that with more accurate modelling these chambers would show better agreement with experimental results compared to chambers from other manufacturers. Except for the CC01 chamber, information about the composition and specifications of the IBA chamber stems have not been made available, so these chambers are modelled with a solid C552 stem. As discussed above, for some cylindrical Exradin chambers (the Exradin A12, A19, A2 and A18) simplified models have been created and the results compared to those obtained using models from chamber blueprints. For the Exradin A12, A2 and A18 chambers, the calculated results using *simplified* models are up to 0.2 % *closer* to measured results than calculations performed using blueprint models while, for the Exradin A19 chamber, the difference is up to 0.4 % in the highest energy beam. Therefore, it appears that the

k_Q factors calculated for IBA C552-walled chambers (which use very simple models for the stem) exhibit misleading agreement with experimental values. A larger discrepancy is expected between experimental and Monte Carlo calculated k_Q factors for C552-walled IBA chambers with a more realistic stem; this topic is discussed below in the context of possible variation in $(W/e)_{air}$.

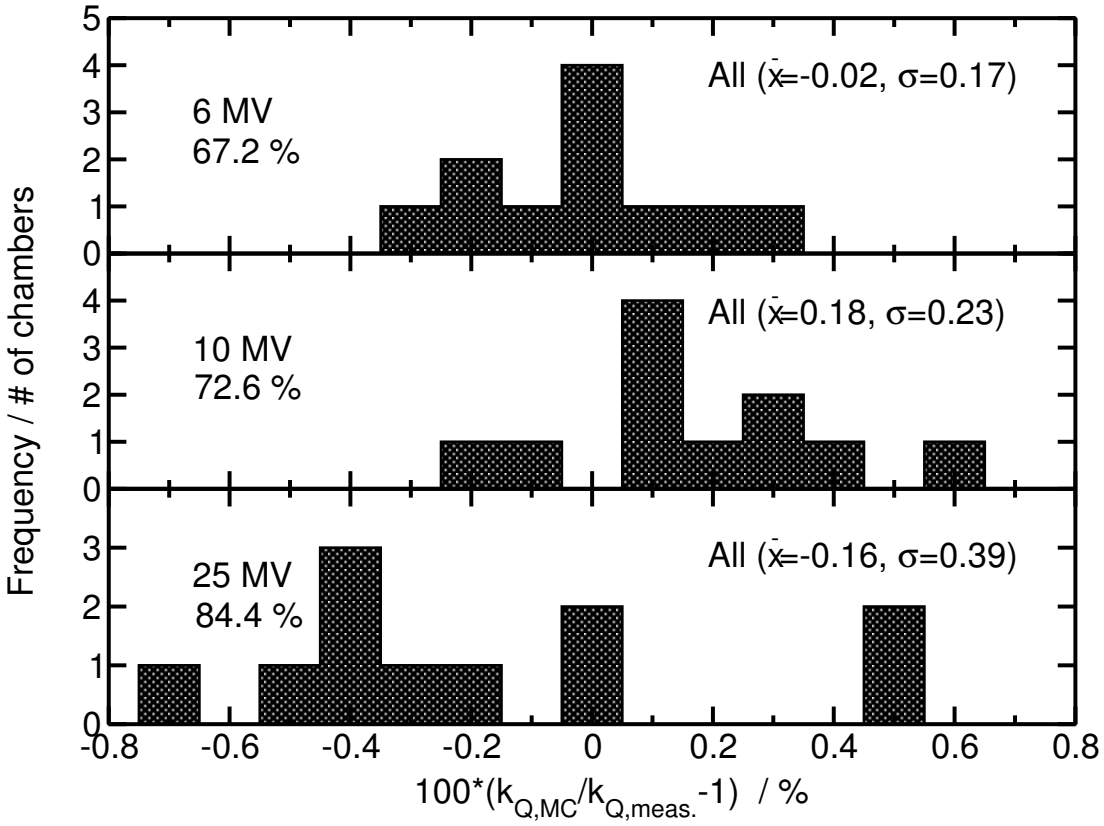

Figure 5.2: As in figure 5.1 but for the measured and calculated k_Q factors determined for plane-parallel chambers in photon beams in this work. No distinction is made between reference and non-reference class plane-parallel chambers. From paper IV.

Figure 5.2 provides histograms showing the percent difference between measured and calculated k_Q factors determined in this work for plane-parallel chambers at each measured beam quality. Table 5.2 shows the percent difference between measured and calculated k_Q factors for plane-parallel chambers in photon beams with the χ^2/df at all energies for each chamber and for all chambers at each energy. For plane-parallel

chambers, the reduced χ^2 is less than unity for all chambers when the sum is over energies and for all energies when the sum is over chambers. The χ^2/df for the entire data set of plane-parallel chambers is 0.3 which again indicates excellent agreement between k_Q calculations and measurements and that the low estimates of systematic uncertainty are reasonable or possibly conservative. Among all energies, only three data points disagree by more than 0.5 %. Average percent differences are -0.02, 0.18 and -0.16 % for 6, 10 and 25 MV beams with standard deviations about the means of 0.17, 0.23 and 0.39 %, respectively. Percent RMS deviations from zero are 0.17, 0.29 and 0.40 % for the 6, 10 and 25 MV beams, respectively, with a % RMS deviation of 0.31 % for the entire data set (all energies). These results indicate systematically lower Monte Carlo calculated k_Q factors in the highest-energy beam but with a 1.2 % spread in the differences. In addition, in the high-energy beam all of the Exradin chambers have calculated k_Q factors systematically lower than measured values. This is the same trend as that for cylindrical chambers discussed above even though the geometries for Monte Carlo calculations with the plane-parallel chambers are independently modelled and very different from the cylindrical chambers.

5.3 The upper limit of $(W/e)_{air}$ variation with beam quality

If there is variation in $\frac{W}{e}$ from cobalt-60 to 25 MV beam energies, then the equation used for the determination of Monte Carlo calculated k_Q factors becomes

$$k_Q = \alpha \left(\frac{D_w}{D_{ch}} \right)_{Co}^{Q}, \tag{5.3}$$

where $\alpha = \left(\frac{W}{e}\right)_{Co}^{Q}$. Replacing Δ_i in equation 5.1 with

$$\Delta_i = \frac{\alpha \times k_{Q,i}(calculated) - k_{Q,i}(measured)}{k_{Q,i}(measured)} \tag{5.4}$$

and calculating χ^2 for the 25 MV beam as a function of α, one obtains figure 5.3 for the subset of reference cylindrical chambers. Since paper III was accepted before the results of paper IV were obtained, this analysis was performed separately for cylindrical reference chambers, the entire data set of cylindrical chambers and plane-parallel chambers. Although the values of χ^2_{min} are different for the subset of reference cylindrical chambers and all cylindrical chambers, the same value of α is obtained for both data sets. The uncertainty on this value is determined by taking the corresponding values of α for $\chi^2_{min}+1$,[109] giving α=1.0024±0.0011, which is independent of the data set used. Finally, assuming that the value of α is normally distributed and using the quantiles of the Normal distribution from Brandt,[110] an upper limit on the variation of $\left(\frac{W}{e}\right)^{25MV}_{Co}$ is obtained as 1.0029, 1.0038 and 1.0042 with confidence levels of 68 %, 90 % and 95 %, respectively. The limit on the variation for the lower energies is less. At the 95 % confidence level, the lower limit on the value of $\frac{W}{e}$ is 1.0006 indicating that $\frac{W}{e}$ does not decrease with beam quality.

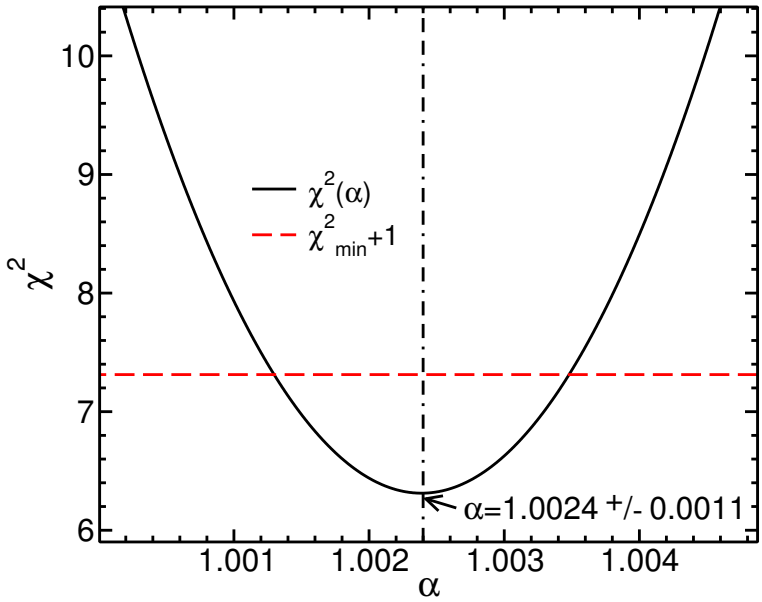

Figure 5.3: Estimation, using equations 5.2 and 5.4, of the upper limit on the variation of $\frac{W}{e}$ with beam quality for the subset of 17 reference cylindrical chambers. The variable α represents the ratio $\left(\frac{W}{e}\right)^{Q}_{^{60}Co}$. From paper III.

This analysis takes no special account of the differences between IBA and Exradin C552-walled ion chambers. To test the effect of using simplified IBA chamber models on the upper limit on the variation of $\frac{W}{e}$ with energy presented above, the method is repeated after reducing Monte Carlo calculated k_Q factors for IBA C552-walled chambers by 0.2 %, the amount suggested by the difference in k_Q factors calculated with blueprint and simplified Exradin chamber models. In the worst case (using only the subset of reference chambers) the results yield an upper limit on $\left(\frac{W}{e}\right)_{Co}^{25MV}$ of 1.0032, 1.0041 and 1.0045 with confidence levels of 68 %, 90 % and 95 %, respectively. This indicates that using simplified models for the IBA chamber stems has an insignificant effect on the above analysis.

Performing the same analysis with plane-parallel chambers yields $\alpha = 1.0012 \pm 0.0017$. As with cylindrical chambers, α is assumed to be normally distributed to obtain an upper limit on $\left(\frac{W}{e}\right)_{Co}^{25MV}$ as 1.0020, 1.0034 and 1.0040 with 68, 90 and 95 % confidence, respectively. The small sample (10) of plane-parallel chamber types indicates that the assumption that α is normally distributed might be a poor one and the uncertainty on the value of α is slightly higher compared with that obtained for cylindrical chambers. However, the results from data sets for cylindrical and plane-parallel chambers are consistent in terms of the percent difference for the 25 MV beam and the value of α. This is impressive since the experimental method[34] required some modifications to adapt it to plane-parallel chambers and the Monte Carlo models for plane-parallel chambers are very different from those used for cylindrical chambers. Minimizing $\chi^2(\alpha)$ with the entire data set, including plane-parallel and reference-type cylindrical ion chambers, a value of $\alpha = 1.0021 \pm 0.0009$ is obtained giving our best estimate of the upper limit of $\left(\frac{W}{e}\right)_{Co}^{25MV}$ as 1.0025, 1.0033 and 1.0036 with 68, 90 and 95 % confidence, respectively. Again, at the 95 % confidence level the lower limit on α is 1.0006 indicating that $\left(\frac{W}{e}\right)_{Co}^{25MV}$ does not decrease with beam quality.

Previously, the question regarding what to take as the uncertainty from possible variation of $(W/e)_{air}$ with beam quality in Monte Carlo calculated k_Q factors remained unanswered. The upper limit of the variation of $(W/e)_{air}$ from cobalt-60 to 25 MV at the 68 % confidence level calculated here is taken as the worst case estimate of the uncertainty from potential variation of $(W/e)_{air}$ with beam quality on Monte Carlo calculated k_Q factors in chapter 4.

5.4 Summary

Overall, outstanding agreement is observed between experimental and Monte Carlo calculated beam quality conversion factors for cylindrical chambers. Mean percent differences for the entire combined data set of cylindrical chambers are -0.08, -0.07 and -0.23 % with standard deviations of 0.17, 0.32 and 0.31 % for 6, 10 and 25 MV beams, respectively. There is a 0.13 % mean percent difference for the entire data set with a sample % RMS deviation of 0.31 %. The χ^2/df for the whole data set is only 0.38. The agreement is well within the estimated uncertainties and suggests that on the whole the chambers investigated experimentally are representative of the individual types.

Although within uncertainties, systematic differences are noted between experimental and Monte Carlo calculated k_Q factors for the Exradin C552-walled chambers. Despite some measures that have been taken to determine the source of the difference, further research is required to explain the discrepancies.

Excellent agreement is observed between measured and calculated k_Q factors for plane-parallel chambers - average percent differences are -0.02, 0.18 and -0.16 % with standard deviations of 0.17, 0.23 and 0.39 % for 6, 10 and 25 MV beams, respectively. The χ^2/df for the entire data set of plane-parallel chambers is 0.3 suggesting excellent agreement and that the low uncertainty estimates are possibly conservative.

Indeed, this level of agreement is somewhat surprising given the variations observed in repeated calibration measurements for plane-parallel chambers.

Using the cylindrical chamber data set, an upper limit on the variation of $(W/e)_{air}$ from cobalt-60 to 25 MV beam energies is determined to be 0.42 % with 95 % confidence (0.29 % with 68 % confidence). If the IBA cylindrical ion chamber calculations are adjusted to include the effect of using a model with a detailed stem, this upper limit changes by only 0.03 % indicating an insignificant effect from the amount of detail in the chamber stem in this situation.

Similarly, the upper limit of variation of $(W/e)_{air}$ with beam quality is investigated for the data set of plane-parallel chambers and amounts to 0.20, 0.34 and 0.40 % with 68, 90 and 95 % confidence, respectively. This is lower than that for cylindrical chambers. However, fewer chambers and chamber types are investigated for plane-parallel chambers and the analysis yields a higher uncertainty. The combined data set consisting of plane-parallel and reference cylindrical ion chambers is used to obtain a best estimate of the upper limit on the variation of $(W/e)_{air}$ with beam quality between ^{60}Co and 25 MV as 0.25, 0.33 and 0.36 % with 68, 90 and 95 % confidence, respectively. The result for the upper limit on the variation of $(W/e)_{air}$ with beam quality at the 68 % confidence level calculated here is used for a final assessment of the uncertainty on Monte Carlo calculated k_Q factors in chapter 4.

Monte Carlo calculated k_Q factors reflect general chamber dimensions as given by the manufacturer while experimental k_Q factors are relevant for the specific ion chamber for which measurements were made. Measured k_Q factors obtained for the user's specific ion chamber would still be more accurate but the exceptional agreement observed here has given the AAPM Working Group confidence in adopting the Monte Carlo calculated k_Q factors of this work for cylindrical chambers for its update to the TG-51 dosimetry protocol.[12]

Chapter 6

Monte Carlo calculations for electron beam reference dosimetry

The focus of this chapter is on Monte Carlo calculations for electron beam reference dosimetry with the PTW Roos and NE2571 chambers. Similar results for several other plane-parallel and cylindrical ion chambers are presented in paper VII. Plane-parallel chambers are recommended for reference dosimetry of low-energy electron beams (E_0 <10 MeV) so literature data are most readily available for the commonly used PTW Roos chamber. Historically, cylindrical ion chambers were not recommended for reference dosimetry of these low-energy electron beams because of potential uncertainties in large replacement correction factors at the reference depth. Given the problems with plane-parallel chambers indicated in chapter 3 in photon beams and similar stability issues discussed in appendix B in electron beams, there is interest in characterizing the use of cylindrical chambers in low-energy electron beams. Determination of k_Q factors with equation 2.6 (p. 28) removes the need for knowledge of any of the individual correction factors that were historically required to indirectly calculate k_Q. Therefore, in this chapter, Monte Carlo calculations as a function of depth are used to investigate dosimetric parameters, such as R_{50}, and determine beam quality conversion factors in clinical electron beams for the plane-parallel PTW Roos chamber for comparison to literature data and the cylindrical Farmer-type NE2571

chamber to characterize its use for electron beam reference dosimetry.

6.1 Comparison of R_{50} determined with D_w to that from D_{ch}

As discussed in chapter 1, current dosimetry protocols[10,17] use R_{50}, the depth at which the absorbed dose falls to 50 % of its maximum value, to specify beam quality for electron beams. In practice, the results of Ding *et al.*[23] are used to convert from I_{50}, the depth at which the measured ionization falls to 50 % of its maximum value to R_{50} (for R_{50} <10 cm) with

$$R_{50} = 1.029 I_{50} - 0.063 \quad \text{(cm)}, \tag{6.1}$$

which is based on calculations of absorbed dose to water and water-to-air stopping power ratios and therefore assumes a perturbation-free ionization chamber without walls, stem or central electrode.

The use of equation 6.1 to convert from I_{50} to R_{50}, where I_{50} is determined using calculations of D_{ch} vs. depth with full ion chamber simulations, gives results which are systematically different by up to 1 mm compared to R_{50} determined using calculations of absorbed dose to water as a function of depth in water. These chamber simulations use the TG-51[10] protocol recommendations to define the point of measurement (the inside of the front face for the Roos chamber and the center of the cavity with a 0.5 r_{cav} shift upstream to determine R_{50} from the NE2571 calculations). The observed differences could be from including the full model of the chamber (equation 6.1 was developed assuming a perturbation-free ion chamber) or from differences between the `EGSnrc` calculations of this work compared to the `EGS4` calculations used by Ding *et al.*[23]

To investigate the source of this discrepancy, the approach of Ding *et al.*[23] - converting from depth-dose calculations to depth-ionization using calculated stopping power ratios - is used to calculate R_{50} as a function of I_{50} for 12 electron beams (7 `BEAMnrc` models and 5 spectra). The resulting relationship is linear with an equation of best fit of $R_{50} = 1.026(\pm 0.003)I_{50} - 0.046(\pm 0.014)$, which is similar to equation (5) of Ding *et al.*[23] (equation 6.1 above), indicating that the observed difference between R_{50} calculated using water and chamber simulations results from including the full model of the ion chamber.

It is found that a shift of the depth-ionization data, different from that recommended by TG-51,[10] can be used to minimize the differences between R_{50} calculated in a water only phantom to that using chamber simulations with equation 6.1 to convert I_{50} to R_{50}. Based on results from 44 beams, the shift is determined to be 1.55±0.03 mm from the front face for the PTW Roos chamber, i.e., the point of measurement is shifted from the back of the front wall into the cavity by 0.42 mm. With the results from 47 beams for the NE2571 chamber, the required shift to minimize the differences between R_{50} determined with water and chamber simulations is $0.34(\pm 0.01)\ r_{cav}$ compared to the shift of $0.5\ r_{cav}$ recommended by TG-51.[10] Using these results, the differences between R_{50} determined with water and chamber simulations for either chamber is less than 0.5 mm for all beams investigated compared to differences of up to 1 mm if the TG-51[10] prescription ($0.5\ r_{cav}$) is used or 2 mm if no shift is used for determination of R_{50} using the NE2571 calculations. The optimal shift causes the overall ion chamber perturbation factor, P_{Q}, (equation 1.5, p. 6) to approach unity at all depths including I_{50} resulting in improved agreement when equation 6.1 is used to convert I_{50} to R_{50} compared to R_{50} calculated in a water only phantom. This topic is discussed further in appendix C.

6.1. COMPARISON OF R_{50} DETERMINED WITH D_W TO THAT FROM D_{CH}

6.2 Beam quality conversion factors

Beam quality conversion factors for the PTW Roos chamber: Figure 6.1 shows beam quality conversion factors, $k_{R_{50}}$, (equation 1.12 [p. 15] with the assumption that P_{gr}^{Q}=1 for the well-guarded PTW Roos chamber) as a function of R_{50} for the PTW Roos chamber calculated using different source models and different effective points of measurement.

A systematic difference is observed between results calculated using realistic `BEAMnrc` accelerator simulations compared to those using electron beam spectra. This discrepancy increases to up to 0.5 % with increasing beam energy. Calculations of $k_{R_{50}}$ factors using the same `BEAMnrc` accelerator simulations but only including electrons incident on the phantom from the `BEAMnrc` simulation are in agreement with the results that use electron beam spectra indicating that the difference is from contaminant photons from the realistic accelerator simulations. The `BEAMnrc` models of electron beams shown in table 2.4 (p. 38) have bremsstrahlung tails up to 5 % whereas the `BEAMnrc` models that only include electrons from the accelerator or sources modelled from electron beam spectra have bremsstrahlung tails of less than 1 % from interactions occurring in the phantom. An increase in calculated water-to-air stopping power ratios at the reference depth with increasing bremsstrahlung tail was also observed by Ding *et al.*,[23] as shown in figure 18 of that work. Using lower energy electron beam spectra with R_{50} up to 6.5 cm, the differences between k_Q factors calculated using `BEAMnrc` simulations or electron beam spectra are not as significant and are on the order of the scatter observed using only `BEAMnrc` simulations. Similar results are observed for calculations using the NE2571 chamber. Since simulations using electron beam spectra take much less time than running full `BEAMnrc` accelerator simulations, electron beam spectra are still used to obtain results. For the remain-

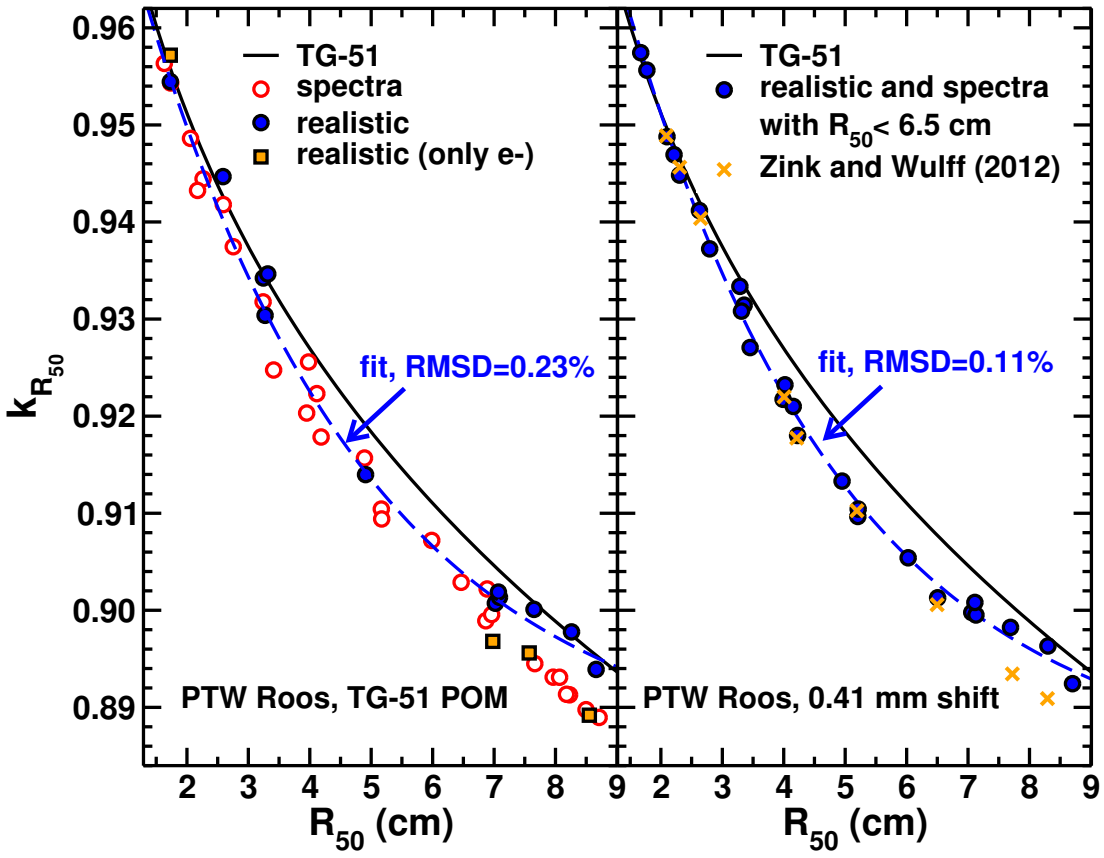

Figure 6.1: Beam quality conversion factors at d_{ref} using different electron beam source models for the PTW Roos chamber. Data from this work are obtained with realistic BEAMnrc simulations (filled dark circles), realistic BEAMnrc simulations that include only electrons incident on the phantom (filled light squares) and collimated point sources using electron beam spectra (open circles). Error bars representing statistical uncertainties are smaller than the size of the symbols. The left panel shows results obtained when the inside of the chamber's front window is used for the point of measurement (TG-51 approach). The right panel shows results using an optimal shift of the data, for realistic simulations (filled dark circles), including all results from realistic BEAMnrc simulations in the left panel and all electron beam spectra with R_{50} less than 6.5 cm. Data from TG-51[10] and Zink and Wulff[26] (light x) are shown for comparison. From paper VI.

der of this chapter, the presented results use electron beam spectra for beams with R_{50} ≤6.5 cm and use BEAMnrc accelerator models at all energies. If, however, there are calculations that use a BEAMnrc model and electron beam spectra representing the same accelerator, only the results obtained using the BEAMnrc accelerator model

are used.

Aside from the systematic differences with increasing beam energy between calculations that use different source models, significant scatter of $k_{R_{50}}$ as a function of R_{50} is observed in the left panel of figure 6.1. In particular, at approximately the same R_{50} value of 4 cm, there is a 0.9 % spread of $k_{R_{50}}$ results. However, if the shift to optimize R_{50} determination described in section 6.1 above is used, the scatter of $k_{R_{50}}$ as a function of R_{50} is reduced. A fit to the optimally shifted $k_{R_{50}}$ vs. R_{50} is provided in paper VI and results in a 0.11 % root-mean-square deviation (RMSD) of the data about the fit. Conversely, if the TG-51[10] recommended point of measurement is used, the RMSD increases to 0.23 %. Figure 6.1 shows that using different shifts does not change the actual trend of the fit to the data significantly but serves to make the distribution of the data about the fit tighter.

Zink and Wulff[26] used an EPOM shift for their calculations of k_Q for parallel-plate ion chambers. The shift was determined by scaling the front wall of the chamber with electron densities and amounts to a 0.17 mm shift inside the chamber cavity for the PTW Roos chamber. The right panel of figure 6.1 shows the excellent agreement in low- to intermediate-energy beams between the present results and those calculated by Zink and Wulff.[26] The discrepancies at high-energy are from the lack of photons in the source model since Zink and Wulff[26] used electron beam spectra for source simulation.

Current dosimetry protocols[10,11] factor $k_{R_{50}}$ via

$$k_{R_{50}} = k'_{R_{50}} k_{ecal}, \tag{6.2}$$

with the electron quality conversion factor, $k'_{R_{50}}$, and the photon-electron conversion factor k_{ecal} which is $k_{R_{50}}$ at R_{50}=7.5 cm. There are practical reasons for this fac-

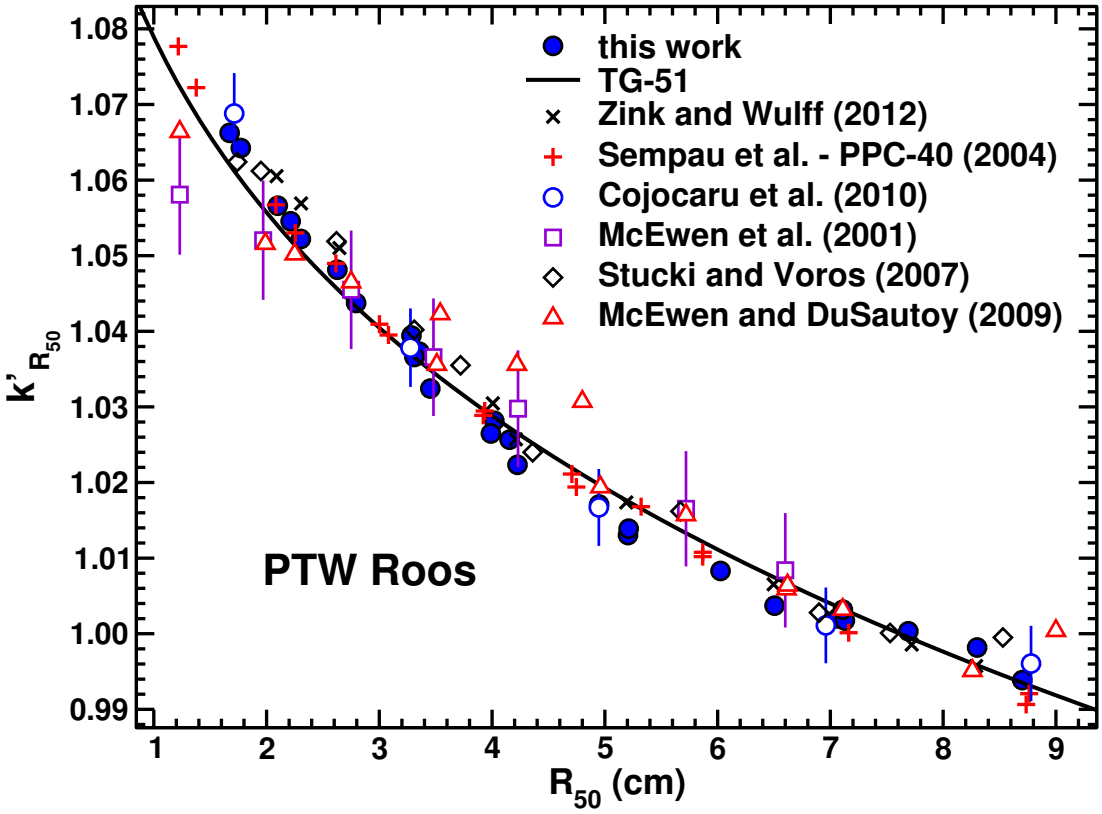

Figure 6.2: The electron quality conversion factor at d_{ref} compared to literature data. The results of this work are represented by filled circles and use sources modelled from realistic `BEAMnrc` accelerator models and/or electron beam spectra with R_{50} less than 6.5 cm. Data obtained using Monte Carlo simulations are from Sempau *et al.*[111] (+) and Zink and Wulff[26] (x) while measured data are from McEwen *et al.*[112] (open squares), Cojocaru *et al.*[113] (open circles), Stucki and Voros[114] (open diamonds) and McEwen and DuSautoy[115] (open triangles). Measurement uncertainties are indicated on the McEwen *et al.*[112] and Cojocaru *et al.*[113] data sets. The shift used here is the optimal shift for accurate R_{50} determination from chamber simulations (0.39 mm from the front of the cavity) while other publications all used water-equivalent scaling of the front window of the PTW Roos chamber (∼0.14 mm from the front of the cavity). However, as explained in the text, small shifts at the reference depth make little difference to the trend of the data but make the distribution about the fit tighter. From paper VI.

torization; chamber-to-chamber variation of $k'_{R_{50}}$ is much less than for $k_{R_{50}}$ and k_{ecal} plays a natural role when cross-calibrating plane-parallel chambers against cylindrical chambers. In addition, if primary standards for absorbed dose in electron beams are available, k_{ecal} can be measured directly. It is therefore more common in the literature

to provide the electron quality conversion factor, $k'_{R_{50}}$. Figure 6.2 shows the agreement between $k'_{R_{50}}$ factors calculated in this work and other published data. Sempau *et al.*[111] calculated $k'_{R_{50}}$ factors using the PENELOPE Monte Carlo code system. They simulated the IBA PPC-40 chamber, which is very similar in construction to the PTW Roos. The excellent agreement between results using different code systems is reassuring. McEwen *et al.*[112] measured absorbed dose calibration coefficients in electron beams compared to the NPL primary standard graphite calorimeter for various chambers, including the PTW Roos and NE2571 chambers. The data appear to follow a linear trend in beams with R_{50} less than 6.6 cm. To compare the results of this work to McEwen *et al.*,[112] a linear fit to their data was made and used to normalize the data to an extrapolation of the fit to R_{50} =7.5 cm since $k'_{R_{50}} = N^{Q}_{D,w}/N^{R_{50}=7.5\ cm}_{D,w}$ (assuming that no gradient corrections are needed). This approach assumes that the calibration coefficients follow the same trend in high-energy beams so the good agreement between our results and those measured in 2001 at NPL[112] may be fortuitous. Cojocaru *et al.*[113] used a hybrid water calorimeter-Fricke dosimetry system to determine measured $k'_{R_{50}}$ factors at NRC. Stucki and Voros[114] used Fricke dosimetry to obtain measured $k'_{R_{50}}$ factors at the METAS standards laboratory and McEwen and DuSautoy[115] compiled measured results from NRC and McGill based on water calorimetry and from NPL that used graphite calorimetry. The results obtained here for the PTW Roos chamber are in excellent agreement, well within systematic uncertainties, with the measured data from various laboratories.

Beam quality conversion factors for the NE2571 chamber: Figure 6.3 (a) shows $k_{R_{50}}$ (equation 1.12, p. 15) for the NE2571 chamber with different shifts used to obtain and remove the gradient correction from calculated k_Q factors. The gradient correction, P^{Q}_{gr}, is calculated as the ratio of the absorbed dose to the air in the chamber cavity at a depth of $d_{ref} + f\ r_{cav}$, where f is a fraction of the cavity radius, to that at

d_{ref},

$$P_{\mathrm{gr}}^{Q} = D_{ch}(d_{ref} + f\, r_{cav})/D_{ch}(d_{ref}). \tag{6.3}$$

Note that the statistical uncertainty in $k_{R_{50}}$ is slightly greater than that in k_Q because of statistical fluctuations of P_{gr}^{Q}. In figure 6.3 (a), results from monoenergetic beams and research accelerators or those no longer used clinically are included. If either the TG-51[10] recommendation of determining the gradient correction with a shift of 0.5 r_{cav} is used or the gradient correction is ignored (including gradient effects in k_Q by definition), significant scatter of $k_{R_{50}}$ at the same value of R_{50} is observed in figure 6.3 (a). However, if an optimized shift of 0.22 r_{cav} is used to determine P_{gr} and applied to remove gradient effects from calculated k_Q factors, $k_{R_{50}}$ factors at similar R_{50} values are much closer together (closed circles in figure 6.3 [a]). Using the optimal shift of 0.22 r_{cav} to determine the gradient correction, a fit to the data as a function of R_{50} from all beams results in an RMSD of only 0.21 %, lower than that of 0.38 % when the TG-51[10] recommendation is used or 0.32 % when P_{gr}^{Q} is not applied.

In figure 6.3 (a), the maximum difference between the calculated $k_{R_{50}}$ factors and a fit to the data vs. R_{50} is 0.5 %, for the Varian *Clinac* 6 MeV beam (R_{50}=2.64 cm). Figure 6.3 (b) shows k_Q factors (as opposed to $k_{R_{50}}$) for beams that are considered 'clinical' and monoenergetic beams to aid in explaining the differences in k_Q factors from different electron beams. The largest difference between the calculated data from clinical beams and a fit to k_Q vs. R_{50} is still for the Varian *Clinac* 6 MeV beam with a difference of about 0.5 %. However, these results are for the Varian *Clinac* accelerator that use the Type II applicator. A low-energy peak was observed[79] in all of the Varian *Clinac* beams caused by electrons passing through one of the layers of the Type II applicator. At about the time of that 1995 report, Varian discontinued the production of the Type II applicator; it was replaced by the Type III applicator, which was designed to reduce the peak from scattered low-energy electrons. If calculations

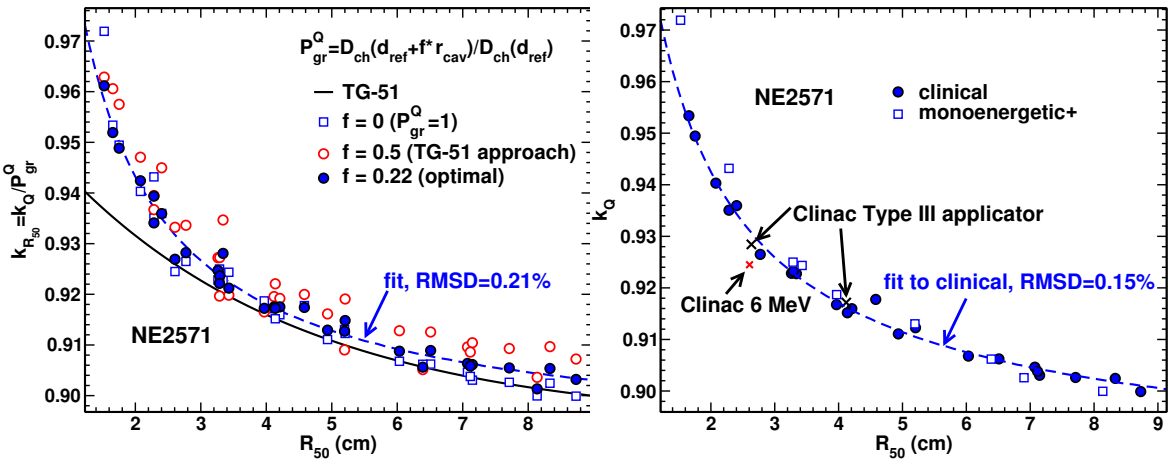

Figure 6.3: Panel (a): The component of k_Q at d_{ref} which is independent of gradient effects, $k_{R_{50}}$ for the NE2571 chamber in a wide variety of beams. Different shifts are used to correct for gradient effects. An optimized gradient correction is determined to reduce scatter for the NE2571 chamber. Panel (b): k_Q factors at d_{ref} when gradient effects are not explicitly corrected (but included in k_Q by definition) for beams considered 'clinical' and electron beams that are not generally used clinically (labelled monoenergetic+). The results using a model of the Varian *Clinac* linear accelerator with different applicators are specifically identified. From paper VI.

of k_Q are performed with the spectra for the Varian *Clinac* 6 and 9 MeV beams that use the Type III applicator, the results for the 6 MeV beam are different by 0.4 % and are in much better agreement with results for other clinical accelerators as shown in figure 6.3 (b). The calculations for the 9 MeV beam that uses the Type III applicator are not significantly different from those with a Type II applicator.

When the shift to optimize R_{50} determination and reduce scatter in $k_{R_{50}}$ is applied, calculations of $k_{R_{50}}$ for the PTW Roos chamber are not sensitive to the differences in electron beam spectra for either the 6 or 9 MeV Varian *Clinac* beams when the different applicator models are used. To investigate this difference in sensitivity to the electron spectrum for the two chambers, calculations of P_{wall} and P_{repl} are performed and extracted at the reference depth for both beams using electron beam

spectra for the Varian *Clinac* with different applicator models. Both P_{wall} and P_{repl} for the PTW Roos are affected by up to 0.24 % in opposite directions when the two different spectra are used, resulting in a negligible difference in D_w/D_{ch}. However, if the front of the cavity is used to define the point of measurement (the TG-51[10] POM), $k_{R_{50}}$ is up to 0.3 % different (consistent with the scatter in the left panel of figure 6.1) when the spectra for the Type II or III applicator models are used. Again, both of P_{wall} and P_{repl} are affected by the differences in input spectra but P_{repl} changes by 0.4 % whereas P_{wall} only changes by 0.1 %. The situation is more extreme when comparing the k_Q calculations for the NE2571 chamber (with the POM at the center of the chamber and including gradient effects by definition) using electron beam spectra for the 6 MeV Varian *Clinac* beam with different applicator models. The difference in the D_w/D_{ch} ratio is 0.4 % with spectra for different applicator models but P_{repl} is different by 0.8 % while P_{wall} changes by only 0.3 %, again in opposite directions. It is clear that the model of the incident electron beam has significant, complicated impacts on the resulting correction factors as well as k_Q factors, indicating that R_{50} may not be an ideal beam quality specifier.

Figure 6.3 (b) also shows that using a fit to k_Q factors at d_{ref} for clinical beams gives an RMSD of 0.15 %. The one outlying 'clinical' point on figure 6.3 (b) at R_{50}=4.57 cm is for a Siemens *MD2* accelerator model which uses a cut-out to shape the field. When $k_{R_{50}}$ values for all investigated beams are considered, removing gradient effects with an optimal shift, as in figure 6.3 (a), provides an advantage in that the RMSD of a fit to $k_{R_{50}}$ is 0.21 % compared to 0.32 % when k_Q (where gradient effects are included by definition and require no correction) is considered for all beams and 0.15 % when only considering clinical beams. The approach taken above to eliminate gradient effects is really only compensating for the inadequacy of R_{50} to completely specify the beam quality for electron beams with different properties

in order to determine accurate k_Q factors. If one only considers results for k_Q from beams that are representative of clinical accelerators, reasonable results are obtained without explicitly accounting for gradient effects as in figure 6.3 (b).

6.3 Comparison of individual correction factors and k_{ecal} factors to other studies

Comparison of individual correction factors to recent Monte Carlo investigations: Table 6.1 shows individual correction factors calculated in cobalt-60 and a high-energy electron beam compared to published data and k_{ecal} values calculated for comparison to TG-51,[10] discussed below. Calculations for the PTW Roos chamber are in good agreement with literature values.[9,26,38] Slight differences are consistent with minor variations in the ion chamber models and statistical fluctuations. Similar differences are observed in cobalt-60 calculations with NACP-02 chamber models that use different back wall specifications (see Wulff and Zink[99] and chapter 4). A stem is not included in the model of the PTW Roos used here nor in any other publications; the assumption is made that P_{stem} is unity for the Roos chamber. This assumption is likely valid considering the distance from the stem to the active cavity (about 1 to 2 cm) in plane-parallel chambers.

Individual correction factors are calculated for the NE2571 chamber with a simple cylindrical model, as done by Buckley and Rogers,[30,33] and with a detailed chamber model with a fully modelled stem and conical chamber tip, like that of Wulff *et al.*[31] Very little difference is observed between calculations of P_{wall} and P_{cel} using detailed and cylindrical models. However, the stem correction, P_{stem}, is determined to be 0.3 and 0.5 % different from unity in cobalt-60 and 18 MeV, respectively. These corrections result in a 0.2 % effect on k_{ecal}, which is not taken into account when using a simple cylindrical chamber model. The calculated P_{stem} determined in this

Table 6.1: Individual correction factors and photon-electron conversion factors, k_{ecal}, for the Roos and NE2571 ion chambers compared to published data. For the NE2571 chamber, calculations are performed with different chamber models (D=detailed, S=simplified, NS=without waterproofing sleeve, WS=with waterproofing sleeve). Statistical uncertainties on correction factors calculated in this work are shown in parentheses. Unless otherwise specified, the calculations of this work use 10 keV photon and electron energy cut-offs and production thresholds. Determination of k_{ecal} for comparison to TG-51[10] is described in the text. Typical statistical uncertainties in the values from other publications are less than 0.1 %. Modified from paper VI.

PTW Roos				
	cobalt-60		Elekta *Precise* 18 MeV (R_{50}=7.04 cm)	
Correction	this work	Literature value	this work	Literature value
P_{wall}	1.0074(05)	1.0088^{a}	1.0057(09)	1.0050^{a}
		1.0080^{b}		1.0040^{b}
		1.0087^{c}		
		$1.003^{TG-51,d}$		$1.0^{TG-51,d}$
P_{wall} (1 keV)	1.0068(04)			
P_{repl}	1.0061(10)	1.0077^{b}	1.0009(10)	1.0021^{b}
				1.0016^{e}
		$1.0^{TG-51,d}$		$1.0^{TG-51,d}$
SPR	1.1338(04)	$1.1335^{TG-51,d}$	1.0304(04)	$1.0276^{TG-51,d}$
k_{ecal} (this work) = 0.8992				
k_{ecal} (using correction factors from this work, R_{50}=7.04 cm) = 0.9026				
k_{ecal} (Mainegra-Hing *et al.*[c]) = 0.896				
k_{ecal} (TG-51[d]) = 0.901				
NE2571				
	cobalt-60		Elekta *Precise* 18 MeV (R_{50}=7.04 cm)	
Correction	this work	Literature value	this work	Literature value
P_{stem} (D)	0.9972(01)	0.9973 (PTFE)[i]	0.9954(02)	0.996^{k}
		0.9985 (PMMA)[i]		
		$1.0^{TG-51,d}$		$1.0^{TG-51,d}$
P_{cel} (D)	0.9918(02)	0.9918^{i}	0.9982(02)	0.998^{k}
		$0.993^{TG-51,d}$		$0.998^{TG-51,d}$
P_{cel} (S)	0.9920(02)	0.9924^{g}	0.9983(01)	0.9985^{g}
P_{sleeve} (D)	0.9988(04)	1.000^{f}	1.0013(09)	1.0015^{f}
		$1.0^{TG-51,d}$		$1.0^{TG-51,d}$
P_{wall} (D,NS)	0.9986(04)	0.9995^{i}	1.0013(06)	
P_{wall} (D,WS)	0.9974(05)	0.998^{i}	1.0027(10)	1.001^{k}
P_{wall} (S,NS)	0.9988(04)	0.9985^{f}	1.0008(04)	1.00099^{f}
		$0.992^{TG-51,d}$		$1.0^{TG-51,d}$
P_{repl}	0.9956(07)	0.9964^{h}	0.9800(07)	0.984^{j}
		$0.992^{TG-51,d}$		0.990^{k}
P_{fl}			0.9854(10)	0.990^{j}
				$0.978^{TG-51,d}$
SPR	1.1338(04)	$1.1335^{TG-51,d}$	1.0304(04)	$1.0276^{TG-51,d}$
k_{ecal} (this work) = 0.9084				
k_{ecal} (using correction factors from this work) = 0.9084				
k_{ecal} (TG-51[d]) = 0.903				

[a]Buckley and Rogers, 2006[9] [b]Zink and Wulff, 2012[26] [c]Mainegra-Hing *et al.*, 2003[38]
[d]Rogers, 2009[13] [e]Wang and Rogers, 2010[116] [f]Buckley and Rogers, 2006[33]
[g]Buckley *et al.*, 2004[30] [h]Wang and Rogers, 2008[7] [i]Wulff *et al.*, 2008[31]
[j]Wang and Rogers, 2009[43] [k]Ono *et al.*, 2010.[117]

work is in good agreement with that of Wulff *et al.*[31] when similar stem materials are used. Including the effect of a waterproofing sleeve results in a 0.3 % effect on k_{ecal}. The replacement correction and fluence correction factors calculated here are in reasonable agreement with those calculated by Wang and Rogers.[7,43,116] The calculations of P_{repl} obtained here are lower than those of Wang and Rogers[43] but they observed that P_{repl} was lower when using the SPR method (used here) compared to other methods. The fluence correction factor calculated here is 0.5 % lower than that of Wang and Rogers.[43] The method used in this study to obtain P_{fl} uses the ratio of P_{repl} to P_{gr}, which is different from the method of Wang and Rogers[43] who observed significant variability of P_{gr} calculations depending on the method employed. Except for the replacement correction factor, individual correction factors calculated in this work are in good agreement with those of Ono *et al.*[117] who used a model of the PTW 30012 chamber, which is similar to the NE2571 chamber model studied here. There are a few possible reasons for the 1 % discrepancy between the results for P_{repl}. In the work of Ono *et al.*,[117] the calculation of P_{repl} provided in table 6.1 is for a beam with R_{50} of 7.6 cm whereas the value reported here is for 7.04 cm. Ono *et al.*[117] show that P_{repl} changes from 0.981 to 0.990 when calculated in beams with R_{50} ranging from 6.27 to 7.6 cm. They also used a shift of 0.5 r_{cav} upstream of the reference depth to determine individual correction factors, which will have an impact on the resulting P_{repl} factor, and explains why their value is closer to the result for the fluence correction factor obtained here since a shift of 0.5 r_{cav} is equivalent to applying the gradient correction.

Calculations of k_{ecal} compared to current dosimetry protocols: In table 6.1, k_{ecal} is extracted from a fit to $k_{R_{50}}$ at R_{50}=7.5 cm with the point of measurement for the PTW Roos chamber as prescribed by TG-51[10] for comparison. This is slightly different from k_{ecal} calculated using individual correction factors because R_{50}=7.04 cm

(instead of 7.5 cm) for the beam used to calculate the individual correction factors and statistical fluctuations in the individual correction factors will affect the resulting k_{ecal} calculation. Mainegra-Hing *et al.*[38] calculated k_{ecal} by updating the TG-51 P_{wall} calculation in cobalt-60 with their more accurate Monte Carlo calculation and the result is within 0.2 % of the value from this work even though several of the other correction factors used for TG-51 k_{ecal} calculations are also different compared to more recent Monte Carlo calculations. Table 6.1 shows that the individual correction factors obtained in this work for the PTW Roos are different from those used by TG-51[10] by up to 0.6 %. However, these differences cancel when k_{ecal} is calculated, resulting in only a 0.2 % difference between the result obtained here and that provided in TG-51.[10] If the EPOM recommended here is used for calculations of $k_{R_{50}}$, the k_{ecal} factor extracted from the fit to the data is 0.898, only slightly different from the value of 0.899 obtained when the TG-51[10] POM is used.

For the NE2571 chamber, k_{ecal} factors are determined in three ways. The first is to calculate k_Q factors, including gradient effects by definition and therefore not applying a gradient correction, as in figure 6.3 (a) when $P_{\text{gr}}^Q = 1$. A fit to the data is made including all investigated beams and $k_{ecal} = k_Q$ (R_{50}=7.5 cm) amounts to 0.903. The second approach is to calculate $k_{R_{50}}$ when the optimal shift is used to calculate and remove the gradient correction. Again, a fit to the data is made and the resulting k_{ecal} factor obtained here amounts to 0.906. TG-51[10] only included the fluence correction in the electron beam component of k_{ecal} from equation 1.11 (p. 10) - the gradient correction was ignored ($P_{\text{repl}} = P_{\text{gr}}P_{\text{fl}}$) for TG-51[10] calculations with the recommendation that the gradient correction, measured in the clinical beam of interest, be applied. Therefore, to compare to TG-51,[10] $k_{R_{50}}$ factors are calculated when the gradient correction is obtained with a shift of 0.5 r_{cav} and removed from k_Q as in figure 6.3 (a). Again, k_{ecal} is extracted from a fit to the calculated $k_{R_{50}}$ factors

and amounts to 0.9084 in table 6.1. The k_{ecal} factor determined with individual correction factors in table 6.1, is calculated by including only the P_{fl} component of P_{repl} in the numerator of equation 1.11, again for comparison to TG-51.[10] As with the PTW Roos chamber, table 6.1 shows that the individual correction factors calculated here with the NE2571 chamber model are up to 0.8 % different from those used by TG-51[10] but, because of cancellation of some differences, the resulting k_{ecal} factors are within 0.5 %.

6.4 Uncertainty in electron beam k_Q calculations

Table 6.2 shows calculated systematic uncertainties in electron beam k_Q factors for the NE2571 chamber, determined by varying quantities that introduce components of uncertainty in k_Q factors within reasonable limits in cobalt-60 and the Elekta *Precise* 18 MeV beam as discussed in chapter 2. Considering uncorrelated photon cross sections, the uncertainty in k_Q amounts to between 0.02 % when varying photon cross sections by 1 % for the air in the chamber cavity and 0.9 % when varying cross sections in the water phantom. These effects are almost entirely from changes in the D_w/D_{ch} ratio in cobalt-60. The calculations in the Elekta *Precise* 18 MeV electron beam are not affected by changes to photon cross sections. This is different from the results of chapter 4 for photon beams where varying the photon cross sections in water introduced a 0.55 % uncertainty in calculated k_Q factors. In that case, the same 0.9 % change occurred in the D_w/D_{ch} ratio in the cobalt-60 beam but was partially compensated by a change in the same direction in the high-energy photon beam. When the more realistic situation that photon cross section uncertainties are correlated is considered, the uncertainty introduced in calculated k_Q factors is only 0.08 %.

Uncertainty in k_Q factors is between 0.06 % when changing the mean excitation

Table 6.2: The systematic uncertainty in calculated electron beam k_Q factors for the NE2571 chamber. Modified from paper VI.

Component of uncertainty	Variation in parameter (%)	Uncertainty in k_Q (%)	Statistical uncertainty (%)
Photon cross sections (uncorrelated)	1.0		
Water		0.90	0.04
Graphite		0.46	0.02
Al		0.05	0.01
Air		0.02	0.01
Total (uncorrelated cross sections)		1.01	
Photon cross sections (correlated)	1.0	0.08	0.05
Mean excitation energy			
Water	1.5	0.06	0.05
Graphite	4.5	0.26	0.02
Al	0.6	0.02	0.01
Air	2.5	0.08	0.02
Total (Stopping powers)		0.28	
Chamber dimensions			
Wall	10.0	0.06	0.02
Cavity	10.0	0.09	0.02
Stem	Change to Al	0.20	0.10
Other sources			
Statistics		0.10	
`EGSnrc`[48]		0.10	
$(W/e)_{air}$ variation[17]		0.50	
Overall uncertainty in k_Q			
uncorrelated, with W/e		1.19	
correlated, with W/e		0.64	
uncorrelated, without W/e		1.08	
correlated, without W/e		0.40	

energy for water and 0.26 % when the change is made to the graphite in the chamber wall. The overall component of uncertainty in k_Q from uncertainty in stopping powers amounts to 0.28 %.

The influence on k_Q factors when changing the wall thickness and cavity radius for the NE2571 chamber by 10 % is only up to 0.09 %. When the model of the stem uses

solid aluminum instead of the realistic stem model, the k_Q factor changes by 0.2 %. This is comparable to the overall effect of the stem correction in table 6.1 (p. 102), indicating that this component of uncertainty is likely a conservative estimate.

The relative statistical uncertainty in calculated k_Q factors is always less than 0.1 %. `EGSnrc` has been shown to be accurate at the 0.1 % level with respect to its own cross sections for calculations of ion chamber response,[48] although this statement applies to a lack of artifacts in the condensed history Monte Carlo implementation of electron transport tested with a 1.25 MeV photon source.

As emphasized above, obtaining k_Q factors with equation 2.6 relies on the assumption that the average energy lost per unit charge released by electrons slowing completely in air, $(W/e)_{air}$, remains constant with beam quality. There is some question as to what component of uncertainty from possible variation of $(W/e)_{air}$ with beam quality should be assigned in table 6.2. In chapter 5, comparison of measured and calculated k_Q factors obtained in photon beams is used to establish an upper limit on the difference between $(W/e)_{air}$ values in a cobalt-60 beam compared to a 25 MV photon beam. Those results indicate that $(W/e)_{air}$ varies by less than 0.36 % with 95 % confidence in high-energy photon beams. However, in this chapter we are concerned with the difference in the value of $(W/e)_{air}$ in cobalt-60 compared to electron beams. The value of $(W/e)_{air}$ for cobalt-60 calculations is for the entire slowing down spectrum of electrons with energies less than 1.33 MeV. In higher energy electron beams the relevant quantity is $w(E)/e$, the energy lost per Coulomb of charge released by electrons of a certain energy, since the spectrum of electrons crossing the cavity in the electron beam simulations is much closer to monoenergetic. The value of $w(E)/e$ is estimated to possibly vary by 0.5 eV (1.5 %) over a range of electron energies from 0 to 40 MeV.[15] TRS-398[17] assigned an uncertainty estimate of 0.5 % in k_Q factors from potential variation of $(W/e)_{air}$ with beam quality based on the

results of Svensson and Brahme.[15] As a conservative estimate, this 0.5 % component of uncertainty in calculated k_Q factors from possible $(W/e)_{air}$ or $(w/e)_{air}$ variation with beam quality is assigned in table 6.2 but the issue warrants further investigation.

Adding the individual components of uncertainty in k_Q factors in table 6.2 in quadrature, an overall uncertainty on calculated k_Q factors is realized. Assuming that photon cross sections are correlated and that $(W/e)_{air}$ does not vary with beam quality, the uncertainty in k_Q factors amounts to 0.4 %. Meanwhile, if the more conservative approach is taken that assumes uncorrelated photon cross sections and $(W/e)_{air}$ or $(w/e)_{air}$ variation of beam quality of 0.5 %, the overall uncertainty in k_Q factors is 1.2 % for the NE2571 chamber.

Zink and Wulff[26] investigated systematic uncertainties in k_Q factors for the PTW Roos chamber which amount to between 0.32 % if correlated photon cross sections are assumed and $(W/e)_{air}$ does not vary with beam quality. However, if one assumes $(W/e)_{air}$ or $(w/e)_{air}$ variation, that result increases to 0.44 % with their assumption that $(W/e)_{air}$ or $(w/e)_{air}$ variation introduces a 0.25 % component of uncertainty in k_Q calculations and if uncorrelated photon cross sections are considered, the uncertainty in k_Q is 1.06 %. Uncertainties on k_Q factors for the PTW Roos chamber are not investigated here, but the results of Zink and Wulff[26] are comparable to those obtained here for the NE2571 chamber. It is reasonable to assume a similar level of uncertainty on the k_Q calculations for the PTW Roos chamber obtained in this work.

6.5 Summary

An investigation of reference dosimetry of electron beams using Monte Carlo simulations is presented. Calculations are performed for the plane-parallel PTW Roos chamber and the Farmer-type NE2571 chamber but similar results are presented for several other ion chambers in paper VII. Differences are observed between the beam

quality specifier, R_{50}, calculated by converting from I_{50} using calculations of the absorbed dose to the air in the ion chamber compared to that obtained from depth-dose calculations in water. It is found that an EPOM shift can be used to reduce these differences for both chamber types. The shifts for accurate determination of R_{50} from ion chamber simulations are 1.55 mm for the PTW Roos chamber and 0.34 r_{cav} for the NE2571 chamber. It is also determined that, for the Roos chamber, the same shift reduces the RMSD of a fit to calculated beam quality conversion factors, $k_{R_{50}}$.

The gradient effect is investigated for the NE2571 chamber and it is found that using a reduced shift of 0.22 r_{cav} compared to the 0.5 r_{cav} shift recommended by TG-51[10] to determine the gradient correction results in a reduced RMSD of a fit to calculated beam quality conversion factors, $k_{R_{50}}$. If only clinical accelerators are considered, the RMSD of a fit to the calculated k_Q factors is low enough to obtain results that are acceptable for reference dosimetry. The shortcomings of R_{50} as a beam quality specifier are discussed. Systematic uncertainties in calculated beam quality conversion factors for the NE2571 chamber are estimated to be 0.4 % if realistic assumptions are made and 1.2 % using conservative assumptions.

Chapter 7

Summary and conclusions

A discussion of differences of up to 1.7 % between recent Monte Carlo calculated individual correction factors and those used to obtain k_Q factors for current dosimetry protocols[10,11] was presented in chapter 1, motivating this comprehensive study on beam quality conversion factors.

7.1 Summary

Measured $N_{D,w}$ coefficients and k_Q factors are obtained for plane-parallel chambers in photon beams in chapter 3 with estimated systematic uncertainties of 0.5 %. Leakage currents and the stability of plane-parallel ion chamber calibrations appear to be more sensitive to environmental conditions, specifically relative humidity levels, than cylindrical chambers. The chamber-to-chamber variability of measured k_Q factors observed here is not a significant problem (generally less than 0.2 % difference for chambers of the same type), contrary to the observations made in early investigations.[36] However, issues with the long-term repeatability of calibration coefficients (up to 1.5 % differences when repeated calibrations are performed after less than a year) are observed for plane-parallel chambers in photon beams. Long-term stability is less problematic when considering measured k_Q factors; the uncertainty in k_Q factors is estimated at 0.19 % from long-term repeatability when measurements to

obtain $N_{D,w}$ coefficients in cobalt-60 and linac beams are obtained close in time.

In chapter 4, selected results are presented from our study to obtain Monte Carlo calculated k_Q factors for 33 cylindrical ion chamber types. These results are being used by the AAPM Working Group in the addendum[12] to the TG-51 protocol. The results of this work are in very good agreement (well within 0.8 %) with published measured and calculated k_Q factors. Generally, differences of up to 0.5 % exist between more accurate correction factors and those used for TG-51 k_Q calculations.[13] The largest difference between the photon beam k_Q calculations of this work for representative cylindrical chambers (excluding small volume chambers that use high-Z electrodes) and TG-51 values is 0.7 %. These differences are explained using Monte Carlo calculated correction factors. Large effects on k_Q factors are observed for small volume ion chambers because of their use of high-Z central electrodes. Calculated k_Q factors are also obtained for 10 plane-parallel ion chamber types and, although the geometries and materials are very different from cylindrical chambers, the level of agreement with measured k_Q factors is similar.

Systematic uncertainties in calculated k_Q factors are investigated for plane-parallel and cylindrical chambers in photon beams and the NE2571 cylindrical chamber in electron beams and amount to less than 0.5 % using realistic assumptions and generally less than 1 % when conservative assumptions are made.

Overall, excellent agreement is observed when comparing the large data sets of measured and calculated photon beam k_Q factors for 25 cylindrical chambers and 10 plane-parallel chambers in chapter 5. For cylindrical chambers, mean percent differences for the entire combined data set of cylindrical chambers are -0.08, -0.07 and -0.23 % with standard deviations of 0.17, 0.32 and 0.31 % for 6, 10 and 25 MV beams, respectively. For plane-parallel chambers, mean percent differences are -0.02, 0.18 and -0.16 % with standard deviations of 0.17, 0.23 and 0.39 % for 6, 10 and 25

MV beams, respectively.

In chapter 5, it is estimated that the upper limit on the variation of $(W/e)_{air}$ in high-energy photon beams is less than 0.36 % with 95 % confidence using the combined data set consisting of plane-parallel and reference cylindrical ion chambers. The results of this exercise indicate that $(W/e)_{air}$ does not decrease with increasing beam energy.

Chapter 6 presents Monte Carlo calculated k_Q factors for the PTW Roos and NE2571 chamber types in electron beams. Individual correction factors are generally found to be in good agreement with previous studies and explain the differences between k_Q factors provided by TG-51 and those calculated here. In a high-energy electron beam, differences of up to 0.8 % are observed between the individual correction factors used for TG-51 $k_{R_{50}}$ calculations and the calculations of this work but k_{ecal} ($k_{R_{50}}$ at R_{50}=7.5 cm) values are within 0.2 % for the PTW Roos and 0.5 % for the NE2571 when using the TG-51 recommendation to account for gradient effects.

A shift of the points of measurement for both of the PTW Roos and NE2571 chambers, different than those recommended by TG-51, is determined in chapter 6 to more accurately determine the electron beam quality specifier, R_{50}, from ion chamber measurements. For the PTW Roos chamber, the same shift reduces scatter in $k_{R_{50}}$ calculations as a function of R_{50}. Gradient effects are investigated for the NE2571 chamber and a shift, again different from that recommended by TG-51, can be used to determine and remove gradient effects to give more accurate $k_{R_{50}}$ factors if results from all electron beams are considered. However, if only results from clinical accelerators are considered, a good fit to calculated k_Q factors is obtained despite there being no need to explicitly correct for gradient effects.

7.2 Conclusions

Monte Carlo calculated k_Q factors can be obtained with systematic uncertainties that are low enough for their use for reference dosimetry. The level of agreement observed between measured and calculated k_Q factors for photon beams indicate that the calculated results of this work are accurate enough for adoption in updated reference dosimetry protocols.

Problems observed with the operation of plane-parallel chambers suggest that plane-parallel chambers are still not suitable for reference dosimetry without cross-calibration against a stable cylindrical chamber.

Comparison of measured and calculated k_Q factors in photon beams indicate that $(W/e)_{air}$ variation with photon beam quality is not a significant issue.

In electron beams, differences are observed between the effective points of measurement determined here compared to those recommended by current dosimetry protocols[10,11] for the PTW Roos and NE2571 chambers. In addition, appendix C shows that beam-dependent shifts are required for both chambers to minimize the variation of the overall ion chamber perturbation factor with depth. For plane-parallel chambers, it is clear that it is too simplistic an approach to use a fixed EPOM determined with either the physical thickness (TG-51 recommendation[10]) or water-equivalent scaling (IAEA recommendation[11]) of the front window of the chamber. Similarly, the results of this work indicate that using a fixed EPOM of 0.5 r_{cav} for cylindrical chambers (recommended by both protocols[10,11]) is an oversimplified approach.

The issues discovered for plane-parallel chambers in photon beams (chapter 3) and electron beams (appendix B) indicate that cylindrical chambers might be more suitable for reference dosimetry of electron beams. This work goes a long way toward characterizing the use of cylindrical chambers in low-energy electron beams but

measurements of k_Q factors are required for comparison and the results of this work indicate that R_{50} may not be an ideal beam quality specifier.

7.3 Future work

Direct measurements of $(W/e)_{air}$ in clinical photon and electron beams are required to verify the accuracy of Monte Carlo calculated k_Q factors. This work indicates that $(W/e)_{air}$ variation is not significant in high-energy photon beams but in electron beams, the situation is not as clear. A study at NRC[118] is underway to obtain updated measurements of $[w(E)/e]_{air}$ in electron beams and the results are highly anticipated.

In this study, the question about whether photon cross sections are correlated or uncorrelated has a large effect on systematic uncertainties in calculated k_Q factors. It is difficult to determine which is the correct approach. However, Ali *et al.*[119] suggest that the 1-2 % uncertainty in photon cross sections in the energy range of interest (used here) is overestimated. They estimate the upper bound for these uncertainties to be 0.7 % at the 95 % confidence level.

Measurement of k_Q factors for both chamber types in electron beams are required to compare to calculated results. The measured results from appendix B will be used to determine electron beam k_Q factors for several chamber types once electron beam calorimetry measurements are performed.

An investigation of k_Q factors for nonstandard beams is needed. Some modern treatment machines cannot realize the reference conditions required by dosimetry protocols (specifically, field size and SSD) so a study on the effects on k_Q factors from variations in these parameters is recommended. A joint IAEA-AAPM Working Group[120] is in the process of establishing a protocol for reference dosimetry of these beams and some progress has been made but there is room for further research.

Appendix A

The central electrode correction factor

A.1 Motivation and methods

Increased adoption of radiation therapy techniques using small fields has provoked the advent of ionization chambers with much smaller volumes than standard Farmer-type chambers. For practical reasons, many of these ion chambers have electrodes composed of high-Z (Z>13) materials. For these chambers, it was noted in chapter 4 that k_Q exhibits the largest deviation from TG-51 type calculations and that Monte Carlo calculations of k_Q for the same chambers without a central electrode are in much better agreement with TG-51 type calculations. In the past, studies of central electrode correction factors have focused on ion chambers with aluminum or graphite electrodes,[28–30,121,122] although other investigations have reported strange behavior with ion chambers using high-Z electrodes.[34,123–126]

The large effects of high-Z electrodes on k_Q factors and the abundance of publications indicating issues with these ion chambers motivated this study on the effect of the central electrode for these chambers. The central electrode correction factor, P_{cel}, is defined as the ratio of the dose to the gas in an ion chamber without the central electrode, $D_{ch}^{no\ el}$, to that with the central electrode, D_{ch}:

$$P_{cel} = \frac{D_{ch}^{no\ el}}{D_{ch}}. \tag{A.1}$$

Note that this is different from the definition of P_{cel} from equation 1.6 (p. 6) in that the chamber stem is included in these calculations. The dose to the gas without the central electrode is calculated by changing the central electrode in the stem to the material adjacent to the electrode and the central electrode in the active region to air. However, calculations of P_{cel} for the NE2571 agree with those of Buckley *et al.*[30] where no stem is considered. Calculations using the previous method (without a stem) and the method used here for the A16 and CC01 chambers exhibit a maximum difference of only 0.25 %. The definition of P_{cel} used here takes into account most of the non-negligible effects on the absorbed dose-to-air introduced by the presence of high-Z materials in the stem as well as in the cavity.

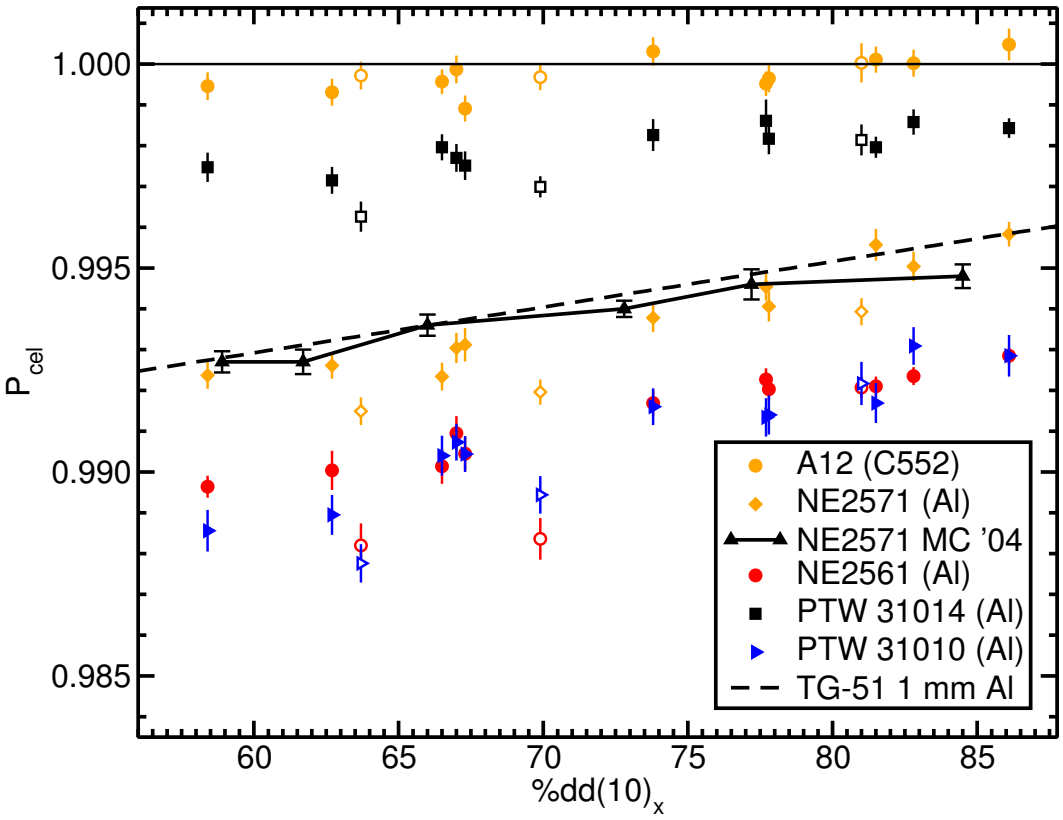

Figure A.1: P_{cel} for ion chambers in photon beams plotted against $\%dd(10)_x$ for chambers with C552 or aluminum electrodes. Solid symbols are filtered beams and open symbols are soft (unfiltered) beams. MC '04 data are from Buckley *et al.*[30] Error bars are smaller than symbols if not visible. From paper II.

For this study, the chambers simulated include the Exradin A16, T14, A14 and A14SL, the IBA CC01, the NE2561 and the PTW 31010, 31006 and 31014 chambers. Additionally, two Farmer-type chambers, the NE2571 and Exradin A12, are studied for comparison to calculations with small volume chambers. Calculations of P_{cel} are performed with the chamber at the reference depth on the central axis of the beam in a 30×30×30 cm^3 water phantom. The results presented here are from selected photon and electron beams discussed in chapter 2 (as well as additional unfiltered photon beams). In paper II results are also presented for central electrode effects as a function of distance from an ^{192}Ir point source in water and as a function of depth in a water phantom on which a 6 MV photon beam or kilovoltage x-ray beam is incident. The effects of using high-Z central electrodes in the ^{192}Ir and x-ray beams are significant: up to 50 % compared to 15 % for the NE2571 chamber that uses an aluminum electrode. Although these results are important, they are not presented here since they are not directly relevant to this thesis.

A.2 Results from photon beams

Figure A.1 shows P_{cel} values for ion chambers with C552 or aluminum electrodes in photon beams as a function of $\%dd(10)_x$. Calculations of P_{cel} for the Exradin A12 chamber with a C552 electrode in figure A.1 are all within 0.1 % of unity, regardless of beam filtration. Traditionally, it is assumed that the central electrode does not need to be taken into account if the electrode is composed of the same material as the wall[13] - the near unity values of P_{cel} for the Exradin A12 chamber confirm the validity of that assumption for this chamber. NE2571 P_{cel} calculations in filtered beams are in good agreement with values provided by Buckley *et al.*[30] and TG-51 P_{cel} values for a 1 mm diameter aluminum electrode.[10] Calculations of P_{cel} for the NE2571 in linear accelerator beams without a flattening filter (unfiltered) are all lower than TG-

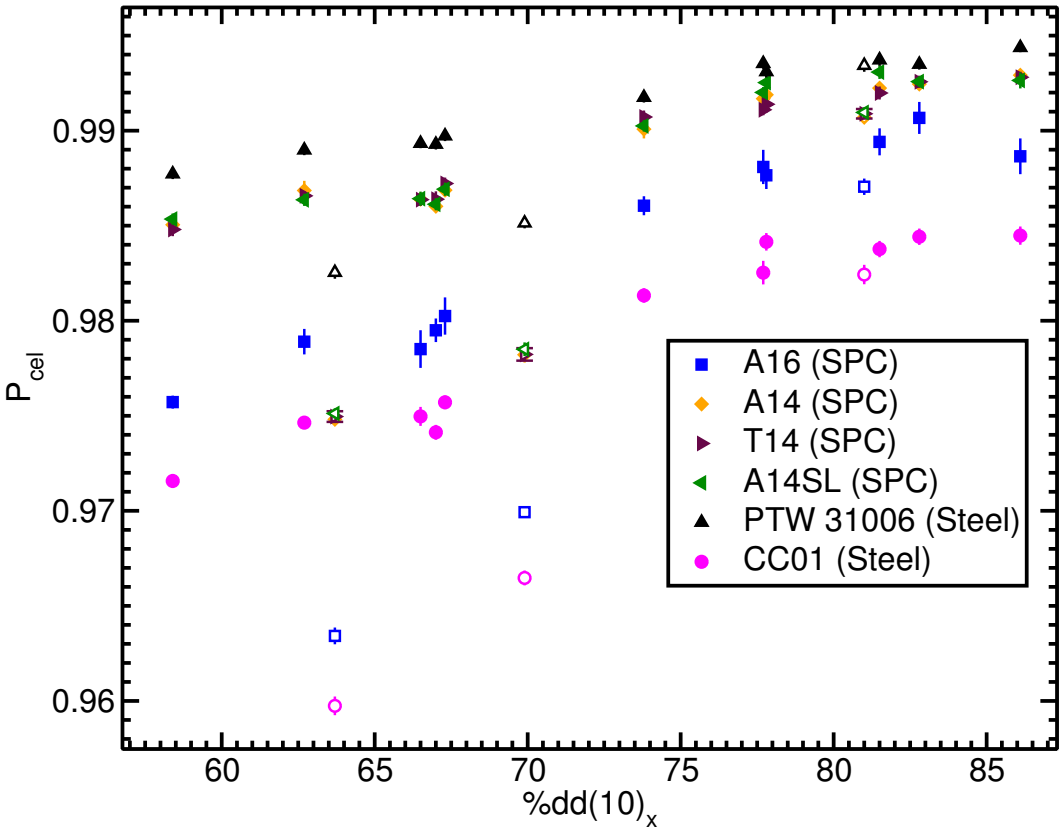

Figure A.2: P_{cel} for ion chambers in photon beams plotted against $\%dd(10)_x$ for chambers with high-Z electrodes. Error bars are smaller than symbols if not visible. Solid symbols are filtered beams and open symbols are soft beams. From paper II.

51 values, by up to 0.2 %. The differences between P_{cel} calculations for different chambers that use aluminum electrodes can be explained by differing fractions of the collecting volume occupied by the electrode (see paper II for details).

Figure A.2 shows P_{cel} calculations for ion chambers with electrodes composed of materials with Z>13 in photon beams. The Exradin A16, A14, A14SL and T14 chambers use silver-plated copper covered steel (SPC) electrodes while the IBA CC01 and PTW 31006 use steel electrodes. The high effective atomic number of these electrodes increases the probability of electrons being created, contributing to a higher dose for ion chambers that include the higher-Z central electrode. The resulting impact on P_{cel} is seen in figure A.2 where P_{cel} is generally much lower than for

those chambers with an aluminum electrode seen in figure A.1. Again, differences between P_{cel} calculations for different chambers that use the same central electrode material can be explained by differing fractions of the collecting volume occupied by the electrode (see paper II for details). There is also a large difference between P_{cel} values in filtered and unfiltered beams for the same chamber in neighbouring beam qualities for all chambers using high-Z electrodes (the same is true if TPR_{10}^{20} is used to specify beam quality). This implies that neither $\%dd(10)_x$ nor TPR_{10}^{20} are adequate beam quality specifiers for these ionization chambers.

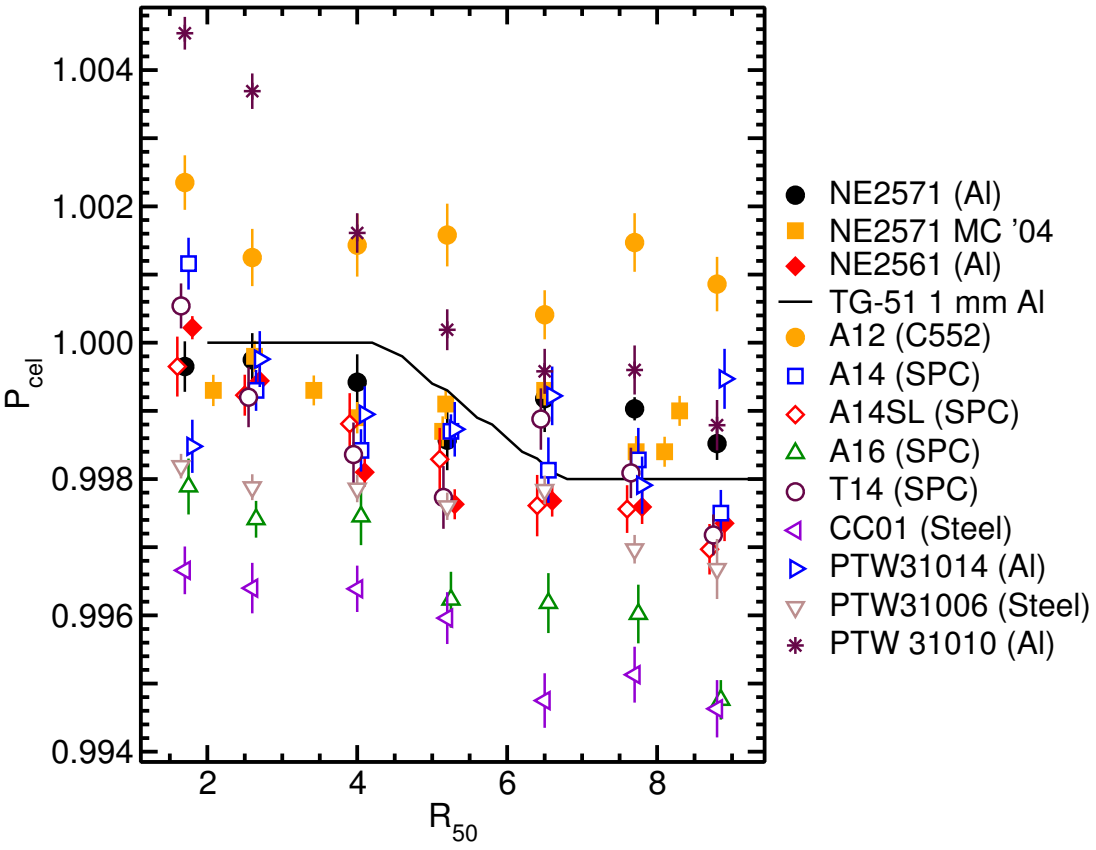

Figure A.3: P_{cel} for ion chambers in electron beams plotted against R_{50}. MC '04 data are from Buckley *et al.*[30] Some R_{50} values have been offset for clarity; offsets are -0.1, -0.05, 0.05, 0.05, 0.1 and 0.1 cm for the A14SL, T14, A14, A16, NE2561 and PTW 31014 chambers, respectively. From paper II.

A.3 Results from electron beams

Figure A.3 shows that the variation of P_{cel} values in electron beams is not as dramatic as that in photon beams. The calculated P_{cel} factors for the Exradin A12 chamber are almost all slightly larger than the previously used value of unity by up to 0.2 %. P_{cel} calculations for the NE2571 chamber agree with the results of Buckley *et al.*[30] Calculations of P_{cel} for the NE2561 chamber with a hollow aluminum electrode are within 0.1 % of the TG-51 calculations for a 1 mm diameter aluminum electrode except for two points that are close to 0.2 % low (for $R_{50} \approx$ 4-5cm). The P_{cel} calculations for the PTW 31014 are in good agreement with TG-51 calculations, except for the highest and lowest energy data points which both differ by 0.15 %. For the PTW 31010 chamber, with a much larger aluminum electrode, P_{cel} calculations are 0.45 % higher than TG-51 calculations at low energies. The difference decreases with increasing beam energy. The P_{cel} calculations for the Exradin A14, A14SL and T14 (SPC electrodes) are surprisingly close to TG-51 values for a 1 mm diameter aluminum electrode, with maximum deviations less than 0.2 %. The calculations of the central electrode correction factor for the PTW 31006 (steel electrode) in the low to mid-energy regime ($R_{50} < 5.5$ cm) have P_{cel} factors that are all about 0.2 % lower than TG-51 calculations. The Exradin A16 (SPC) and IBA CC01 (steel) chambers exhibit the worst deviations from TG-51 calculations with a 1 mm diameter aluminum electrode. Calculations of P_{cel} for the A16 chamber are between 0.2 and 0.3 % lower than TG-51 values while calculations for the CC01 chamber are 0.2 to 0.4 % lower.

A.4 Effects on beam quality conversion factors

For dosimetry protocols, the ratio of P_{cel} values in a beam of quality Q to that in a ^{60}Co beam is the relevant quantity for beam quality conversion factors, k_Q. In

the worst case, for the Exradin A16 chamber, the ratio of P_{cel} in a photon beam of quality Q to that in a ^{60}Co beam varies from 0.987 for an unfiltered, low-energy beam (Varian 6 MV flattening filter free) to 1.015 for a filtered, high-energy beam (Elekta SL25 25 MV) while the same ratio for the NE2571 chamber only varies from 0.9991 to 1.0027 for the same beams, respectively. However, the A16 represents a worst case for photon beams and if one ignores the flattening filter free beams, the $(P_{cel})_Q/(P_{cel})_{^{60}Co}$ ratio varies from 1.000 to 1.008 for all of the other detectors.

These values of P_{cel} for high-Z electrodes cause a much larger change in k_Q factors for electron beam dosimetry because of the large values of P_{cel} in ^{60}Co beams. The ratio of P_{cel} in an electron beam of quality Q to that in a ^{60}Co beam for the Exradin A16 is between 1.0227 and 1.0195 for the lowest and highest energy electron beams, respectively, while for the NE2571 chamber the ratio is between 1.0073 and 1.0062. For electron beams there are six chambers for which this ratio exceeds 1.010 for all values of R_{50}.

A.5 Conclusions

The central electrode correction factors for chambers with high-Z electrodes, which were not characterized by current dosimetry protocols,[10,11,103] are different from those for chambers with aluminum electrodes. The difference between P_{cel} for high-Z compared with aluminum electrodes is dramatic for photon beams but less problematic for electron beams. These results are superficially misleading since what is important for dosimetry protocols is the variation of P_{cel} compared to that in a cobalt-60 beam. In photon beams, the variation is not so dramatic although still significant. A much larger change is observed in electron beams because of the non-unity values of P_{cel} in cobalt-60 beams. These observations indicate that k_Q values from current dosimetry protocols should not be used for chambers with high-Z electrodes. Beam filtration

also affects P_{cel} for high-Z electrodes in photon beams.

It is important that clinical medical physicists be aware of the issues presented in paper II for chambers with high-Z electrodes. If possible, it would be best for manufacturers to avoid producing chambers that employ high-Z electrodes.

Appendix B

Electron beam measurements of absorbed-dose calibration coefficients

Paper V presents a method, similar to that of chapter 3, to obtain absorbed-dose calibration coefficients but as a function of depth in water in electron beams. Absorbed-dose calibration coefficients for a given chamber relative to reference chambers are investigated. A water calorimeter-based primary standard in electron beams has yet to be realized at NRC but once established, these results can be used to obtain absolute $N_{D,w}$ coefficients and k_Q factors for a wide variety of ion chambers by measuring them for secondary standard reference chambers. The issue of the effective point of measurement (EPOM) is also investigated in paper V by comparing R_{50} values obtained with 'user' chambers to those determined with reference chambers but the results are not presented here. A very brief review of this paper is presented here and the reader is referred to paper V for details.

B.1 Depth-ionization measurements

Equation 1.8 (p. 7) can be used to obtain relative $N_{D,w}$ coefficients as

$$\frac{N_{D,w,ref}}{N_{D,w,ch}} = \frac{M_{ch}}{M_{ref}} \tag{B.1}$$

which relates $N_{D,w}$ coefficients and ion chamber readings for two ion chambers - reference and 'user' ion chambers. In this work, measurements are made with National Research Council of Canada (NRC) reference ion chambers and various 'user' ion chambers from major ion chamber manufacturers as the chambers are scanned through a water phantom. Ratios of ion chamber readings are then used to derive relative calibration coefficients as a function of depth as per equation B.1. In this way, ratios of ion chamber readings obtained as a function of depth can be used to get a better estimate of the ratio of ion chamber calibration coefficients at the reference depth.

For electron beams incident on the surface of a water phantom, the mean electron energy as a function of depth z, $\bar{E}_z$ varies smoothly with depth in water. An approach is sought by which we can combine depth-ionization data from electron beams with different energies. An obvious choice would appear to be $\bar{E}_z$ and it is difficult to identify any other single parameter that could be used. Ratios of chamber measurements can therefore be investigated as a function of $\bar{E}_z$ instead of the depth of measurement. In this work, determination of $\bar{E}_z$ uses the approach of the IPEM[127,128] reports.

The NRC Elekta *Precise* linear accelerator is set up for beam delivery in a horizontal geometry. This linac can deliver electron beams with nominal energies of 4, 8, 12, 18 and 22 MeV. Even in high-energy electron beams, results are obtained with the calibration field size shaped by the 10×10 cm^2 applicator although preliminary measurements were obtained with a 14×14 cm^2 field size. Two reference Farmer-type chambers are mounted on the upstream side of the applicator for beam monitoring such that they do not affect the collimated beam at the phantom. Measurements of the charge collected by reference and 'user' ion chambers are made relative to the monitor chambers as a given chamber is scanned through the phantom to transfer the calibration coefficient from the NRC secondary standard reference chamber to the

'user' chamber. The standard deviation of the ratio of signals from the two reference monitor chambers and the drift in the ratio of the monitor chamber readings over the course of a single set of measurements are less than 0.1 % indicating that the uncertainty from the transfer of calibration coefficients is not significant.

Measurements are performed in a 30×30×30 cm^3 water phantom with the thin PMMA entrance window at an SSD of 100 cm. Chambers are preirradiated to 1000 MU, then scanned through the phantom along the beam axis in both directions - to investigate any systematic effect on the charge reading - with step sizes between 0.05 and 0.25 cm depending on beam energy. At each step, charge is collected for five seconds. Before making changes to the set-up, scans are performed with positive and negative applied voltages (typically 100 V) for polarity correction. Raw ion chamber readings are corrected with equation 1.10 (p. 9). Correction of the reduced signal due to ion recombination losses is performed using the results of chapter 3 with P_{ion} expressed in terms of the charge liberated in the chamber per pulse. Polarity corrections obtained in this work are discussed in detail with comparison to literature data in paper V.

The plane-parallel chambers investigated in this work are the same as those used for chapter 3 (list of chambers given on p. 23-24 in chapter 2). Two additional IBA NACP-02 and PTW Markus chambers are also evaluated. In addition, measurements are made with a small sample of cylindrical ion chambers. These are:

NE 2571 (2),

IBA FC65-G (2).

These cylindrical chambers are graphite-walled Farmer-type chambers that employ aluminum central electrodes. The important geometric specifications are given for all chambers in chapter 2. NRC reference chambers include the two PTW Roos chambers, the two NACP-02 chambers manufactured by Scanditronix and one NE 2571

chamber.

Since the proposed method requires the use of ratios of ion chamber readings as a function of depth, the ability to accurately set the depth of measurement is crucial. To this end, verification of the measurement depth and the depth to which useful data can be extracted before positioning uncertainties dominate is discussed in detail in paper V. The scanning system described by McEwen *et al.*[58] is used for depth-ionization measurements. The measurement depth is set using a calibrated 10 cm brass bar such that the initial depth is at 10.2 g/cm^2 accounting for the water-equivalent thickness of the phantom entrance window. All chambers are centred on the beam axis. Plane-parallel chambers are positioned with the outer front face of the chamber window at the initial depth. Cylindrical chambers are positioned with the chamber axis centred at the initial depth. Chambers are set up many times over the course of this work and repeated positioning by the same and by different operators indicate that the typical standard uncertainty in positioning is 0.1 mm.

B.2 Selected results

Relative calibration coefficients vs. depth and the effect of shifting data: This work presents ratios of ion chamber readings; any shift of a given chamber from the initial depth only shifts that chamber relative to the other chamber being used for the ratio. In this work, a negative shift moves the point of measurement of a chamber upstream toward the radiation source relative to the initial depth of the PTW Roos reference chamber. The effect of using different shifts on ratios of ion chamber readings is shown in figure B.1. An analysis of the EPOM for all of the chambers investigated is presented in paper V and the optimum relative EPOM found there, -0.17 mm, is used here.

Stability of relative calibration coefficients: Comparing the ratio of signals

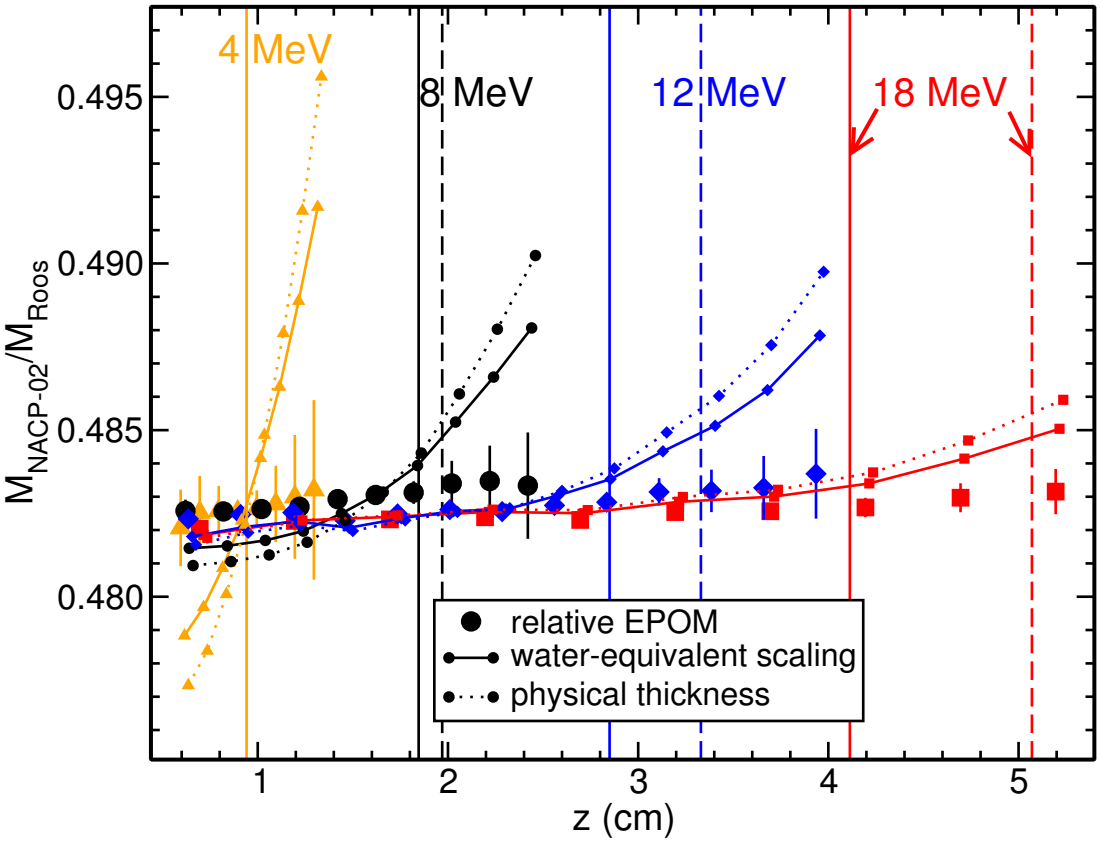

Figure B.1: The ratio of ion chamber signals from reference chambers, Scanditronix NACP-02 to PTW Roos, as a function of depth, z, in the 4 (triangles), 8 (circles), 12 (diamonds) and 18 MeV (squares) beams when the chambers are positioned using the relative EPOM determined through comparison of R_{50} values (-0.17 mm). The error bars reflect the standard uncertainty from a 0.14 mm positioning uncertainty along the beam axis. The dashed lines show the maximum depths to which the uncertainty in the chamber ratio from positioning uncertainty is less than 0.1 % (which almost never occurs in the 4 MeV beam) while the solid lines show the reference depths. The ratio of ion chamber signals is also shown when positioning is performed using water-equivalent scaling of the front window of the chambers (IAEA TRS-398[11] recommendation - filled symbols connected with solid lines, -0.42 mm) or using the physical thickness of the chamber windows (TG-51[10] recommendation - filled symbols connected with dotted lines, -0.53 mm). From paper V.

from two chambers on different days allows an investigation of the repeatability of the ratio of signals from two chambers and the stability of calibration coefficients derived using these results. The average ratio of signals near the reference depth from the reference NACP-02 to the reference PTW Roos chambers with the percent

difference compared to the initial calibration is investigated from various days. Field-size dependence of the ratio of signals is not observed and similar results are obtained with fixed depth calibrations compared to those from a depth-ionization acquisition. The standard deviation of all (10) calibrations of the reference NACP-02 against the PTW Roos chamber in an 18 MeV beam is only 0.17 %. We observed that the short- and long-term stabilities of relative calibration coefficients for plane-parallel chambers are very similar. Preliminary results obtained within four days of each other differ by 0.3 % at the reference depth. This is similar to the repeatability of the ratio of signals from the two chambers after a time period of six years.

Table B.1: The maximum difference between repeated ion chamber calibrations from the 8, 12 or 18 MeV beams when a given 'user' ion chamber is calibrated against a reference chamber. The average ratio of signals is taken near the reference depth. Modified from paper V.

Type	Chamber	Maximum difference (%)
Reference	IBA NACP-02	0.28
	PTW Roos	0.24
	NE2571	0.11
User (plane-parallel)	Exradin A10	0.39
	Exradin P11	0.30
	Exradin A11	0.19
	IBA NACP-02	0.22
	IBA PPC-05	0.06
	IBA PPC-40	0.49
User (cylindrical)	NE2571	0.03
	IBA FC65-G	0.12

Table B.1 shows the maximum difference between calibrations when the reading from a given chamber is compared to that from a reference plane-parallel chamber or, in the case of cylindrical 'user' chambers, the reference NE2571 chamber. The maximum difference between calibrations of the reference NACP-02 chamber against the reference PTW Roos is up to 0.28 %. For another reference PTW Roos chamber, the maximum difference between calibrations is up to 0.24 %. Although a 0.3 % change in the ratio of chamber readings in a time period of over a year is not large it is con-

cerning; this just meets the minimum requirement for a reference-class chamber that the stability of calibration coefficients be within 0.3 % over a period of two years.[12,95] Similar findings were observed in chapter 3 in photon beams for the same plane-parallel ion chambers compared to a stable reference cylindrical chamber. Bass *et al.*[87] observed comparable levels of stability when calibrating plane-parallel chambers at the reference depth. On average, the calibration coefficients determined in electron beams in that work[87] only changed by 0.1-0.2 % between calibrations but for some chambers the difference was up to 1 %. The same authors[87] performed Strontium-90 check source measurements with NACP-02 and PTW Roos chambers and observed stability at the 0.3 % level independent of whether the measurements were made over the course of a few weeks or a longer period up to several years.

Table B.1 also shows the maximum difference between relative calibration coefficients for several plane-parallel and cylindrical 'user' chambers when calibrations are repeated after a time period of a year to two years. The plane-parallel chambers investigated here generally show repeatability at the 0.5 % level, although the relative calibration coefficient of one of the NACP-02 chambers (not included in table B.1, considered to have failed) was different by 1.2 %. Table B.1 shows that for the NE2571 reference chamber, which has been stable at the 0.1 % level in photon beams for a period of 15 years (see paper III), the maximum difference between calibrations relative to a reference plane-parallel chamber is only 0.11 %. Although repeated results are only obtained here for two cylindrical chambers, table B.1 indicates that the calibration coefficients relative to the NE2571 reference chamber for these chambers are stable in electron beams at the 0.1 % level after a time period of almost two years.

Energy dependence of relative calibration coefficients: Figure B.2 shows the ratio of signals from the NACP-02 to the PTW Roos chambers from the 8, 12 and 18 MeV beams normalized to the average of ratios of chamber readings at $\bar{E}_z$=6.1 MeV,

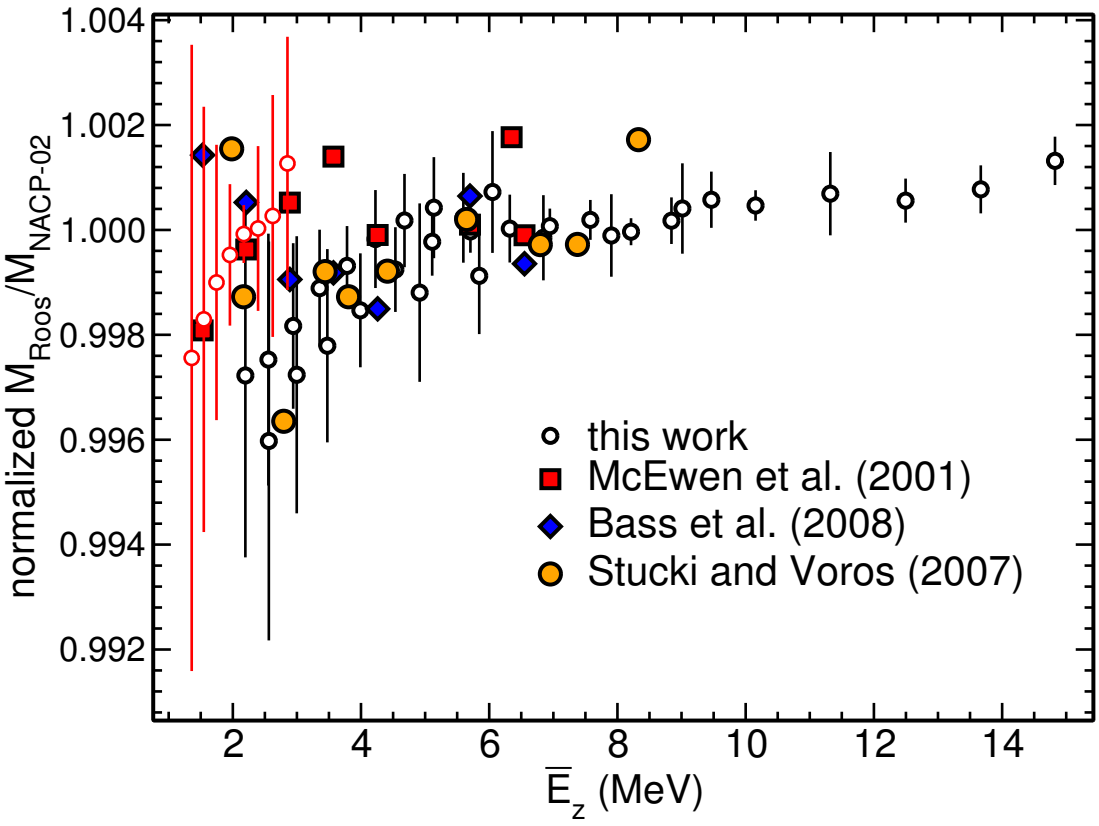

Figure B.2: The normalized ratio of the response of a reference Roos chamber to a reference NACP-02 chamber compared to data from other publications.[87,112,114] Open symbols are measurements obtained here with thicker dark (thin light) symbols representing data from the 8, 12 and 18 MeV (4 MeV) beams. From paper V.

corresponding to the average of the two highest energy points provided by McEwen *et al.*[112] and Bass *et al.*[87] at NPL. When comparing ratios of ion chamber readings to literature data, one must be sure to use the same shift as was used in the published work. These results are compared to measured results from other publications and the shift of the chambers relative to each other is -0.1 mm, the same as was used at NPL. Error bars represent standard uncertainty from the stability of the ratio of chamber readings from 2011 to 2012, any effect of scan direction/irradiation time, which is accounted for by averaging the two nearest neighbouring data points, and uncertainty in the ratio of signals from positioning uncertainty along the beam axis. The data obtained in this work in the 4 MeV beam are also provided. The results

from the 4 MeV beam show behavior which is different from the results obtained for other beam energies although the error bars are much larger at low $\bar{E}_z$ and do overlap. This type of behavior is observed for different ion chamber types and is sometimes much worse. Similar plots for other chambers for which literature values are available for comparison are in paper V.

Figure B.2 shows that the normalized ratio of response from the Roos and NACP-02 chambers as a function of average electron energy is in good agreement with measured data from other publications obtained at the reference depth.[87,112,114] Similar energy dependence of the ratios of chamber readings (or relative chamber perturbation factors) is observed among all studies. At low electron energies, all investigations observe variability of the ratio of $N_{D,w}$ coefficients with energy, albeit with larger uncertainties.

B.3 Conclusions

Although not presented here, the issue of the effective point of measurement is analyzed by comparing R_{50} values determined with reference PTW Roos chambers compared to that obtained with other ion chambers. The results of paper V show that using water-equivalent scaling of the front window of a plane-parallel chamber to estimate the EPOM may be too simplistic an approach. The shifts determined here are not generally equivalent to the EPOM determined with water-equivalent scaling and, for some chambers, beam-dependent shifts are observed.

The variability of relative calibration coefficients for chambers other than the PTW Roos compared to the NACP-02 at similar average electron energies indicates that the mean electron energy at depth is not a sufficient quality specifier to combine results from different electron beams.

The proposed method of obtaining dosimetric data in electron beams allows the efficient collection of ratios of ion chamber calibration coefficients at all clinically relevant electron energies. This method obtains more information regarding energy dependence of relative chamber measurements in less time while reproducing the results from other publications using the conventional fixed-depth method. However, the results obtained with the proposed method are only useful at shallow depths before effects from small shifts, linac drift or minor differences in chamber construction dramatically affect the results. The results presented in paper V show that absolute calibration coefficients can be obtained for well-behaved chambers with uncertainty less than 0.5 %. However, the short- and long-term stabilities of the plane-parallel ion chambers investigated continue to pose problems. The results of this work indicate that stable cylindrical ion chambers might be better suited for electron beam dosimetry.

Appendix C

Monte Carlo calculations of overall ion chamber perturbation factors with depth

This thesis has focused on the determination of more accurate reference dosimetric data. The discussion is now shifted to the accurate determination of depth-dose data from depth-ionization measurements, needed for clinical treatment planning systems to determine absorbed dose for real treatments. The discussion presented here focuses on the PTW Roos ion chamber but similar results are obtained for the NE2571 chamber in paper VI.

C.1 Determination of overall ion chamber perturbation factors and minimization of variation with depth

The calculated D_w/D_{ch} ratios from electron beams obtained for calculations of k_Q factors in chapter 6 along with Spencer-Attix water-to-air mean restricted mass collision stopping power ratios, $\left(\overline{L}/\rho\right)_{air}^{water}$, are used to obtain the overall ion chamber perturbation factor, P_{Q}, (defined in equation 1.5, p. 6) with

$$P_{\mathrm{Q}} = \left(\frac{D_w}{D_{ch}}\right) \Big/ \left(\frac{\bar{L}}{\rho}\right)_{air}^{water} . \tag{C.1}$$

Stopping power ratios as a function of depth in water are obtained using the `SPRRZnrc`[53] user-code with a subset of the source models described in chapter 2. Since the RZ user-codes can only model cylindrical geometries, point sources using electron beam spectra are modelled with a radius of 5.64 cm (equivalent to a 10×10 cm^2 field size) on the surface of the phantom. The water phantom is cylindrical with a radius of 20 cm, 30 cm thick. Calculations are performed in seventy discs starting at the surface of the phantom with 0.5 cm radii and thicknesses between 0.05 and 0.2 cm, depending on the incident beam energy. The results for stopping power ratios obtained here are generally in agreement down to the projected range within 1 % with calculations using the fit as a function of depth and R_{50} provided in equation 7 of Burns *et al.*[24] and recommended in TG-51.[10] Tighter agreement is not expected due to the general nature of the fit.[25]

Kawrakow[129] and Tessier and Kawrakow[123] studied the issue of the effective point of measurement (EPOM) in photon beams. By varying the shift, Δz, of a given chamber's point of measurement they determined the optimal shift to minimize the variation of the ratio of the absorbed dose to water to the absorbed dose to the gas in an ion chamber, $D_w(z+\Delta z)/D_{ch}(z)$, with depth, z. χ^2-minimization was used to determine the optimal EPOM shift. In photon beams, except near the surface, the stopping power ratio is nearly independent of depth so, in those publications, the variation of the stopping power ratio was ignored. In this work, a similar procedure is employed except that, instead of minimizing the variation of D_w/D_{ch} we investigate the variation of calculated P_{Q} factors from equation C.1 with depth. χ^2 is calculated as a function of the shift, Δz, as

$$\chi^2(\Delta z) = \sum_{i=1}^{N_z} \frac{(P_{\mathrm{Q}}(z_i+\Delta z) - \overline{P_{\mathrm{Q}}})^2}{P_{\mathrm{Q}}^2(z_i+\Delta z)(s_{D_w}^2 + s_{D_{ch}}^2 + s_{SPR}^2)}, \tag{C.2}$$

where the sum is over depths, z_i. In this equation, the overall chamber perturbation factor, $P_{\mathrm{Q}}(z_i + \Delta z)$, is compared to the mean overall chamber perturbation factor $\overline{P_{\mathrm{Q}}}$ and the components of uncertainty s_{D_w}, $s_{D_{ch}}$, and s_{SPR} are the fractional statistical uncertainties in calculated doses to water, the gas in the chamber and the stopping power ratio. Minimization of χ^2 with respect to Δz is performed in order to determine the optimum shift to minimize the variation of P_{Q} with depth from depths close to the phantom surface to either the projected range, R_p, or R_{50}.

C.2 Selected results

Figure C.1 shows the overall ion chamber correction factor, P_{Q}, calculated with equation C.1 as a function of depth for the PTW Roos chamber. Results for P_{Q} shown in figure C.1 use the Elekta *Precise* 8 and 18 MeV `BEAMnrc` accelerator models. The inset shows the results obtained when the point of measurement for the PTW Roos chamber is taken as the inside of the front face of the chamber window determined using the physical thickness as recommended by TG-51.[10] Also shown in figure C.1 are P_{Q} corrections when the optimal shift to minimize the variation of P_{Q} as a function of depth to either R_p or R_{50} is determined with the χ^2-minimization procedure discussed above.

Figure C.1 shows that using optimal shifts results in P_{Q} approaching unity. This explains the observation discussed in chapter 6, that a shift of the chamber data results in a reduced difference between R_{50} calculated from chamber simulations with equation 6.1 (which assumes a perturbation-free ion chamber, i.e., P_{Q}=1) compared to that calculated from dose to water simulations. The shift to reduce that difference for the PTW Roos chamber (1.55 mm) is very close to the average values of the optimal shifts, Δz, presented in figure C.2 (a).

In figure C.1, different shifts are required to minimize the variation of the overall

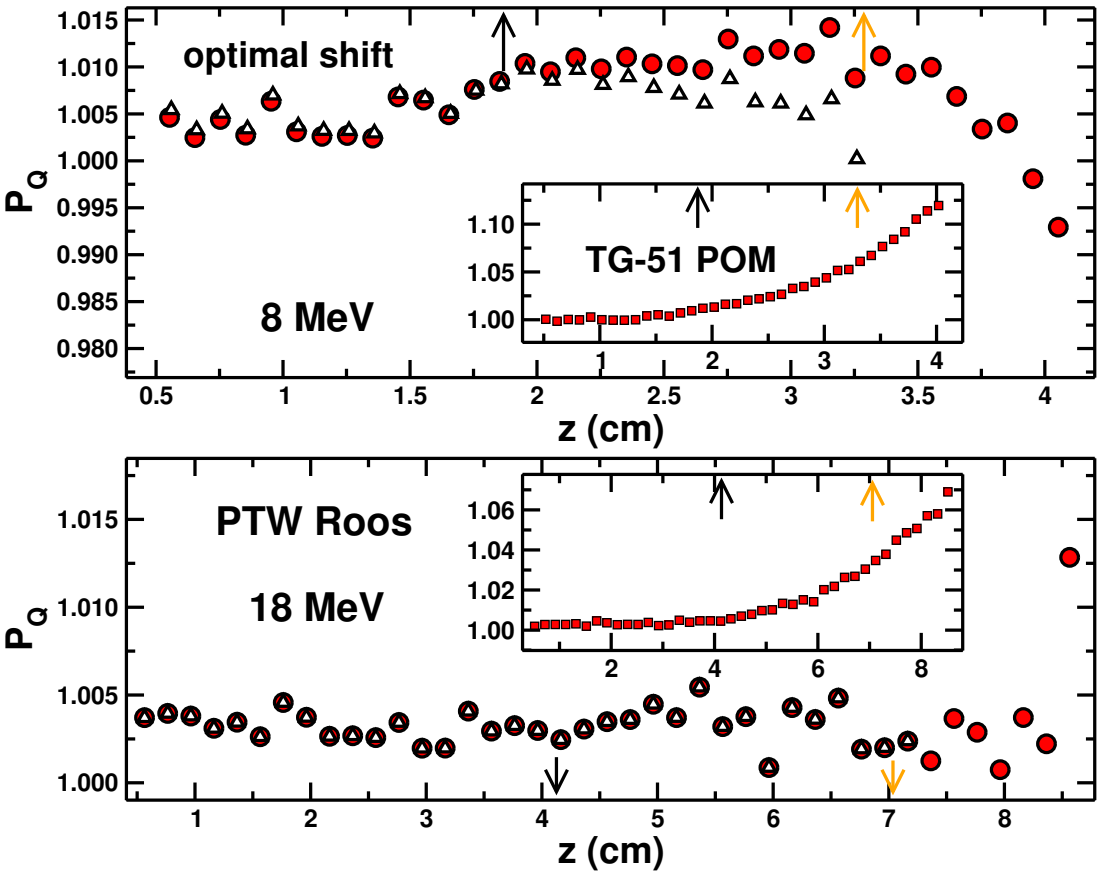

Figure C.1: The overall ion chamber correction factor (equation C.1) as a function of depth in an 8 and 18 MeV beam for the PTW Roos chamber. Results are shown with the point of measurement at the inside of the front face of the PTW Roos chamber (TG-51 POM) and using optimal shifts to minimize the variation of P_Q with depth to R_p (filled circles) or to R_{50} (open triangles). The shift values are 1.55 mm (1.48 mm) and 1.58 mm (1.59 mm) in the 8 and 18 MeV beams, respectively, for minimization of P_Q variation with depth to R_{50} (R_p). Dark and light arrows indicate d_{ref} and R_{50}, respectively. From paper VI.

ion chamber perturbation factor with depth for the PTW Roos chamber if the calculated data are considered to different depths, R_p or R_{50}. Figure C.2 (a) shows that if the depth-dependence is considered to only R_{50}, the resulting shifts are systematically higher for most beams than if the data are considered to R_p. Lacroix *et al.*[130] made a similar observation when considering measured data - when minimization of the variation of P_Q was performed to R_{50} their resulting shift was systematically slightly

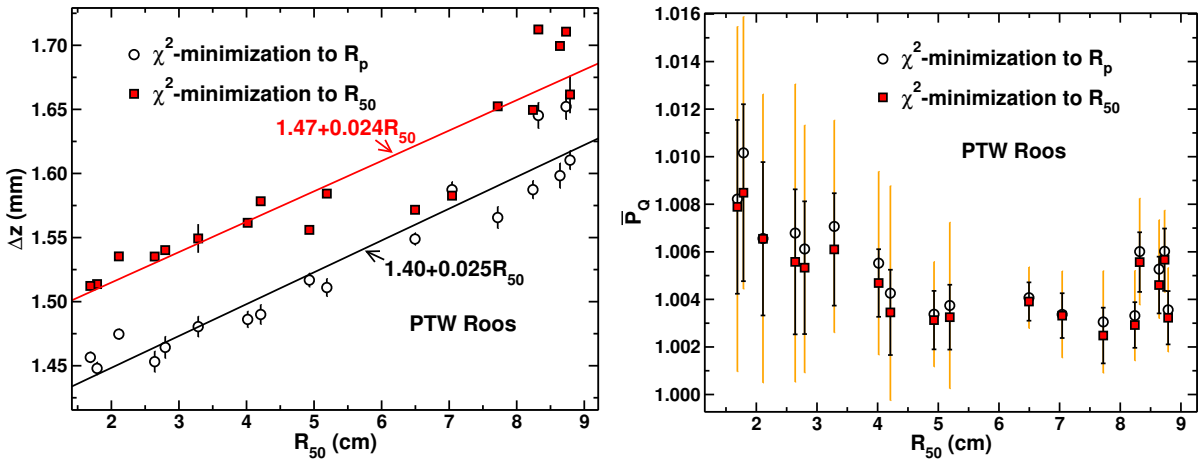

(a) (b)

Figure C.2: Panel (a): Optimal shifts, Δz, to minimize the variation of P_{Q} with depth to R_p (circles) or to R_{50} (squares) as a function of R_{50} in beams with different energies for the PTW Roos chamber. Panel (b): The average overall ion chamber correction factor, $\overline{P}_{\mathrm{Q}}$, for the shift which minimizes χ^2 in equation C.2 as a function of R_{50} for the PTW Roos chamber. Error bars in panel (b) represent the standard deviation of the P_{Q} values as a function of depth from the mean values. From paper VI.

higher than when the data were considered to R_p. Figure C.2 (a) shows the optimal shift of the point of measurement for the PTW Roos chamber as a function of R_{50} in several different beams when the minimization procedure is performed to either R_p or R_{50}. The optimal shifts in figure C.2 (a) do appear to be energy dependent with Δz varying between 1.45 mm in the Elekta *Precise* 4 MeV beam to 1.65 mm in the 22 MeV beam from the same accelerator when data are considered to R_p.

Figure C.2 (b) shows that the actual average value of the overall perturbation factor is not largely affected when considering the data to different depths. However, the standard deviations of the P_{Q} results from the mean values, $\overline{P}_{\mathrm{Q}}$, shown by the error bars in figure C.2 (b), are much lower when the minimization of the variation of P_{Q} is only performed to R_{50}. Using optimal shifts, the standard deviation from the mean of the overall beam-specific ion chamber correction factor as a function of depth for the PTW Roos chamber is between 0.13 to 0.72 % considering data to R_p (0.08

to 0.37 % considering data to R_{50}). For the NE2571 chamber, the variation is much more dramatic - the standard deviation is up to 5.3 % when the data are considered to R_p but if the results are only considered to R_{50} the standard deviation is at most 1.5 % in low-energy beams. In high-energy beams, the standard deviation of P_{Q} from the mean value is less sensitive when considering data to different depths. These results indicate that a shift of the point of measurement along with the application of the stopping power ratio as a function of depth might be appropriate to convert from depth-ionization measurements to obtain a depth-dose curve but could result in unacceptable errors if the NE2571 chamber is used in low-energy beams.

Other publications have investigated optimal EPOM shifts to minimize the variation of P_{Q} with depth in electron beams. Lacroix *et al.*[130] used ionization measurements from plane-parallel ion chambers compared to an (assumed perturbation-free) plastic scintillation detector to determine optimal shifts. These amount to 1.12±0.1, 1.40±0.1 and 1.90±0.2 mm for the Roos chamber in 6, 12 and 18 MeV beams, respectively, and given their large uncertainties are in reasonable agreement with the results obtained here. In this work and in Lacroix *et al.*,[130] an energy dependent optimal EPOM is observed which increases with increasing beam energy. Using Monte Carlo simulations, Zink and Wulff[131] determined that the optimal EPOMs for a Roos chamber in 6, 11 and 21 MeV beams are 1.48±0.03, 1.51±0.05 and 1.51±0.05 mm, respectively. Again, these results are in reasonable agreement with those obtained here, although the results observed by Zink and Wulff[131] are nearly independent of beam energy. Zink and Wulff[131] also determined that a shift of 0.17 mm from the front of the cavity minimizes the variation of the wall perturbation factor with depth for the PTW Roos chamber. The calculated EPOM of Wang and Rogers[132] for a bare Roos chamber without walls was 0.18 mm from the front of the cavity in a 6 MeV beam. Adding these two optimal shifts that minimize variation of effects from

the wall and cavity separately, along with the physical thickness of the window of the PTW Roos chamber, gives a shift of 1.48 mm, very close to the resulting optimal Δz obtained here in low-energy beams.

C.3 Discussion and conclusions

The question remains as to what should be recommended to obtain clinical depth-dose curves. As mentioned above, the stopping power ratios calculated here agree within 1 % of the fit as a function of depth and R_{50} provided by Burns *et al.*[24] When using the optimal EPOM for the PTW Roos chamber, the low values of the standard deviation of the overall chamber perturbation factor with depth indicate that it would be reasonable to obtain a depth-ionization curve in the clinical beam with the shift of the ion chamber to minimize P_{Q} variation with depth and correct the curve using the stopping power ratio calculated with the Burns *et al.*[24] fit. For the NE2571 chamber, the high values of standard deviation of the overall chamber perturbation factor with depth indicate that the same approach will likely result in unacceptable errors in the percentage depth-dose curve if data are considered to R_p but may be acceptable if data are only considered to R_{50}. The optimal shifts and average chamber perturbation factors are more important for reference dosimetry if data are only considered to R_{50} instead of R_p because (i) all reference dosimetry parameters are determined in the region between the surface and R_{50}; and, (ii) the discrepancies between the local P_{Q} and the average value past R_{50} may be large but introduce a small component of error when converting to dose to water as a fraction of D_{max}.

The results of this investigation explain the observation discussed in chapter 6, that a shift of the chamber data results in a reduced difference between R_{50} calculated from chamber simulations with equation 6.1 (p. 91) compared to that calculated from dose to water simulations, because the shift causes P_{Q} to approach unity at R_{50}.

References

[1] P. R. Almond, A Historical Perspective: A Brief History of Dosimetry, Calibration Protocols, and the Need for Accuracy, in *Clinical Dosimetry Measurements in Radiotherapy*, edited by D. W. O. Rogers and J. E. Cygler, pages 1 – 27, Medical Physics Publishing, Madison, Wisconsin, 2009.

[2] E. G. A. Aird and F. T. Farmer, The design of a thimble chamber for the Farmer dosemeter, Phys. Med. Biol. **17**, 169 – 174 (1972).

[3] L. A. DeWerd, S. D. Davis, L. J. Bartol, and F. Grenzow, Ionization chamber instrumentation, in *Clinical dosimetry measurements in radiotherapy*, edited by D. W. O. Rogers and J. E. Cygler, Medical Physics Publishing, Madison, Wisconsin, 2009.

[4] F. H. Attix, *Introduction to Radiological Physics and Radiation Dosimetry*, Wiley, New York, 1986.

[5] L. V. Spencer and F. H. Attix, A theory of cavity ionization, Radiat. Res. **3**, 239 – 254 (1955).

[6] J. Seuntjens and D. W. O. Rogers, Monte Carlo applications in measurement dosimetry, in *Clinical Dosimetry Measurements in Radiotherapy*, edited by D. W. O. Rogers and J. E. Cygler, pages 147 – 180, Medical Physics Publishing, Madison, Wisconsin, 2009.

[7] L. L. W. Wang and D. W. O. Rogers, Calculation of the replacement correction factors for ion chambers in megavoltage beams by Monte Carlo simulation, Med. Phys. **35**, 1747 – 1755 (2008).

[8] F. W. Wittkämper, H. Thierens, A. Van der Plaetsen, C. de Wagter, and B. J. Mijnheer, Perturbation correction factors for some ionization chambers commonly applied in electron beams, Phys. Med. Biol. **36**, 1639 – 1652 (1991).

[9] L. A. Buckley and D. W. O. Rogers, Wall correction factors, P_{wall}, for parallel-plate ionization chambers, Med. Phys. **33**, 1788 – 1796 (2006).

[10] P. R. Almond, P. J. Biggs, B. M. Coursey, W. F. Hanson, M. S. Huq, R. Nath, and D. W. O. Rogers, AAPM's TG–51 protocol for clinical reference dosimetry of high-energy photon and electron beams, Med. Phys. **26**, 1847 – 1870 (1999).

[11] IAEA, *Absorbed Dose Determination in External Beam Radiotherapy: An International Code of Practice for Dosimetry Based on Standards of Absorbed Dose to Water V12*, volume 398 of *Technical Report Series*, IAEA, Vienna, 2006.

[12] M. R. McEwen, L. A. DeWerd, G. S. Ibbott, D. S. Followill, D. W. O. Rogers, S. M. Seltzer, and J. P. Seuntjens, Addendum to the AAPM's TG–51 protocol for clinical reference dosimetry of high-energy photon beams, Med. Phys. **40**, submitted May (2013).

[13] D. W. O. Rogers, The physics of the AAPM's TG-51 protocol, in *Clinical Dosimetry Measurements in Radiotherapy*, edited by D. W. O. Rogers and J. E. Cygler, pages 239 – 296, Medical Physics Publishing, Madison, Wisconsin, 2009.

[14] D. W. O. Rogers and C. K. Ross, The role of humidity and other correction factors in the AAPM TG–21 dosimetry protocol, Med. Phys. **15**, 40 – 48 (1988).

[15] H. Svensson and A. Brahme, Recent Advances in Electron and Photon Dosimetry, in *Radiation Dosimetry*, edited by C. G. Orton, pages 87 – 170, Plenum Press, New York, 1986.

[16] S. R. Domen and P. J. Lamperti, Comparisons of calorimetric and ionometric measurements in graphite irradiated with electrons from 15 to 50 MeV, Med. Phys. **3**, 294 – 301 (1976).

[17] IAEA, *Absorbed Dose Determination in External Beam Radiotherapy: An International Code of Practice for Dosimetry Based on Standards of Absorbed Dose to Water*, volume 398 of *Technical Report Series*, IAEA, Vienna, 2001.

[18] J. P. Seuntjens, C. K. Ross, K. R. Shortt, and D. W. O. Rogers, Absorbed-dose beam quality conversion factors for cylindrical chambers in high-energy photon beams, Med. Phys. **27**, 2763 – 2779 (2000).

[19] A. Kosunen and D. W. O. Rogers, Beam quality specification for photon beam dosimetry, Med. Phys. **20**, 1181 – 1188 (1993).

[20] N. I. Kalach and D. W. O. Rogers, Which accelerator photon beams are "clinic-like" for reference dosimetry purposes?, Med. Phys. **30**, 1546 – 1555 (2003).

[21] G. Xiong and D. W. O. Rogers, Relationship between $\%dd(10)_x$ and stopping-power ratios for flattening filter free accelerators: A Monte Carlo study, Med. Phys. **35**, 2104 – 2109 (2008).

[22] D. W. O. Rogers and C. L. Yang, Corrected relationship between $\%dd(10)_x$ and stopping-power ratios, Med. Phys. **26**, 538 – 540 (1999).

[23] G. X. Ding, D. W. O. Rogers, and T. R. Mackie, Calculation of stopping-power ratios using realistic clinical electron beams, Med. Phys. **22**, 489 – 501 (1995).

[24] D. T. Burns, G. X. Ding, and D. W. O. Rogers, R_{50} as a beam quality specifier for selecting stopping-power ratios and reference depths for electron dosimetry, Med. Phys. **23**, 383 – 388 (1996).

[25] D. W. O. Rogers, Accuracy of the Burns equation for stopping-power ratio as a function of depth and R_{50}, Med. Phys. **31**, 2961 – 2963 (2004).

[26] K. Zink and J. Wulff, Beam quality corrections for parallel-plate ion chambers in electron reference dosimetry, Phys. Med. Biol. **57**, 1831–1854 (2012).

[27] F. Verhaegen, R. Zakikhani, A. DuSautoy, H. Palmans, G. Bostock, D. Shipley, and J. Seuntjens, Perturbation correction factors for the NACP-02 plane-parallel ionization chamber in water in high-energy electron beams, Phys. Med. Biol. **51**, 1221 – 1235 (2006).

[28] C.-M. Ma and A. E. Nahum, Effect of size and composition of central electrode on the response of cylindrical ionisation chambers in high-energy photon and electron beams, Phys. Med. Biol. **38**, 267 – 290 (1993).

[29] A. Palm and O. Mattsson, Experimental study on the influence of the central electrode in Farmer-type ionization chambers, Phys. Med. Biol. **44**, 1299 – 1308 (1999).

[30] L. A. Buckley, I. Kawrakow, and D. W. O. Rogers, CSnrc: correlated sampling Monte Carlo calculations using EGSnrc, Med. Phys. **31**, 3425 – 3435 (2004).

[31] J. Wulff, J. T. Heverhagen, and K. Zink, Monte-Carlo-based perturbation and beam quality correction factors for thimble ionization chambers in high-energy photon beams, Phys. Med. Biol. **53**, 2823 – 2836 (2008).

[32] P. R. Almond and H. Svensson, Ionization chamber dosimetry for photon and electron Beams, Acta Radiol. Ther. Phys. Biol. **16**, 177 – 186 (1977).

[33] L. A. Buckley and D. W. O. Rogers, Wall correction factors, P_{wall}, for thimble ionization chambers, Med. Phys. **33**, 455 – 464 (2006).

[34] M. R. McEwen, Measurement of ionization chamber absorbed dose k_Q factors in megavoltage photon beams, Med. Phys. **37**, 2179 – 2193 (2010).

[35] C. K. Ross and K. R. Shortt, The effect of waterproofing sleeves on ionization chamber response, Phys. Med. Biol. **37**, 1403 – 1411 (1992).

[36] A. Kosunen, H. Järvinen, and P. Sipilä, Optimum calibration of NACP type plane-parallel ionization chambers for absorbed dose determinations in low energy electron beams, in *Proc. of Symp. on Meas. Assurance in Dosimetry*, pages 505 – 513, IAEA–SM–330/419, IAEA, Vienna, 1994.

[37] D. W. O. Rogers, A new approach to electron beam reference dosimetry, Med. Phys. **25**, 310 – 320 (1998).

[38] E. Mainegra-Hing, I. Kawrakow, and D. W. O. Rogers, Calculations for plane-parallel ion chambers in ^{60}Co beams using the EGSnrc Monte Carlo code, Med. Phys. **30**, 179 – 189 (2003).

[39] K. A. Johansson, L. O. Mattsson, L. Lindborg, and H. Svensson, Absorbed-dose determination with ionization chambers in electron and photon beams having energies between 1 and 50 MeV, in *IAEA Symposium Proceedings*, pages 243 – 270, IAEA–SM–222/35, IAEA, Vienna, 1978.

[40] J. R. Cunningham and M. R. Sontag, Displacement corrections used in absorbed dose determinations, Med. Phys. **7**, 672 – 676 (1980).

[41] L. L. W. Wang and D. W. O. Rogers, The replacement correction factors for cylindrical chambers in high-energy photon beams, Phys. Med. Biol. **54**, 1609 – 1620 (2009).

[42] A. Van der Plaetsen, J. Seuntjens, H. Thierens, and S. Vynckier, Verification of absorbed doses determined with thimble and parallel-plate ionization chambers in clinical electron beams using ferrous sulphate dosimetry, Med. Phys. **21**, 37 – 44 (1994).

[43] L. L. W. Wang and D. W. O. Rogers, Replacement correction factors for cylindrical ion chambers in electron beams, Med. Phys. **36**, 4600 – 4608 (2009).

[44] K. Zink and J. Wulff, Monte Carlo calculations of beam quality correction factors k_Q for electron dosimetry with a parallel-plate Roos chamber, Phys. Med. Biol. **53**, 1595 – 1607 (2008).

[45] I. Kawrakow, Accurate condensed history Monte Carlo simulation of electron transport. I. EGSnrc, the new EGS4 version, Med. Phys. **27**, 485 – 498 (2000).

[46] I. Kawrakow, E. Mainegra-Hing, D. W. O. Rogers, F. Tessier, and B. R. B. Walters, The EGSnrc Code System: Monte Carlo simulation of electron and photon transport, NRC Technical Report PIRS-701 v4-2-3-2, National Research Council Canada, Ottawa, Canada. http://www.irs.inms.nrc.ca/inms/irs/EGSnrc/EGSnrc.html, 2011.

[47] W. R. Nelson, H. Hirayama, and D. W. O. Rogers, The EGS4 code system, Report SLAC–265, Stanford Linear Accelerator Center, Stanford, California, 1985.

[48] I. Kawrakow, Accurate condensed history Monte Carlo simulation of electron transport. II. Application to ion chamber response simulations, Med. Phys. **27**, 499 – 513 (2000).

[49] J. Wulff, K. Zink, and I. Kawrakow, Efficiency improvements for ion chamber calculations in high energy photon beams, Med. Phys. **35**, 1328– 1336 (2008).

[50] I. Kawrakow, E. Mainegra-Hing, F. Tessier, and B. R. B. Walters, The EGSnrc C++ class library, Technical Report PIRS–898 (rev A), National Research Council of Canada, Ottawa, Canada. http://www.irs.inms.nrc.ca/EGSnrc/PIRS898/, 2009.

[51] D. W. O. Rogers, B. A. Faddegon, G. X. Ding, C.-M. Ma, J. Wei, and T. R. Mackie, BEAM: A Monte Carlo code to simulate radiotherapy treatment units, Med. Phys. **22**, 503 – 524 (1995).

[52] D. W. O. Rogers, B. Walters, and I. Kawrakow, BEAMnrc Users Manual, NRC Technical Report PIRS-509(A) revL, National Research Council of Canada, Ottawa, Canada. http://www.irs.inms.nrc.ca/BEAM/beamhome.html, 2011.

[53] D. W. O. Rogers, I. Kawrakow, J. P. Seuntjens, B. R. B. Walters, and E. Mainegra-Hing, NRC user codes for EGSnrc, NRC Technical Report PIRS-702 (rev C), National Research Council of Canada, Ottawa, Canada. http://www.irs.inms.nrc.ca/EGSnrc/PIRS702/, 2011.

[54] R. P. Kapsch, G. Bruggmoser, G. Christ, O. S. Dohm, G. H. Hartmann, and E. Schüle, Experimental determination of p_{Co} perturbation factors for plane-parallel chambers, Phys. Med. Biol. **52**, 7167 – 7181 (2007).

[55] R. P. Kapsch and I. Gomola, Beam quality correction factors for plane parallel chambers in photon beams , IAEA–E2-CN-182, *Book of Extended Synopses for Symp. on Standards, Applications and Quality Assurance in Medical Radiation Dosimetry* (IAEA, Vienna) , 35 – 36 (2010).

[56] C. K. Ross, J. P. Seuntjens, N. V. Klassen, and K. R. Shortt, The NRC Sealed Water Calorimeter: Correction Factors and Performance, in *Proceedings of NPL Workshop on Recent Advances in Calorimetric Absorbed Dose Standards*, edited by A. J. Williams and K. E. Rosser, pages 90–102, National Physical Laboratory, Teddington, UK, 2000.

[57] M. R. McEwen and C. K. Ross, Direct calibration of ionization chambers in linac photon beams, Med. Phys. (abstract) **32**, 2128 (2005).

[58] M. R. McEwen, I. Kawrakow, and C. K. Ross, The effective point of measurement of ionization chambers and the build-up anomaly in MV x-ray beams, Med. Phys. **35**, 950 – 958 (2008).

[59] J. P. McCaffrey, B. Downton, H. Shen, D. Niven, and M. McEwen, Pre-irradiation effects on ionization chambers used in radiation therapy, Phys. Med. Biol. **50**, N121 – N133 (2005).

[60] L. L. Campos and L. V. E. Caldas, Induced effects in ionization chamber cables by photon and electron irradiation, Med. Phys. **18**, 522 – 526 (1991).

[61] D. T. Burns and M. R. McEwen, Ion recombination corrections for the NACP parallel-plate chamber in a pulsed electron beam, Phys. Med. Biol. **43**, 2033 – 2045 (1998).

[62] J. W. Boag, Ionization measurements at very high intensities. I. Pulsed radiation beams, Brit. J. Radiol. **23**, 601 – 611 (1950).

[63] J. W. Boag, Ion chambers, in *Radiation Dosimetry, Vol II*, edited by F. H. Attix and W. C. Roesch, pages 1 – 72, Academic Press, New York, 1966.

[64] G. Bruggmoser, R. Saum, A. Schmachtenberg, F. Schmid, and E. Schule, Determination of the recombination correction factor k_S for some specific plane-parallel and cylindrical ionization chambers in pulsed photon and electron beams, Phys. Med. Biol. **52**, N35 – N50 (2007).

[65] C. Zankowski and E. B. Podgorsak, Determination of saturation charge and collection efficiency for ionization chambers in continuous beams, Med. Phys. **25**, 908 – 915 (1998).

[66] D. M. González-Castaño, G. H. Hartmann, F. Sánchez-Doblado, F. Gómez, R.-P. Kapsch, J. Pena, and R. Capote, The determination of beam quality correction factors: Monte Carlo simulations and measurements, Phys. Med. Biol. **54**, 4723 – 4741 (2009).

[67] L. Tantot and J. P. Seuntjens, Modelling ionization chamber response to non-standard beam configurations, J of Phys: Conf Series **102**, 012023 (9 pp) (2008).

[68] F. Erazo and A. M. Lallena, Calculation of beam quality correction factors for various thimble ionization chambers using the Monte Carlo code PENELOPE, Physica Medica **29**, 163 – 170 (2013).

[69] M. J. Berger, J. H. Hubbell, S. M. Seltzer, J. Chang, J. S. Coursey, R. Sukumar, D. S. Zucker, and K. Olsen, XCOM: Photon cross section database (version 1.5), Technical report, NIST, Gaithersburg, MD, http://physics.nist.gov/xcom, 2010.

[70] S. M. Seltzer and M. J. Berger, Bremsstrahlung spectra from electron interactions with screened atomic nuclei and orbital electrons, Nucl. Inst. Meth. B **12**, 95 – 134 (1985).

[71] S. M. Seltzer and M. J. Berger, Bremsstrahlung energy spectra from electrons with kinetic energy from 1 keV to 10 GeV incident on screened nuclei and orbital electrons of neutral atoms with Z = 1 – 100, Atomic Data and Nuclear Data Tables **35**, 345 – 418 (1986).

[72] J. Wulff, J. T. Heverhagen, K. Zink, and I. Kawrakow, Investigation of systematic uncertainties in Monte Carlo-calculated beam quality correction factors, Phys. Med. Biol. **55**, 4481 – 4493 (2010).

[73] O. Chibani and C. M. Ma, On the discrepancies between Monte Carlo dose calculations and measurements for the 18 MV Varian photon beam, Med. Phys. **34**, 1206 – 1216 (2007).

[74] C.-M. Ma and A. E. Nahum, Calculation of absorbed dose ratios using correlated Monte Carlo sampling, Med. Phys. **20**, 1189 – 1199 (1993).

[75] D. J. La Russa, M. McEwen, and D. W. O. Rogers, An experimental and computational investigation of the standard temperature-pressure correction factor for ion chambers in kilovoltage x rays, Med. Phys. **34**, 4690 – 4699 (2007).

[76] G. Mora, A. Maio, and D. W. O. Rogers, Monte Carlo simulation of a typical ^{60}Co therapy source, Med. Phys. **26**, 2494 – 2502 (1999).

[77] D. Sheikh-Bagheri and D. W. O. Rogers, Monte Carlo calculation of nine megavoltage photon beam spectra using the BEAM code, Med. Phys. **29**, 391 – 402 (2002).

[78] R. Mohan, C. Chui, and L. Lidofsky, Energy and angular distributions of photons from medical linear accelerators, Med. Phys. **12**, 592 – 597 (1985).

[79] G. X. Ding and D. W. O. Rogers, Energy spectra, angular spread, and dose distributions of electron beams from various accelerators used in radiotherapy, NRC Report PIRS–0439, NRC, Ottawa, K1A 0R6, 1995.

[80] G. G. Zhang, D. W. O. Rogers, J. E. Cygler, and T. R. Mackie, Effects of changes in stopping-power ratios with field size on electron beam ROFs, Med. Phys. **25**, 1711 – 1724 (1998).

[81] ICRU, Stopping powers for electrons and positrons, ICRU Report 37, ICRU, Bethesda, MD., 1984.

[82] International Standards Organization (ISO), Guide to the Expression of Uncertainty in Measurement, ISO report, International Standards Organization, ISO, Geneva, Switzerland, 2005.

[83] J. H. Hubbell, Review of photon interaction cross section data in the medical and biological context, Phys. Med. Biol. **44**, R1 – R22 (1999).

[84] M. J. Berger, J. H. Hubbell, S. M. Seltzer, J. S. Coursey, and D. S. Zucker, XCOM: Photon cross section database (version 1.2), Report NBSIR87-3597, NIST, Gaithersburg, MD, 1999, see http://physics.nist.gov/xcom.

[85] D. W. O. Rogers and I. Kawrakow, Monte Carlo calculated correction factors for primary standards of air-kerma, Med. Phys. **30**, 521 – 543 (2003).

[86] M. R. McEwen, S. Duane, and R. A. S. Thomas, Absorbed dose calibration factors for parallel-plate chambers in high energy photon beams, in *Standards and Codes of Practice in Medical Radiation Dosimetry; Proc. Int'l Symp, Vienna 25 – 28 Nov 2002*, volume 1, pages 335 – 341, IAEA, Vienna, 2003.

[87] G. Bass, R. Thomas, and J. Pearce, The calibration of parallel-plate electron ionization chambers at NPL for use with the IPEM 2003 code of practice: summary data, Phys. Med. Biol. **54**, N115 – N124 (2009).

[88] M. Berg and O. Noerrevang, Recombination factors for the cylindrical FC65-G ionization chamber in pulsed photon beams and the plane-parallel Roos ionization chamber in pulsed electron beams, Phys. Med. Biol. **49**, 5309 – 5318 (2004).

[89] J. Pearce, R. Thomas, and A. DuSautoy, The characterization of the Advanced Markus ionization chamber for use in reference electron dosimetry in the UK, Phys. Med. Biol. **51**, 473 – 483 (2006).

[90] K. Derikum, Correcting for ion recombination effects in ionization chambers consistently in continuous and pulsed radiation, in *Standards and Codes of Practice in Medical Radiation Dosimetry; Proc. Int'l Symp, Vienna 25 – 28 Nov 2002*, volume 1, pages 353 – 359, IAEA, Vienna, 2003.

[91] A. Nisbet and D. I. Thwaites, Polarity and ion recombination correction factors for ionization chambers employed in electron beam dosimetry, Phys. Med. Biol. **43**, 435 – 443 (1998).

[92] K. Derikum, Evaluation of different methods for determining the magnitude of inital recombination in ionization chambers, *Proceed. of Absorbed Dose and Air Kerma Primary Standards Workshop*, LNHB, Paris , http://www.nucleide.org/ADAKPS_WS/ (May, 2007).

[93] G. Christ, O. S. Dohm, G. Bruggmoser, and E. Schüle, The use of plane-parallel chambers in electron dosimetry without any cross-calibration, Phys. Med. Biol. **47**, N121 – N126 (2002).

[94] A. Palm, L. Czap, P. Andreo, and O. Mattsson, Performance analysis and determination of the p_{wall} correction factor for ^{60}Co γ-ray beams for Wellhöfer Roos-type plane-parallel chambers, Phys. Med. Biol. **47**, 631 – 640 (2002).

[95] IAEA, *Calibration of Reference Dosimeters for External Beam Radiotherapy*, volume 469 of *Technical Report Series*, IAEA, Vienna, 2009.

[96] A. Krauss and R.-P. Kapsch, Calorimetric determination of k_Q factors for NE 2561 and NE 2571 ionization chambers in 5 cm $\times$ 5 cm and 10 cm $\times$ 10 cm radiotherapy beams of 8 MV and 16 MV photons, Phys. Med. Biol. **52**, 6243 – 6259 (2007).

[97] H. Palmans, W. Mondelaers, and H. Thierens, Absorbed dose beam quality correction factors k_Q for the NE2571 chamber in a 5 MV and 10 MV photon beam, Phys. Med. Biol. **44**, 647–663 (1999).

[98] V. Panettieri, J. Sempau, and P. Andreo, Chamber-quality factors in ^{60}Co for three plane-parallel chambers for the dosimetry of electrons, protons and heavier charged particles: PENELOPE Monte Carlo simulations, Phys. Med. Biol. **53**, 5917 – 5926 (2008).

[99] J. Wulff and K. Zink, Chamber quality factors for the NACP-02 chamber in ^{60}Co beams: Comparison of EGSnrc and PENELOPE Monte Carlo simulations, IAEA–E2-CN-182, *Book of Extended Synopses for Symp. on Standards, Applications and Quality Assurance in Medical Radiation Dosimetry* (IAEA, Vienna), 269 – 270 (2010).

[100] E. Chin, D. Shipley, M. Bailey, J. Seuntjens, H. Palmans, A. DuSautoy, and F. Verhaegen, Validation of a Monte Carlo model of a NACP-02 plane-parallel ionization chamber model using electron backscatter experiments, Phys. Med. Biol. **53**, N119 – N126 (2008).

[101] M. Pieksa, L. De Prez, E. van Dijk, and A. Aalbers, Measurements of k_Q beam quality correction factors for the NE 2611A chamber in high energy photon beams using the Nederlands Meetinstituut water calorimeter, IAEA–CN–96/17P in Vol 1, *Proc. of Int'l Symp. on Standards and Codes of Practice in Medical Radiation Dosimetry*, (IAEA, Vienna), 93 – 102 (2003).

[102] J. Medin, C. Ross, N. Klassen, H. Palmans, E. Grusell, and J. Grindborg, Experimental determination of beam quality factors, k_Q, for two types of Farmer chamber in a 10 MV photon and a 175 MeV proton beam, Phys. Med. Biol. **51**, 1503 – 1521 (2006).

[103] A. H. L. Aalbers, M. T. Hoornaert, A. Minken, H. Palmans, M. W. H. Pieksma, L. A. de Prez, N. Reynaert, S. Vynckier, and F. W. Wittkamper, Code of Practice for the Absorbed Dose Determination in High Energy Photon and Electron Beams, NCS Report 18 of the Netherlands Commission on Radiation Dosimetry (2008).

[104] K. R. Shortt, C. K. Ross, M. Schneider, K. Hohlfeld, M. Roos, and A.-M. Perroche, A comparison of absorbed dose standards for high energy X-rays, Phys. Med. Biol. **38**, 1937 – 1955 (1993).

[105] M. Boutillon, B. M. Coursey, K. Hohlfeld, B. Owen, and D. W. O. Rogers, Comparison of primary water absorbed dose standards, in *Proc. of Symp. on Measurement Assurance in Dosimetry*, pages 95 – 111, IAEA–SM–330/48, IAEA, Vienna, 1994.

[106] C. K. Ross, K. R. Shortt, D. W. O. Rogers, and F. Delaunay, A Test of TPR_{10}^{20} as a Beam Quality Specifier for High-Energy Photon Beams, in *Proc. of Symp. on Measurement Assurance in Dosimetry*, pages 309 – 321, IAEA–SM–330/10, IAEA, Vienna, 1994.

[107] A. S. Guerra, R. F. Laitano, and M. Pimpinella, Experimental determination of the beam quality dependence factors, k_Q, for ionization chambers used in photon and electron dosimetry, Phys. Med. Biol. **40**, 1177 – 1190 (1995).

[108] S. Duane and M. Simon, Experimental Determination of the Quality-Dependent Correction Factors, k_Q, for Ionisation Chambers of Type NE 2561 and NE 2611, 11th Radiotherapy Standards Users' Group meeting (2008).

[109] D. W. O. Rogers, Analytic and graphical methods for assigning errors to parameters in non-linear least squares fitting, Nucl Inst and Meth **127**, 253 – 260 (1975).

[110] S. Brandt, *Data Analysis: Statistical and Computational Methods for Scientists and Engineers (Third Edition)*, Springer-Verlag, New York, 1999.

[111] J. Sempau, P. Andreo, J. Aldana, J. Mazurier, and F. Salvat, Electron beam quality correction factors for plane-parallel ionization chambers: Monte Carlo calculations using the PENELOPE system, Phys. Med. Biol. **49**, 4427 – 4444 (2004).

[112] M. R. McEwen, A. J. Williams, and A. R. DuSautoy, Determination of absorbed dose calibration factors for therapy level electron beam ionization chambers, Phys. Med. Biol. **46**, 741 – 755 (2001).

[113] C. Cojocaru, G. Stucki, M. McEwen, and C. Ross, Determination of absorbed dose to water in megavoltage electron beams using a calorimeter-Fricke hybrid system, IAEA–E2-CN-182, *Book of Extended Synopses for Symp. on Standards, Applications and Quality Assurance in Medical Radiation Dosimetry* (IAEA, Vienna), 27 – 28 (2010).

[114] G. Stucki and S. Voros, Experimental $k_{Q,Q0}$ Electron Beam Quality Correction Factors for the Types NACP02 and PTW34001 Plane-parallel Chambers, *Proceed. of Absorbed Dose and Air Kerma Primary Standards Workshop*, LNHB, Paris, http://www.nucleide.org/ADAKPS_WS/ (May, 2007).

[115] M. R. McEwen and A. R. DuSautoy, Primary standards of absorbed dose for electron beams, Metrologia **46**, S59–S79 (2009).

[116] L. L. W. Wang and D. W. O. Rogers, Replacement correction factors for plane-parallel ion chambers in electron beams, Med. Phys. **37**, 461 – 465 (2010).

[117] T. Ono, F. Araki, and F. Yoshiyama, Perturbation correction factors for cylindrical ionization chambers in high-energy electron beams, Radiol Phys Technol **3**, 93 – 97 (2010).

[118] C. D. Cojocaru and C. K. Ross, Extracting W_{air} from the 1976 electron beam measurements of Domen and Lamperti, Med. Phys. **39**, 4645 (abstract) (2012).

[119] E. S. M. Ali, B. Spencer, M. R. McEwen, and D. W. O. Rogers, Towards a more-realistic estimate of the uncertainty of photon cross sections at radiation therapy energies, Phys. Med. Biol. , to be submitted (2013).

[120] R. Alfonso, P. Andreo, R. Capote, M. S. Huq, W. Kilby, P. Kjall, T. R. Mackie, H. Palmans, K. Rosser, J. Seuntjens, W. Ullrich, and S. Vatnitsky, A new formalism for reference dosimetry of small and nonstandard fields, Med. Phys. **35**, 5179 – 5186 (2008).

[121] M. Kristensen, Measured influence of the central electrode diameter and material on the response of a graphite ionization chamber to ^{60}Co gamma-rays, Phys. Med. Biol. **28**, 1269 – 1278 (1983).

[122] F. Ubrich, J. Wulff, R. Kranzer, and K. Zink, Thimble ionization chambers in medium-energy x-ray beams and the role of constructive details of the central electrode: Monte Carlo simulations and measurements, Phys. Med. Biol. **53**, 4893 – 4906 (2008).

[123] F. Tessier and I. Kawrakow, Effective point of measurement of thimble ion chambers in megavoltage photon beams, Med. Phys. **37**, 96 – 107 (2010).

[124] T. Shimono, K. Kochida, H. Nambu, K. Matsubara, H. Takahashi, and H. Okuda, Polarity effect in commercial ionization chambers used in photon beams with small fields, Radiol. Phys. Technol. **2**, 97 – 103 (2009).

[125] R. Hill, Z. Mo, M. Haque, and C. Baldock, An evaluation of ionization chambers for the relative dosimetry of kilovoltage x-ray beams, Med. Phys. **36**, 3971 – 3981 (2009).

[126] F. Crop, N. Reynaert, G. Pittomvils, L. Paelinck, C. D. Wagter, L. Vakaet, and H. Thierens, The influence of small field sizes, penumbra, spot size and measurement depth on perturbation factors for microionization chambers, Phys. Med. Biol. **54**, 2951 – 2969 (2009).

[127] D. I. Thwaites, D. T. Burns, S. C. Klevenhagen, A. E. Nahum, and W. G. Pitchford, The IPEMB code of practice for electron dosimetry for radiotherapy beams of initial energy from 2 to 50 MeV based on air kerma calibration, Phys. Med. Biol. **41**, 2557 – 2603 (1996).

[128] D. I. Thwaites, A. R. DuSautoy, T. Jordan, M. R. McEwen, A. Nisbet, A. E. Nahum, and W. G. Pitchford, The IPEMB code of practice for electron dosimetry for radiotherapy beams of initial energy from 4 to 25 MeV based on an absorbed dose to water calibration, Phys. Med. Biol. **48**, 2929 – 2970 (2003).

[129] I. Kawrakow, On the effective point of measurement in megavoltage photon beams, Med. Phys. **33**, 1829 – 1839 (2006).

[130] F. Lacroix, M. Guillot, M. McEwen, C. Cojocaru, L. Gingras, A. S. Beddar, and L. Beaulieu, Extraction of depth-dependent perturbation factors for parallel-plate chambers in electron beams using a plastic scintillation detector, Med. Phys. **37**, 4331 – 4342 (2010).

[131] K. Zink and J. Wulff, Positioning of a plane-parallel ionization chamber in clinical electron beams and the impact on perturbation factors, Phys. Med. Biol. **54**, 2421 – 2435 (2009).

[132] L. L. W. Wang and D. W. O. Rogers, Study of the effective point of measurement for ion chambers in electron beams by Monte Carlo simulation, Med. Phys. **36**, 2034 – 2042 (2009).